INSTITUTO SUPERIOR TÉCNICO
Universidade Técnica de Lisboa

Data Rate Performance Gains in UMTS Evolution at the Cellular Level

Gonçalo Nuno Coelho e Ferraz de Carvalho

Dissertation submitted for obtaining the degree of
Master in Electrical and Computer Engineering

Jury

Supervisor: Prof. Luís M. Correia

Co-Supervisor: Mr. David Antunes

President: Prof. José Bioucas Dias

Member: Prof. António Rodrigues

October 2009

To my family

Acknowledgements

First of all, I would like to thank Professor Luís Correia for giving me the opportunity to write this thesis, and for the constant knowledge and experience sharing. I am thankful for his orientation, availability, constant support and advising, which were key factors to finish the work with the demanded and desired quality.

To Optimus, especially to David Antunes and Luís Santo, for all the suggestions, technical support and for having the time to answer all my doubts. I also would like to thank the opportunity to carry out measurements in the Optimus network, which allowed me to improve my technical knowledge.

To Daniel Sebastião, for his availability to help me with Microsoft Access software.

I also want to thank my colleagues from RF2 Lab, Nuno Jacinto and João Araújo, for their friendship, suggestions and constructive critics. Without their good company and support, this journey would have been much harder.

To my girlfriend Joana, for her love, friendship, encouragement, dedication and understanding throughout the years.

To my friends from Instituto Superior Técnico, for all the moments spent during the academic life. A special thank to my futsal team mates, for all their fellowship.

To my great friends from 'Os Cariocas', for all their support and friendship since our childhood.

Finally, I would to thank my family, especially my parents and siblings, for their unconditional support, patience, love and care, which are of vital importance to me.

Abstract

The main purpose of this thesis was to analyse UMTS/HSPA+ performance at the cellular level. For this purpose, measurements were performed in a single user scenario. The behaviour of some performance parameters was studied, using several settings and under different radio channel conditions. The comparison between the measured and theoretical data was done, pointing out explanations for the deviations shown in some cases. In downlink, the highest measured throughput was 16.3 and 12.6 Mbps, considering instantaneous and average value, respectively. It was confirmed that, given the same radio channel conditions, the increase of available power does not necessarily imply the achievement of a better performance. In uplink, the greatest instantaneous throughput was 5.32 Mbps, while the maximum average value was 4.27 Mbps.

Keywords

UMTS, HSPA+, Performance, Throughput, Measurements.

Resumo

O principal objectivo desta tese foi estudar o desempenho do sistema UMTS/HSPA+ a nível celular. Para tal, foram realizadas medidas num cenário de monoutilizador, tendo sido estudado o comportamento de alguns parâmetros que medem o desempenho do sistema, usando várias configurações e com diferentes condições de canal. Foi feita a comparação entre os resultados medidos e teóricos, e procurou-se encontrar explicações para as disparidades encontradas em alguns casos. No sentido descendente, o maior débito binário medido foi 16,3 e 12,6 Mbps, considerando valor instantâneo e médio, respectivamente. Demonstrou-se que, nas mesmas condições de canal, um aumento de potência disponível não implica necessariamente que se obtenha uma melhor performance. No sentido ascendente, o débito binário instantâneo máximo medido foi de 5,32 Mbps, sendo que 4,27 Mbps foi o maior valor médio.

Palavras-chave

UMTS, HSPA+, Desempenho, Débito Binário, Medidas.

Table of Contents

List of Figures

List of Tables

List of Acronyms

2G	Second Generation
3G	Third Generation
3GPP	Third Generation Partnership Project
AMC	Adaptive Modulation and Coding
AoA	Angle of Arrival
ARQ	Automatic Repeat Request
BLEP	Block Error Probability
BLER	Block Error Ratio
BPSK	Binary Phase Shift Keying
BS	Base Station
CIR	Channel Impulse Response
CN	Core Network
CPICH	Common Pilot Channel
CPC	Continuous Packet Connectivity
CQI	Channel Quality Indicator
CRC	Cyclic Redundancy Check
CS	Circuit Switch
DCH	Dedicated Channel
DL	Downlink
DOB	DL Optimised Broadcast
DRX	Discontinuous Reception
DS-CDMA	Direct-Sequence Code Division Multiple Access
DTX	Discontinuous Transmission
E-AGCH	E-DCH Absolute Grant Channel
E-DCH	Enhanced DCH
E-DPCCH	E-DCH Dedicated Physical Control Channel
E-DPDCH	E-DCH Dedicated Physical Data Channel
E-HICH	E-DCH HARQ Indicator Channel
EIRP	Equivalent Isotropic Radiated Power
eNB	Evolved Node B
EPC	Evolved Packet Core
E-RGCH	E-DCH Relative Grant Channel
E-UTRAN	Evolved UTRAN
FACH	Forward Access Channel

F-DCH	Fractional-DCH
FDD	Frequency Division Duplex
FDMA	Frequency Division Multiple Access
FRC	Fixed Reference Channel
GGSN	Gateway GPRS Support Node
GPRS	General Packet Radio Service
GSM	Global System for Mobile Communications
HARQ	Hybrid Automatic Repeat Request
HLR	Home Location Register
HOM	Higher-Order Modulation
HSDPA	High-Speed Downlink Packet Access
HS-DPCCH	High-Speed Dedicated Physical Control Channel
HS-DSCH	High-Speed Downlink Shared Channel
HSPA	High-Speed Packet Access
HSPA+	HSPA Evolution
HS-PDSCH	High-Speed Physical Downlink Shared Channel
HS-SCCH	High-Speed Shared Control Channel
HSUPA	High-Speed Uplink Packet Access
L1	Layer-1
L2	Layer-2
LTE	Long Term Evolution
MAC	Media Access Control
MBSFN	Multicast/Broadcast Single-Frequency Network
MCS	Modulation and Coding Scheme
ME	Mobile Equipment
MIMO	Multiple Input Multiple Output
MME	Mobility Management Entity
MMS	Multimedia Messaging Service
MSC	Mobile Switching Centre
MT	Mobile Terminal
OFDMA	Orthogonal Frequency Division Multiple Access
OVSF	Orthogonal Variable Spreading Factor
PDN	Packet Data Network
PDU	Protocol Data Unit
P-GW	PDN Gateway
PLMN	UMTS Public Land Mobile Network
PS	Packet Switch
P-SCH	Primary-Synchronisation Channel
QAM	Quadrature Amplitude Modulation
QoS	Quality of Service

QPSK	Quaternary Phase Shift Keying
RF	Radio Frequency
RLC	Radio Link Control
RMG	Relative MIMO Gain
RMSE	Root Mean Square Error
RNC	Radio Network Controller
RNS	Radio Network Sub-System
RRM	Radio Resource Management
RSCP	Received Signal Code Power
RTT	Round Trip Time
Rx	Receiver
SC	Single Carrier
SF	Spreading Factor
SGSN	Serving GPRS Support Node
S-GW	Serving Gateway
SINR	Signal-to-Interference-plus-Noise Ratio
SISO	Single Input Single Output
SMS	Short Messaging Service
SNR	Signal-to-Noise Ratio
S-SCH	Secondary-Synchronisation Channel
TBS	Transport Block Size
TDD	Time Division Duplex
TTI	Transmission Time Interval
ToA	Time of Arrival
Tx	Transmitter
UDP	User Datagram Protocol
UE	User Equipment
UL	Uplink
UMTS	Universal Mobile Telecommunications System
USIM	UMTS Subscriber Identity Module
UTRA	UMTS Terrestrial Radio Access
UTRAN	UMTS Terrestrial Radio Access Network
VLR	Visitor Location Register
VoIP	Voice over Internet Protocol
WCDMA	Wideband Code Division Multiple Access

List of Symbols

α	DL orthogonality factor
Δf	Signal bandwidth
η_{BLER}	HS-DSCH BLER
η_{DL}	DL load factor
η_{UL}	UL load factor
$\bar{\xi}$	Mean correlation between links in a MIMO system
ρ_{IN}	SINR
ρ_{N}	SNR
ρ_{pilot}	CPICH E_c/N_0
σ	Standard deviation
Ω	CQI
a_{pd}	Average power decay
C_{MIMO}	Capacity of a MIMO system
C_{SISO}	Capacity of a SISO system
$\bar{e}$	Relative mean error
E_b	Bit energy
E_c	Chip energy
e_{RMS}	RMSE
g	Geometry factor
G_{div}	Diversity gain
G_p	Processing gain
G_{MHA}	Masthead amplifier gain
$G_{M/S}$	Relative MIMO gain
G_r	Receiving antenna gain
G_t	Transmitting antenna gain
F	Noise figure
F_a	Activity factor
h_{kl}	CIR between signal from the l^{th} Tx antenna to the k^{th} Rx antenna
$\mathbf{H_n}$	Normalised channel transfer matrix related to **T**
I_{inter}	Received inter-cell interference
$I_{inter\ n}$	Normalised inter-cell interference
I_{intra}	Received intra-cell interference
$\mathbf{I_{NR}}$	N_R dimensional identity matrix

L_c	Cable losses between transmitter and antenna
L_{int}	Indoor penetration losses
L_p	Path loss
L_u	User losses
L_{ref}	Propagation model losses
M_{FF}	Fast fading margin
M_I	Interference margin
M_{SF}	Slow fading margin
N	Total noise power
N_0	Noise power spectral density
N_R	Number of Rx antennas
N_{RF}	Noise power at the RF band
N_s	Number of samples
N_T	Number of Tx antennas
P_{BS}^{Rx}	Node B received power
P_{BS}^{Tx}	Total Node B transmit power
$P_{HS-DSCH}^{Rx}$	Received power of the HS-DSCH summing over all active HS-PDSCH codes
$P_{HS-DSCH}^{Tx}$	HS-DSCH transmit power
P_{MT}^{Tx}	MT transmit power
P_{pilot}^{Rx}	CPICH RSCP
P_{pilot}^{Tx}	CPICH transmit power
P_r	Power available at the receiving antenna
P_{Rx}	Received power at receiver input
$P_{Rx\ min}$	Receiver sensitivity
$P_{S\&C}$	Signalling and control power
P_t	Power fed to the transmitting antenna
R	Cell radius
r^2	Correlation factor
R_b	Data rate
R_c	Chip rate
SF_{16}	HS-PDSCH spreading factor of 16
$\mathbf{T}$	Non-normalised channel transfer matrix, containing the channel transfer gains for each pair of antennas
z_i	Sample *i*
z_r	Reference value

List of Software

Microsoft Access	Database management tool
Microsoft Excel	Calculation tool
Microsoft Word	Text editor tool
TEMS Investigation	Data collection tool

Chapter 1

Introduction

This chapter gives a brief overview of the work. It provides the scope and the motivations of the thesis. At the end of the chapter, the work structure is presented.

Access to information and communication technologies has a direct and measurable impact on social and economic development. In emerging markets, the uptake of the mobile phone has driven advances in commerce, education, healthcare and entertainment as well as social inclusion. The boost to emerging economies provided by the deployment of mobile telephony will be further amplified when there is also widespread access to the internet [Eric09].

The analogue cellular systems, known as first-generation systems, provided only the voice service. Second Generation (2G) telecommunications systems, such as the Global System for Mobile Communications (GSM), were already digital and have enabled voice traffic to go wireless in many of the leading markets – the number of mobile phones surpasses the number of landline phones, and the mobile phone penetration is approaching 100% in those markets – and provided new services, such as text messaging and internet access, which started to grow rapidly [HoTo07].

In 1999, the Third Generation Partnership Project (3GPP) launched Universal Mobile Telecommunications System (UMTS), the first Third Generation (3G) system, called Release 99. 3G systems are designed for multimedia communication: with these, person-to-person communication can be enhanced with high-quality images and video, and access to information and services on public and private networks were enhanced by the higher data rates and new flexible communication capabilities of 3G systems [HoTo07]. UMTS uses Wideband Code Division Multiple Access (WCDMA) as air interface, providing data rates up to 384 kbps for the Downlink (DL) and Uplink (UL) in its Release 99, despite having a theoretical maximum for DL of 2 Mbps. In UMTS, there are two different modes of operation possible: Time Division Duplex (TDD) and Frequency Division Duplex (FDD). Only the latter was commercially deployed.

In March 2002, High-Speed Downlink Packet Access (HSDPA) was set as standard in Release 5. HSDPA became available in 2005, providing 1.8 Mbps, increasing to 3.6 Mbps in 2006 and achieving 7.2 Mbps in 2007, with the maximum peak data rate of 14.4 Mbps being currently offered by some operators. The DL packet-data enhancements of HSDPA are complemented by High-Speed Uplink Packet Access (HSUPA). HSUPA was standardised in 3GPP's Release 6, commercially deployed during 2007, with data rates up to 5.76 Mbps. HSDPA and HSUPA are commonly known as High-Speed Packet Access (HSPA).

HSPA Evolution (HSPA+) is specified by 3GPP in Release 7. HSPA+ offers a number of enhancements, providing substantial improvements to end-user performance and network capacity. The aim of HSPA+ is to further improve the performance of UMTS through higher peak rates, lower latency, greater capacity and increased battery times [BEGG08]. The introduction of Multiple Input Multiple Output (MIMO) and Higher-Order Modulation (HOM) extends the peak data rate to 42 Mbps in DL and 11.5 Mbps in UL. In 3GPP's Release 8 is specified Long Term Evolution (LTE), which is the next emergent technology. LTE uses a new access technique called Orthogonal Frequency Division Multiple Access (OFDMA) and further pushes radio capabilities higher, with a larger bandwidth and a lower latency. The peak data rate evolution of 3GPP technologies is presented in Figure 1.1.

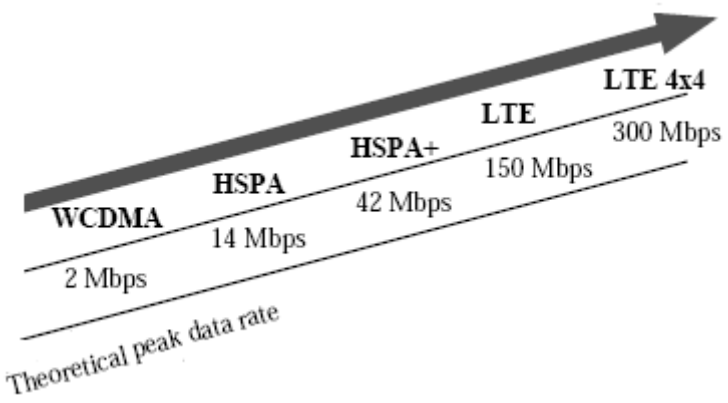

Figure 1.1. Peak data rate evolution of 3GPP technologies (adapted from [HoTo09]).

The global cellular technology market is shown in Figure 1.2. The number of subscriptions surpasses four billions, with GSM having the largest market share. There is a continued strong growth of the mobile industry, with the global market on the path to reach six billion connections by 2013 [GSMW09].

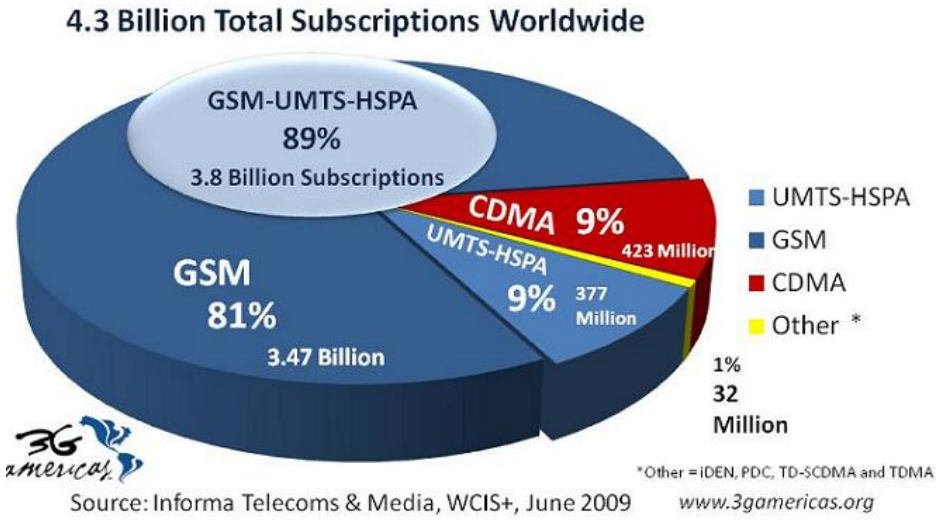

Figure 1.2. Global cellular technology market (extracted from [3GAM09]).

The number of mobile subscribers has increased tremendously in recent years. Voice communication has become mobile in a massive way and the mobile phone is the preferred way for voice communication. At the same time, data usage has grown fast with the introduction of HSPA, indicating that users find value in broadband wireless data. The average data consumption exceeds hundreds of MB per subscriber per month. End users expect data performance similar to the fixed lines, which can be a reality with all new technologies rising [HoTo09].

On the one hand, LTE is still perhaps three to four years away from being ready. On the other, HSPA+ is already being deployed in some countries, including Portugal, so it is of interest to evaluate the actual performance of this system.

The main scope of this thesis is to analyse HSPA+ performance at the cellular level. This goal is

accomplished by carrying out measurements in a single user scenario, studying the behaviour of parameters such as throughput, Channel Quality Indicator (CQI) and modulation, using several settings and under different radio channel conditions.

This thesis was made in collaboration with the Portuguese mobile telecommunications operator Optimus. HSPA+ measurements were performed on Optimus' network. Note that at the time of the measurements HOM had already been introduced, unlike MIMO.

The main contribution of this thesis is the analysis of HSPA+ performance at the cellular level, in a single user scenario, in both DL and UL. The comparison between measured and theoretical data is also done.

This thesis is composed of 4 chapters, besides the current one, followed by a set of annexes.

In Chapter 2, an introduction to the main technologies that are related to the scope of this thesis is presented, mainly focusing on the architecture, coverage and capacity aspects. First, a description of HSPA and HSPA+ is provided. Later, a brief comparison between HSPA+ and LTE is shown. At the end of the chapter, current services and applications are addressed.

Chapter 3 presents the theoretical models that are used in this work, as well as the parameters required to compare expected and experimental data.

In Chapter 4, the measurements' scenario is presented, describing the environment and the power configurations. Afterwards, the HSPA+ DL and UL results are analysed, and the comparison with the theoretical models is done.

Finally, in Chapter 5, the main conclusions of this work are drawn, along with future work suggestions.

A set of annexes with auxiliary information and additional results is also included. Annex A contains the basic aspects of MIMO. In Annex B, one presents the detailed link budget. Finally, in Annex C, one shows additional HSPA+ DL results.

Chapter 2

Basic Concepts

This chapter gives an introduction to the main technologies that are related to the scope of this thesis, mainly focusing on the architecture, coverage and capacity aspects. First, a description of HSPA and HSPA+ is provided. Later, a brief comparison between HSPA+ and LTE is presented. At the end of the chapter, current services and applications are addressed.

2.1 UMTS/HSPA

In this section, based on [HoTo06], UMTS Releases 5 and 6 basic concepts are presented, namely network architecture, radio interface and performance aspects.

2.1.1 Network Architecture

The UMTS architecture is represented in Figure 2.1, the network being grouped into three high-level modules, which are specified by 3GPP:

- User Equipment (UE);
- UMTS Terrestrial Radio Access Network (UTRAN);
- Core Network (CN).

UE is, basically, the interface with the user, UTRAN deals with all radio related functionality, and finally, CN handles switching and routing calls and data connection to external networks.

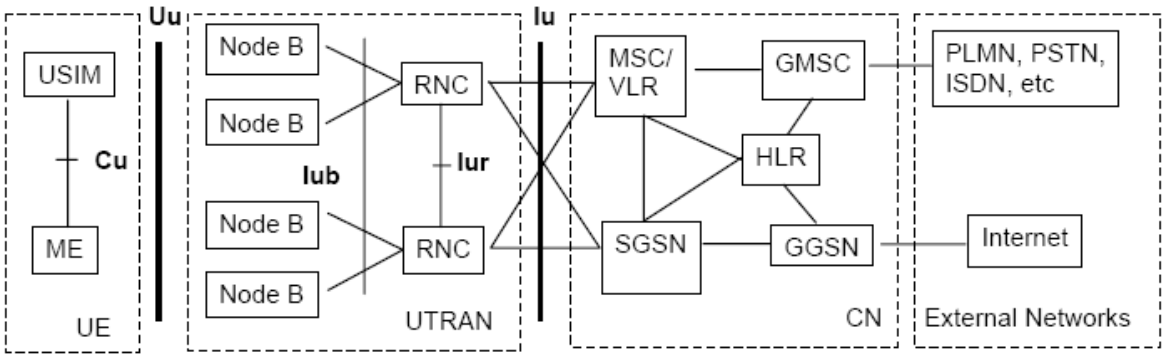

Figure 2.1. UMTS network architecture (extracted from [HoTo04]).

The UE is composed of the Mobile Equipment (ME) and the UMTS Subscriber Identity Module (USIM). The ME is the Mobile Terminal (MT) used for radio communication over the *Uu* interface and the USIM is a smart card that holds the subscriber identity, performs authentication algorithms and stores information. USIM and ME communicate over the *Cu* interface.

UTRAN consists of one or more Radio Network Sub-Systems (RNSs), being composed of two different elements:

- Node B, the Base Station (BS), switches the data flow between the *Iub* and *Uu* interfaces, with some functionalities in the Radio Resource Management (RRM);
- Radio Network Controller (RNC) owns and controls the radio resources in Node Bs connected to it by the *Iub* interface, carrying the major RRM functions, e.g., outer loop power control, packet scheduling and handover control.

In UTRAN, RNCs are connected to each other by the *Iur* interface.

CN is adapted from GSM CN, the main elements being:

- Home Location Register (HLR) is a database located in the user's home system;
- Mobile Switching Centre/Visitor Location Register (MSC/VLR) is the switch and the database that serves the UE in its current location for Circuit-Switched (CS) services;
- Gateway MSC (GMSC) is the switch at the point where UMTS Public Land Mobile Network (PLMN) is connected to external CS networks; it is where all incoming and outgoing CS connections carry by;
- Serving GPRS Support Node (SGSN) that has similar functionalities to MSC/VLR, but is normally used for Packet-Switched (PS) services;
- Gateway GPRS Support Node (GGSN) functionality is close to that of GMSC, but relative to PS services.

2.1.2 Radio Interface

In the radio interface (identified as *Uu* in Figure 2.1), UMTS uses WCDMA, a wideband Direct-Sequence Code Division Multiple Access (DS-CDMA) air interface. It has a chip rate of 3.84 Mcps, which leads to a channel bandwidth of 4.4 MHz, with a channel separation of 5 MHz. Currently, UMTS uses only FDD, UMTS Terrestrial Radio Access (UTRA) occupying the band [1920, 1980] MHz for UL and [2110, 2170] MHz for DL [Moli05].

WCDMA uses two types of codes for spreading and multiple access: channelisation and scrambling. Channelisation codes, on spreading, are responsible for separating transmissions from the same source, in DL at the same sector, and in UL are used to separate physical data and control information from the same UE. These codes are Orthogonal Variable Spreading Factor (OVSF) ones, which allow the Spreading Factor (SF) to be changed and orthogonality between codes to be maintained. Therefore, the number of channelisation codes is given by SF. Scrambling codes are mainly used to distinguish between cells and users. Scrambling is used on top of spreading so that the signal bandwidth is not changed; in DL, it differentiates the sectors of the cell, and in UL it separates MTs from each other, which allows the use of identical spreading codes for several transmitters.

HSDPA and HSUPA are Release 99 evolutions, both known as HSPA, and patented by 3GPP as Release 5 and Release 6, respectively. While in Release 99 the scheduling control is based on the RNC, and the Node B only has power control functionalities, in HSDPA capacity and spectral efficiency are improved. Scheduling and fast link adaptation based on physical layer retransmissions were moved to the Node B, reducing latency and providing a whole change in RRM.

In Release 99, radio transmissions are structured in frames of 10 ms, and transport data blocks are transmitted over an integer number of frames. The Transmission Time Interval (TTI), which is the transmission duration, is, usually, between 10 and 80 ms. HSPA supports a frame length of 2 ms,

which leads to the reduction of latency and a fast scheduling among different users.

HSDPA does not support soft handover or fast power control. Higher data rates are accomplished through the use of 16 Quadrature Amplitude Modulation (QAM), which can only be used under good radio channel conditions. Quaternary Phase Shift Keying (QPSK) is mainly used to maximise coverage and robustness. HSDPA introduces Adaptive Modulation and Coding (AMC), which adjusts the modulation and coding scheme to the radio channel conditions, and, together with 16QAM, allows higher data rates.

Several new channels have been introduced for HSDPA operation. For user data, there are the High-Speed Downlink Shared Channel (HS-DSCH) and the High-Speed Physical Downlink Shared Channel (HS-PDSCH). For the associated signalling needs, there are two channels: High-Speed Shared Control Channel (HS-SCCH) in the DL, and the High-Speed Dedicated Physical Control Channel (HS-DPCCH) in the UL direction. For Release 6, the Fractional Dedicated Channel (F-DCH) was created for handling power control when only packet services are active, allowing a larger number of users with lower data rates [HoTo06].

The HS-DSCH supports the new 16QAM modulation. Node B scheduling with TTI of 2 ms and fast physical layer transmission using Hybrid Automatic Repeat Request (HARQ) with two types of retransmission are used. For user data transmission, HSDPA uses a fixed SF of 16, which means that user data can be transmitted using up to 15 orthogonal codes, since the 16^{th} is reserved for HS-SCCH, allowing a theoretical peak bit rate of 14.4 Mbps. The HS-SCCH carries critical signalling information for de-spreading of the correct codes and ARQ information providing the repetition of the previous transmission based on received transmissions. It uses QPSK modulation and an SF of 128.

In order to keep a balanced evolution, there was the need to enhance UL as well. In Release 6, HSUPA was introduced as an extension of Release 99, with the goal of achieving higher data rates compared to Release 99's 384 kbps in general urban outdoor scenarios, and later reaching 2 Mbps in hot-spot, indoor areas.

HSUPA has some of the features of HSDPA, namely fast Layer-1 (L1) HARQ, fast Node B based scheduling and, optionally, a shorter TTI of 2 ms, brought to UL with a new transport channel, the Enhanced DCH (E-DCH). The HARQ used in HSUPA is fully synchronous, avoiding the need for sequence numbering, and it can operate in soft handover. The modulation is Binary Phase Shift Keying (BPSK), since transmission with multiple channels was adopted, instead of using higher order modulation, avoiding severe changes on technical issues at the UE.

New operation channels were introduced. In UL, the E-DCH Dedicated Physical Control Channel (E-DPCCH) is used for new control information, and for carrying data there is the E-DCH Dedicated Physical Data Channel (E-DPDCH). In DL, the E-DCH Absolute Grant Channel (E-AGCH) and the E-DCH Relative Grant Channel (E-RGCH) are used for scheduling control and the E-DCH HARQ indicator channel (E-HICH) is used for retransmission support. The DCH channels from Release 99

were left unchanged. In HSUPA, the E-DCH is a dedicated channel, similar to Release 99, but with fast retransmission and scheduling, while for HSDPA, the HS-DSCH is a shared one [HoTo06].

In HSDPA, one of the criteria for admission of new users is the available transmit power. On the other hand, in HSUPA the common resource is the UL noise factor, directly connected to the interference level, since each UE has its own transmitter. The scheduling main function is to keep the UL noise factor low enough to allow a high cell capacity, assuring that cell overload is not reached.

Table 2.1 lists the applicability of key features for Release 99, HSDPA and HSUPA.

Table 2.1. Comparison between UMTS stages (adapted from [HoTo06]).

Feature	Release 99	Release 5 (HSDPA)	Release 6 (HSUPA)
Variable Spreading Factor	Yes	No	Yes
Adaptive Modulation	No	Yes	No
Soft Handover	Yes	No	Yes
Fast Power Control	Yes	No	Yes
Node B based scheduling	No	Yes	Yes
Fast L1 HARQ	No	Yes	Yes
TTI length [ms]	80, 40, 20, 10	2	10, 2
Maximum data rate [Mbps]	0.384 (urban outdoor) / 2 (indoor)	14.4	5.7

2.1.3 Coverage and Capacity

The trade-off between capacity and interference is of key importance in cellular networks. In UMTS, capacity depends, essentially, on the number of users and on the type of services, via the interference margin and the sharing of transmitting power. This margin is given by [Corr06]:

$$M_{I[\mathrm{dB}]} = -10\log(1-\eta) \tag{2.1}$$

where:

- η is the load factor.

A raise of the load factor leads to a reduction in coverage, via the increase of the interference margin. The load factor depends on the services, and since there is asymmetry between UL and DL, it is different between the two; it should not be higher than 50% in UL and 70% in DL. These factors, for a given user *j*, are given by [Corr06]:

$$\eta_{UL} = (1 + I_{inter\,n}) \sum_{j=1}^{N_u} \frac{1}{1 + \dfrac{R_c / R_{b\,j}}{\rho_{N\,j} \cdot F_{a\,j}}} \tag{2.2}$$

$$\eta_{DL} = (1 + I_{inter\,n}) \sum_{j=1}^{N_u} F_{a\,j} \cdot \frac{\rho_{N\,j}}{R_c / R_{b\,j}} \left[(1 - \alpha_j) + I_{inter\,n\,j} \right] \tag{2.3}$$

where:

- η_{UL} is the UL load factor;
- η_{DL} is the DL load factor;
- $I_{inter\,n}$ is the normalised inter-cell interference (between [40, 60] % in UL and 0% in DL);
- N_u is the number of active users;
- R_c is the chip rate of WCDMA (3.84 Mcps);
- $R_{b\,j}$ is the data rate associated to service of user *j*;
- $\rho_{N\,j}$ is the Signal-to-Noise ratio (SNR) of user *j*;
- $F_{a\,j}$ is the activity factor of user of user *j* (50% for voice and 100% for data);
- α_j is the code orthogonality factor of user *j* (typically in [0.5, 0.9]).

The radius of a given cell can be estimated using the definition of the path loss and the model of the average power decay with distance. The radius of a cell is given by [Corr06]:

$$R_{[\mathrm{km}]} = 10^{\frac{P_{t[\mathrm{dBm}]} + G_{t[\mathrm{dBi}]} - P_{r[\mathrm{dBm}]} + G_{r[\mathrm{dBi}]} - L_{ref[\mathrm{dB}]}}{10 \cdot a_{pd}}} \tag{2.4}$$

where:

- P_t is the power fed to the transmitting antenna;
- G_t is the gain of the transmitting antenna;
- P_r is the power available at the receiving antenna;
- G_r is the gain of the receiving antenna;
- L_{ref} are propagation model losses;
- a_{pd} is the average power decay.

Release 99 uses E_b/N_0, energy per bit to noise power spectral density ratio, as a metric to evaluate its performance. In HSDPA, the bit rate can change every TTI using different modulation and coding schemes. Therefore, the metric used for HSDPA is the average HS-DSCH Signal-to-Interference-plus-Noise Ratio (SINR) that represents the narrowband SINR after the process of de-spreading of HS-PDSCH. Link adaptation selects the modulation and coding schemes with the purpose of optimising throughput and delay for the instantaneous SINR [HoTo06].

The HS-DSCH SINR for a single antenna Rake receiver is expressed by [HoTo06]:

$$\rho_{IN} = SF_{16} \frac{P_{HS-DSCH}^{Rx}}{(1 - \alpha) \cdot I_{intra} + I_{inter} + N_{RF}} \tag{2.5}$$

where:

- ρ_{IN} is the SINR;
- SF_{16} is a HS-PDSCH spreading factor of 16;
- $P_{HS-DSCH}^{Rx}$ is the received power of the HS-DSCH summing over all active HS-PDSCH codes;
- I_{intra} is the received intra-cell interference;
- I_{inter} is the received inter-cell interference;
- N_{RF} is the noise power at the radio frequency (RF) band.

HS-DSCH SINR is an important measure to network dimensioning and link budget planning. It is also used to accomplish a certain Block Error Ratio (BLER) for the number of HS-PDSCH codes, modulation and coding scheme used. Figure 2.2 illustrates the average throughput, including link adaptation and HARQ, as a function of the average HS-DSCH SINR. Results are shown for 5, 10 and 15 HS-PDSCH codes.

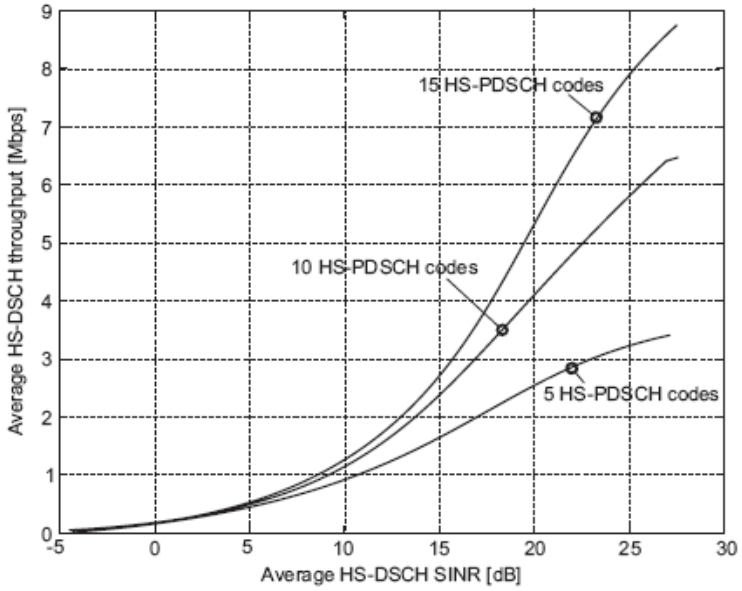

Figure 2.2. HSDPA data rate as function of the average HS-DSCH SINR (extracted from [Pede05]).

The average cell throughput increases with the number of HS-PDSCH codes, having a growth of 50% when the number of codes is modified from 5 to 10. HARQ, fast link adaptation and turbo-coding contribute to have a capacity gain of almost 70% compared to Release 99 [HoTo06].

On the other hand, with the increase of the power allocated to HS-DSCH the data rates would be higher as well, until it creates greater interference. For example, with 5 HS-PDSCH codes, 16QAM, the HS-DSCH SINR should be in the range of [-3, 17] dB, [Salv08].

Network capacity depends on type of user and the respective scenario, type of service provided, and number of HS-PDSCH codes used.

The Common Pilot Channel (CPICH) E_c/N_0, pilot energy per chip to noise power spectral density ratio, is frequently used to network dimensioning and to estimate single user throughput. SINR can be

expressed as a function of the pilot E_c/N_0 [HoTo06]:

$$\rho_{IN} = SF_{16} \frac{P_{HS-DSCH}^{Tx}}{\frac{P_{pilot}^{Tx}}{\rho_{pilot}} - \alpha \cdot P_{BS}^{Tx}} \tag{2.6}$$

where:

- $P_{HS-DSCH}^{Tx}$ is the HS-DSCH transmit power;
- P_{pilot}^{Tx} is the CPICH transmit power;
- ρ_{pilot} is the CPICH E_c/N_0;
- P_{BS}^{Tx} is the total Node B transmit power.

The HSDPA transmit power can be expressed as a function of the SINR, thus, as a function of the desired data rate at the cell edge using:

$$P_{HS-DSCH}^{Tx} \geq \rho_{IN} \cdot (1 - \alpha + g^{-1}) \frac{P_{BS}^{Tx}}{SF_{16}} \tag{2.7}$$

where:

- g is the geometry factor, defined as:

$$g = \frac{I_{intra}}{I_{inter} + N_{RF}} \tag{2.8}$$

As in HSDPA, performance in HSUPA depends highly on network algorithms, deployment scenarios, UE transmitter capability, Node B performance and capability and type of traffic. For performance testing purposes, 3GPP defined a set of E-DCH channel configurations called Fixed Reference Channels (FRCs). FRC5 represents the first HSUPA phase UE, while FRC2 and FRC6 represent the incoming UE's releases with advanced capabilities, like higher coding rate and support 2 ms for TTI.

The performance metric used in HSUPA is E_c/N_0. A high E_c/N_0 at the Node B is necessary to achieve higher data rates, leading to an increased UL noise and, as a result, a decreased cell coverage area. For this reason, a maximum level for the UL noise may be defined for macro-cells, to guarantee the coverage area, otherwise, limiting high data throughputs. In Figure 2.3, one presents the expected data rate for vehicular UE as a function of the available E-DCH E_c/N_0.

The relation between E_b/N_0 and E_c/N_0 is given by:

$$E_b / N_{0[\text{dB}]} = E_c / N_{0[\text{dB}]} + G_{P[\text{dB}]} \tag{2.9}$$

where:

- G_p is the processing gain, defined as:

$$G_{p[\mathrm{dB}]} = 10\log\left(\frac{R_c}{R_b}\right) \tag{2.10}$$

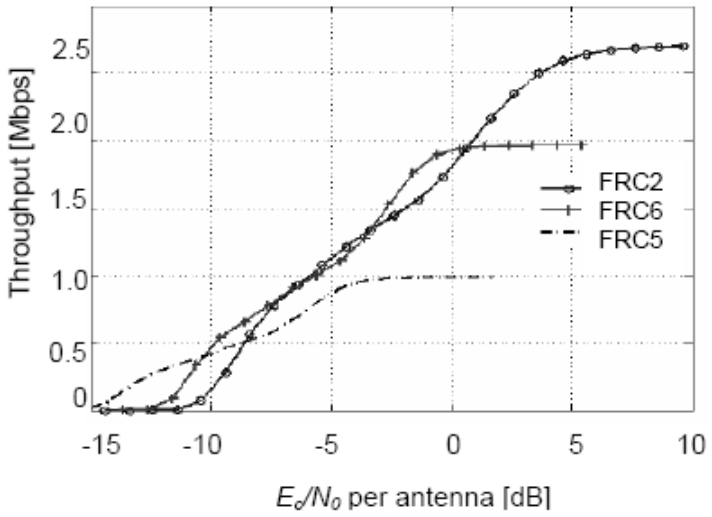

Figure 2.3. HSUPA throughput in Vehicular A at 30 km/h, without power control (extracted from [HoTo06]).

It is clear that the curves corresponding to FRC2 with 2 ms TTI and FRC6 with 10 ms TTI are similar. Nevertheless, FRC2 can reach higher throughputs in circumstances of high enough E_c/N_0 values, which in real scenarios may be difficult to achieve. Values of received E_c/N_0 higher than 0 dB allow, in both cases, to obtain throughputs beyond 2 Mbps [HoTo06].

HSUPA, by using HARQ and a soft combination of HARQ retransmissions, allows a decrease of the necessary E_b/N_0 at the Node B, when comparing similar data rates with Release 99. Increasing the Block Error Probability (BLEP) at first transmission increases the UL spectral efficiency and again consequently a lower E_b/N_0. The capacity improvement due to the use of HARQ is expected to be between 15% and 20% [HoTo06].

Considering Node B based scheduling, it can provide the system two main advantages: faster reallocation of radio resources among users, and tighter control of total received UL power. The former dynamically takes resources from users with low utilisation of allocated radio resources and redistributes them among users with high utilisation, while the latter allows faster adaptation to interference variations. The use of HARQ and Node B scheduling improves a capacity gain of 15 to 60%, according to [Lope08], depending on the service and scenario.

There are 2 TTIs available: the 2 ms is used under good channel conditions and only for high data rates, while the 10 ms is the default value for cell edge coverage suffering from a high number of retransmissions due to the increased associated path loss [HoTo06].

2.2 HSPA+

In this section, HSPA+ main concepts are presented, based on [BEGG08] and [PWST07].

The aim of HSPA+ is to further improve UMTS performance, through higher peak data rates, greater capacity, lower latency, and greater spectral efficiency. In order to support these enhanced capabilities, HSPA+ introduces:

- HOM;
- MIMO;
- Continuous Packet Connectivity (CPC);
- Advanced Receivers;
- Layer-2 (L2) protocol enhancements;
- Multicast/Broadcast Single-Frequency Network (MBSFN);
- Enhanced Cell Forward Access Channel (CELL_FACH);
- Support optimisation for Voice over Internet Protocol (VoIP).

These new concepts will yield substantially higher peak data rates. In Release 8, for example, the peak data rates will theoretically reach up to 42 Mbps in DL and 11.5 Mbps in UL (per 5 MHz carrier) [BEGG08]. Additionally, for next specification releases, 3GPP is considering Downlink-Optimised Broadcast (DOB) and multi-carrier operation.

HOM enables users to experience significantly higher data rates, under favourable radio conditions, with the introduction in Release 6 of BPSK and QPSK in the UL and QPSK and 16QAM for the DL. Furthermore, Release 7 incorporates 64QAM in DL, increasing the peak data rate to the double [HoTo07] from 14.4 Mbps to around 28 Mbps in a 2x2 MIMO configuration.

MIMO increases the data rate by transmitting multiple transport blocks in parallel, using multiple antennas, to a single user; taking advantage of spatial multiplexing, the receiver uses the channel, modulation and coding schemes in order to separate the encoded streams. In Annex A, the basic aspects of MIMO are presented.

The potential gain reachable with MIMO and HOM is illustrated in Figure 2.4 for the 90^{th} percentile throughput, for DL. The improvements verified for UL can be observed in Figure 2.5. Note the slightly differences in DL with the use of multiple receiver branches SIMO, which extend the benefits of HOM in lower SNRs, and the better power efficiency resulting in a better performance of QPSK compared with 16QAM, when the data rate target is under 4 Mbps in the UL.

Moreover, in order to support the signalling of the new modulation schemes, larger transport block sizes (TBS), HARQ per stream, and larger range for CQI, 3GPP updates several physical channels, like HS-SCCH, HS-DPCCH, E-AGCH and E-DPCCH. Modulation and Coding Scheme (MCS) tables determine the best combination of modulation and coding rate for a given SNR, leading to a limited

peak data rate, due to the use of the higher modulation and least amount of coding possible, for each value of SNR.

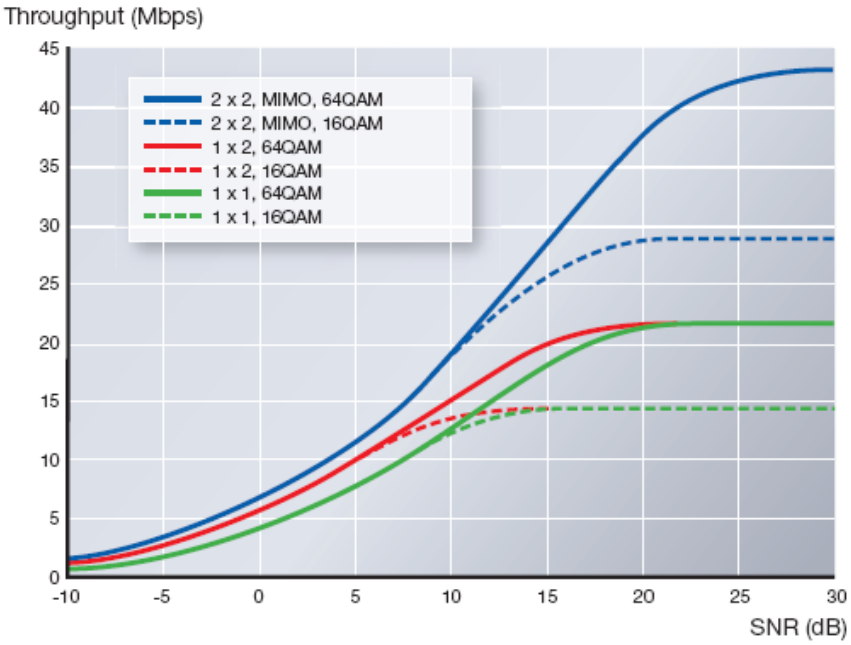

Figure 2.4. The 90th percentile throughput for DL HOM and MIMO (extracted from [BEGG08]).

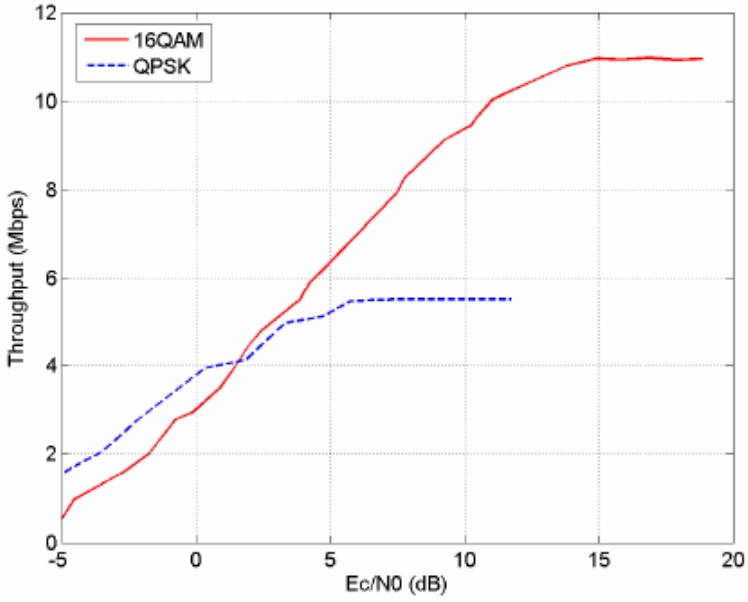

Figure 2.5. Throughput as a function of E_c/N_0 for UL HOM (extracted from [PWST07]).

The receiver structures in UEs and Node Bs are constantly being improved to raise system performance and increase user data bit rates. Release 6 and 7 introduced the use of receive diversity antennas type-1, linear equalisers type-2, and the combination of linear equaliser with receive diversity antennas. Release 8 introduces requirements for even more advanced receivers (type-3), with inter-cell interference cancellation support.

With the activity level of packet users varying considerably over time, there is a need to efficiently support continuously connected applications. The solution presented by 3GPP in Release 7 is CPC, which has two main features called UE Discontinuous Transmission and Reception (UE DTX/DRX) and HS-SCCH-less operation. The introduction of UE DTX/DRX leads to benefits, such as, reduced battery consumption and increased capacity. In some situations of dense traffic transmission the control channel HS-SCCH can carry a significant code overhead that is decreased by the “less operation” referred above. In fact, this operation reduces code usage as well as interference from control signalling and increases capacity. Simulations in [HGMT05] exhibit that the introduction of CPC in Release 7 increases VoIP capacity by 40% in the UL and 10% in the DL.

The DL peak data rate is limited by the size of Radio Link Control (RLC) window, RLC Protocol Data Unit (PDU) and by the RLC Round Trip Time (RTT). In order to support MIMO and 64QAM, a larger RLC Protocol Data Unit is needed, therefore, in Release 7, flexible RLC PDU sizes are adopted as well as Media Access Control (MAC) segmentation and MAC multiplexing for DL transmission. L2 protocol overhead is reduced, by reducing RLC header overhead, which is a consequence of the ability of the transmitter to flexibly select the size of RLC PDUs. At the Node B level, a new protocol was created, the MAC-ehs, which carries on the possibility of RLC PDUs segmentation, improving the system coverage and reducing processing tasks at L2 [BEGG08].

The greater use of HSPA for Internet connections currently causes an impact on load and network characteristics. Therefore, 3GPP has worked to enhance the CELL_FACH state in Release 7 and 8 in order to keep up the data traffic level that has been carrying out. In Release 7, CELL_FACH has been activated for the DL, whereas in Release 8, 3GPP improved the transport channel E-DCH in CELL_FACH, enabling continuous data transmissions without interruptions even when channel switching occurs. A critical enhancement in Release 7 that eliminates inter-cell interference is the use of a common scrambling code on DL carriers for MBSFN transmission. The power efficiency is improving beyond new levels, while now the limiting factor is associated with codes rather than power, resulting in a larger ability of WCDMA technology concerning radio transmissions.

In Table 2.2, one presents the characteristics of MT categories for FDD HS-DSCH physical layer, meaning HSDPA and HSPA+ DL. The inter-TTI parameter indicates the capability to sustain the peak data rate over multiple continuous TTIs. Categories with a value of 1 correspond to devices that can also sustain the peak rate during 2 ms over multiple TTIs, while terminals with an inter-TTI value greater than 1 must wait for 2 or 4 ms after each received TTI [HoTo06].

Table 2.3 shows the HSUPA and HSPA+ UL MT categories’ characteristics.

3GPP standardised for HSDPA the common categories that go up to the 12th and the following ones were frozen from Release 7 and 8, with the introduction of MIMO systems and in some cases dual cell operation (21st to 24th MT categories).

Table 2.2. FDD HS-DSCH physical layer categories (adapted from [3GPP09a] and [HoTo07]).

MT Category	Maximum number of HS-PDSCH codes received	Minimum inter-TTI	Supported Modulation	Supported Modulations with MIMO	Maximum theoretical peak data rate [Mbps]
1	5	3	QPSK & 16QAM	Not applicable (MIMO configurations not supported)	1.22
2					1.22
3		2			1.82
4					1.82
5		1			3.65
6					3.65
7	10				7.21
8					7.21
9	15				10.20
10					14.40
11	5	2	QPSK		0.91
12		1			1.82
13	15		QPSK, 16QAM & 64QAM		17.64
14					21.10
15			QPSK & 16QAM	QPSK & 16QAM	23.37
16					27.95
17			QPSK, 16QAM & 64QAM		23.37
18					27.95
19				QPSK, 16QAM & 64QAM	35.28
20					42.20
21			---	---	23.37
22			---	---	27.95
23			---	---	35.28
24			---	---	42.20

Table 2.3. FDD E-DCH physical layer categories (adapted from [3GPP09a] and [HoTo06]).

MT Category	Maximum number of E-DCH codes transmitted	Minimum SF	TTI length [ms]	Supported Modulation	Maximum theoretical peak data rate [Mbps]
1	1	SF_4	10	QPSK	0.71
2	2	2 x SF_4	10, 2		1.45
3			10		1.45
4		2 x SF_2	10, 2		2.89
5			10		2.00
6	4	2 x SF_4 + 2 x SF_2	10, 2		5.74
7				QPSK & 16QAM	11.50

The creation of a 7th E-DCH category respects to the introduction of HOM in UL, meaning 16QAM, which belongs to the 3GPP specifications of Release 7. Note that the highest data rate supported with 10 ms TTI is 2 Mbps.

2.3 Comparison between HSPA+ and LTE

HSPA+ and LTE are the top class technologies for mobile cellular communications that we have been developed, regarding 3GPP's latest releases. Both systems target the packet data service as a main objective.

In Table 2.4, one shows some features of HSPA+ and LTE. The radio interface is one of the main differences between the systems: while in HSPA+ the multiple access method is WCDMA, in LTE the OFDMA new interface is used. Regarding the use of OFDMA, a flexible spectrum usage is possible with LTE; it is possible to scalable the bandwidths, and with that the increase of data rates can be achieved; this feature is not possible over WCDMA systems, since in HSPA+ only 5MHz bandwidths are used.

Table 2.4. Features comparison of HSPA+ and LTE.

Attribute	HSPA+	LTE
Duplex mode	FDD	
Multiple Access	WCDMA	OFDMA (DL) / SC-FDMA (UL)
Frequency [MHz]	[1920,1980] for UL; [2110, 2170] for DL	900, 1800, 2100, 2600
Channel Bandwidth [MHz]	5	1.4, 3, 5, 10, 15, 20
Frame size [ms]	2	1
Modulation	QPSK, 16QAM (UL); QPSK, 16QAM, 64QAM (DL)	
DL theoretical Peak Data Rate [Mbps]	42 (MIMO 2×2, 64QAM)	325.1 (20MHz, MIMO 4×4, 64QAM)
UL theoretical Peak Data Rate [Mbps]	11.5 (SISO, 16QAM)	86.4 (20MHz, Single Antenna)

LTE has a better spectrum efficiency, by a factor of 2 at least, since it can transmit the double of the information over the same bandwidth, as noticed by the higher data rate values in Table 2.4. Low latencies and shorter TTI are also achieved in LTE, while in HSPA+ the whole system has a greater delay coming from signalling.

In Table 2.5, one presents the comparison between UMTS and LTE network elements. In LTE, the UMTS RNC functionalities are divided between evolved Node B (eNB), the single element of the Evolved UTRAN (E-UTRAN), and Serving Gateway (S-GW), which has also the functionalities of SGSN. The Packet Data Network (PDN) Gateway (P-GW) is similar to GGSN, while the Mobility Management Entity (MME) has the functionalities of HLR and VLR in UMTS. MME, S-GW and P-GW compose the Evolved Packet Core (EPC).

Table 2.5. Comparison between UMTS and LTE network elements.

Element	UMTS	LTE
Base Station	Node B	eNB
Controller	RNC	---
Core Network / Evolved Packet Core	HLR - MSC/VLR	MME
	SGSN	S-GW
	GGSN	P-GW

The LTE architecture is an IP-based flat one, with fewer elements and consequently simpler than the hierarchical architecture used in HSPA+. On the other hand, HSPA+ is easier to implement, since there is no need to modify the current network architecture, whereas in LTE there are several new interfaces and functional upgrades.

2.4 Services and Applications

In order to manage the access to the different services and optimise system capacity, 3GPP defined four classes of services based on their Quality of Service (QoS) requirements: Conversational, Streaming, Interactive and Background. There are some important factors to distinguish them, such as traffic delay, the guaranteed bit rate and the different priorities.

The Conversational class is mainly intended for speech services (e.g., CS or VoIP). Real time services require tighter delay requirements to maintain a minimum quality of service. The delay order should not overtake 400 ms [HoTo07], i.e., the maximum end-to-end delay given by the human perception for audio and video conversation. Traffic is nearly symmetric between UL and DL. Video telephony has even tighter Bit Error Ratio (BER) requirements than voice, due to video compression. When it works on the PS domain, and in order to guarantee an efficient VoIP, service IP header compression and QoS differentiation are needed. This class has priority over others, because voice is a primary service and the one that is most required.

The Streaming class represents the audio and video streamings. This type of service enables the end user to access the data before the transfer is complete, which is possible with the use of buffers in the

final applications and a continuous stream transmission. In this class, traffic is not symmetric, thus, DL traffic is the most significant. Larger delays than in Conversational class can be tolerated, as the receiver typically buffers several seconds of Streaming material.

The Interactive class has a very asymmetric traffic and is tolerant to delay. This class includes Web browsing, online multiplayer games and push-to-talk applications, services that are based on PS connections. These are characterised by requesting response patterns and preservation of payload contents. Nevertheless, there are upper limits to tolerable delay, such as the time between choosing a certain Website and its actual appearance on the screen, which should not exceed a few seconds. For online multiplayer games, RTT is a very important parameter, especially in real time action games, where the end-to-end delay should be below 100 ms [Lope08].

The Background class covers services where transmissions delays are not critical (e.g., Short Messaging Service (SMS), Multimedia Messaging Service (MMS), E-mail), as opposed to the Interactive one, where the end user is not waiting for a response within a short time; however, this class is intolerant to transmission errors. Applications in this traffic class only use resource transmissions when none of the other classes is active.

The main differences between the 3GPP classes are presented in Table 2.6.

Table 2.6. Services and applications according to 3GPP (extracted from [3GPP08]).

Service Class	Conversational	Streaming	Interactive	Background
Real time	Yes	Yes	No	No
Symmetric	Yes	No	No	No
Guaranteed bit rate	Yes	Yes	No	No
Delay	Minimum Fixed	Minimum Variable	Moderate Variable	High Variable
Buffer	No	Yes	Yes	Yes
Bursty	No	No	Yes	Yes
Switching Type	CS	CS	PS	PS
Example	Voice	Video Streaming	Web Browsing	E-mail

Chapter 3

Models

This chapter presents the theoretical models used throughout this work, as well as the parameters needed to compare expected and experimental data.

3.1 HSPA+ DL

In this section, one presents the HSPA+ DL theoretical models of the several parameters under analysis. For all the link budget aspects, refer to Annex B.

As mentioned in the previous chapter, the metric used in HSPA+ DL to evaluate the performance is HS-DSCH SINR. Equations (2.5) and (2.6) give SINR as a function of HS-DSCH received power and CPICH E_c/N_0, respectively. It is also possible to relate SINR with the CPICH Received Signal Code Power (RSCP), which is the received power on one code after de-spreading, measured on the Primary CPICH [3GPP09b].

The HSPA+ DL power scheme is presented in Figure 3.1. Note that the propagation losses in the CPICH and in the HS-DSCH are the same, so the HS-DSCH received power can be expressed as [HoTo06]:

$$P^{Rx}_{HS-DSCH\,[\mathrm{dBm}]} = P^{Rx}_{pilot\,[\mathrm{dBm}]} + 10 \cdot \log\left(\frac{P^{Tx}_{HS-DSCH\,[\mathrm{W}]}}{P^{Tx}_{pilot\,[\mathrm{W}]}}\right) \tag{3.1}$$

where:

- P^{Rx}_{pilot} is the CPICH RSCP;
- $P^{Tx}_{HS-DSCH}$ is the HS-DSCH transmit power, given by:

$$P^{Tx}_{HS-DSCH\,[\mathrm{W}]} = P^{Tx}_{BS\,[W]} - P_{S\&C\,[W]} \tag{3.2}$$

  where:

  - $P_{S\&C}$ is the signalling and control power.

Manipulating (2.5) and (3.1), one has the SINR as a function of CPICH RSCP. Moreover, CPICH E_c/N_0 can also be expressed as a function of CPICH RSCP [3GPP09b]:

$$\rho_{pilot\,[\mathrm{dB}]} = 10 \cdot \log\left(\frac{P^{Rx}_{pilot\,[\mathrm{W}]}}{I_{intra\,[\mathrm{W}]} + I_{inter\,[\mathrm{W}]} + N_{RF\,[\mathrm{W}]}}\right) \tag{3.3}$$

where:

- I_{intra} is the received intra-cell interference, given by [HoTo06]:

$$I_{intra\,[\mathrm{dBm}]} = P^{Rx}_{pilot\,[\mathrm{dBm}]} + 10 \cdot \log\left(\frac{P^{Tx}_{BS\,[\mathrm{W}]}}{P^{Tx}_{pilot\,[\mathrm{W}]}}\right) \tag{3.4}$$

- N_{RF} is the noise power at the RF band, expressed as [Corr06]:

$$N_{RF\,[\mathrm{dBm}]} = -174 + 10 \cdot \log(\Delta f_{[\mathrm{Hz}]}) + F_{[\mathrm{dB}]} \tag{3.5}$$

where:

- Δf is the signal bandwidth, taken as the chip rate;
- F is the receiver's noise figure.

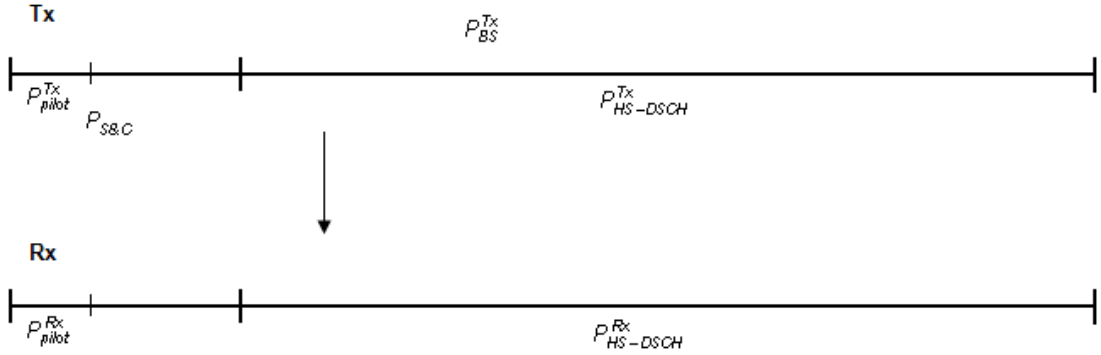

Figure 3.1. HSPA+ DL power scheme.

The received intra-cell interference is calculated by (3.4) similarly to the HS-DSCH received power calculation in (3.1). The latter is obtained given the HS-DSCH transmit power, which is the power available for data, while the former takes the total Node B transmit power into account. Regarding the noise power at the RF band, it is the thermal receiver noise power added to the receiver's noise figure.

This thesis does not address the inter-cell interference, since it was not experienced during the measurements, i.e., the HSPA+ DL user was subject only to intra-cell interference and noise power at the RF band.

SINR may be related to CQI, in order to establish theoretical models for parameters, such as HS-DSCH throughput or modulation as functions of CPICH RSCP and CPICH E_c/N_0. Equations (3.6) and (3.7) give two models relating SINR and CQI, Ω, Figure 3.2, from [BBSS04] and [3GGP02], respectively:

$$\Omega = \begin{cases} 0, & \rho_{IN\,[\mathrm{dB}]} \le -3.96 \\ \dfrac{\rho_{IN\,[\mathrm{dB}]}}{1.02} + 4.81, & -3.96 \le \rho_{IN\,[\mathrm{dB}]} < 26.04 \\ 30, & \rho_{IN\,[\mathrm{dB}]} \ge 26.04 \end{cases} \tag{3.6}$$

$$\Omega = \rho_{IN\,[\mathrm{dB}]} + 4.5 \tag{3.7}$$

Figure 3.2 shows that both models are similar and it was decided to use the one in (3.6). Note that the BLER is considered to be less than or equal to 10%.

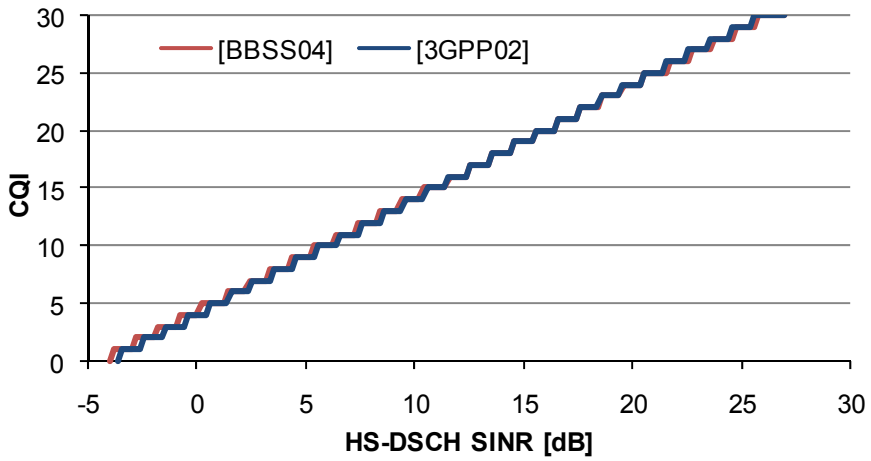

Figure 3.2. CQI as a function of HS-DSCH SINR.

For CQI definition, the UE reports the highest tabulated CQI value for which a single HS-DSCH sub-frame formatted with the TBS, number of HS-PDSCH codes and modulation corresponding to the reported or lower CQI value could be received with a BLER not exceeding 10% [3GPP09c]. The CQI mapping tables for MT categories 8 and 14 are presented in Table 3.1 and Table 3.2, respectively. These tables define the TBS, number of codes and modulation that the MT should use for each CQI and are used as a theoretical model throughout this thesis. The HS-DSCH throughput using these UEs is approximated by dividing the TBS by TTI length (2 ms) and considering 16.7% for the necessary overheads – 6.7% due to the RLC and MAC layers and 10% for BLER and application [Lope08].

BLER is defined as the ratio of the number of erroneous blocks received to the total number of blocks sent. An erroneous block is defined as a transport block, the cyclic redundancy check (CRC) of which is wrong [3GPP09d]. HS-DSCH BLER can analytically be well approximated by [BBSS04]:

$$\eta_{BLER} = \left[10^{\left(\frac{2^{\rho_{IN[dB]} - 1.03 \cdot \Omega + 5.26}}{\sqrt{3} - \log(\Omega)} \right)} + 1 \right]^{-1/0.7} \tag{3.8}$$

where:

- η_{BLER} is the HS-DSCH BLER.

BLER on the HS-DSCH is illustrated in Figure 3.3 as a function of SINR for six different values of CQI, from 5 to 30. One can observe a trend to a decrease of BLER with the increase of SINR for all CQI values. Note that the higher the SINR the greater the obtained CQI, given (3.6). Consequently, the SINR needed to achieve BLER less than 10% increases when one considers higher CQIs.

Table 3.1. CQI mapping table for MT category 8 (adapted from [3GPP09c]).

CQI value	Transport Block Size [bits]	Number of HS-PDSCH Codes	Modulation
1	137	1	QPSK
2	173		
3	233		
4	317		
5	377		
6	461		
7	650	2	
8	792		
9	931		
10	1262	3	
11	1483		
12	1742		
13	2279	4	
14	2583		
15	3319	5	
16	3565		16QAM
17	4189		
18	4664		
19	5287		
20	5887		
21	6554		
22	7168		
23	9719	7	
24	11418	8	
25	14411	10	
26	14411		
27	14411		
28	14411		
29	14411		
30	14411		

Table 3.2. CQI mapping table for MT category 14 (adapted from [3GPP09c]).

CQI value	Transport Block Size [bits]	Number of HS-PDSCH Codes	Modulation
1	136	1	QPSK
2	176		
3	232		
4	320		
5	376		
6	464		
7	648	2	
8	792		
9	928		
10	1264	3	
11	1488		
12	1744		
13	2288	4	
14	2592		
15	3328	5	
16	3576		16QAM
17	4200		
18	4672		
19	5296		
20	5896		
21	6568		
22	7184		
23	9736	7	
24	11432	8	
25	14424	10	
26	15776		64QAM
27	21768	12	
28	26504	13	
29	32264	14	
30	38576	15	

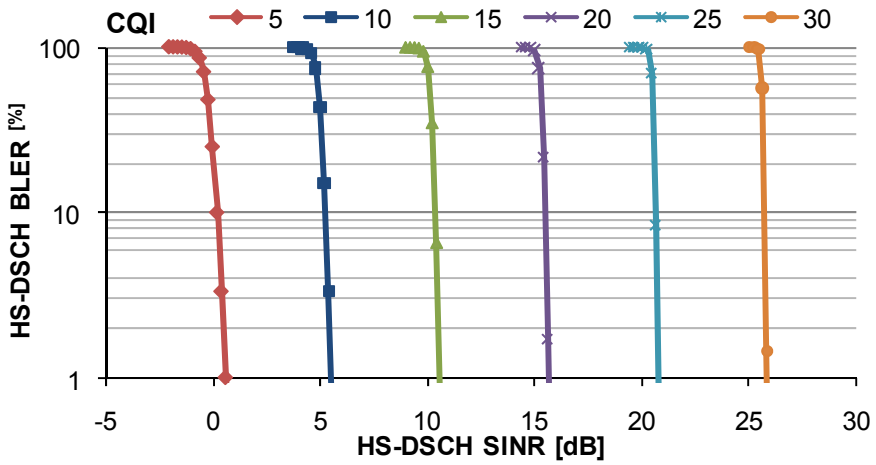

Figure 3.3. BLER as a function of SINR on HS-DSCH, considering different CQI values.

3.2 HSPA+ UL

As stated earlier, the performance metric used in HSPA+ UL is E-DCH E_c/N_0. Physical throughput as a function of E_c/N_0 is given by (3.9) and (3.10), considering TTIs of 10 and 2 ms, respectively, and the usage of QPSK [Preg08]. E-DCH throughput is obtained considering MAC and RLC overheads of 5.1% and BLER and application overhead equal to 10% [Lope08].

$$R_{b[\text{Mbps}]} = \begin{cases} 0.055\cdot(E_c/N_{0[\text{dB}]})^2 + 1.405\cdot(E_c/N_{0[\text{dB}]}) + 9.02, -13 \le E_c/N_{0[\text{dB}]} \le -10 \\ 0.0021\cdot(E_c/N_{0[\text{dB}]})^2 + 0.141\cdot(E_c/N_{0[\text{dB}]}) + 1.7137, \ -10 < E_c/N_{0[\text{dB}]} \le -5 \\ -0.0048\cdot(E_c/N_{0[\text{dB}]})^3 - 0.0431\cdot(E_c/N_{0[\text{dB}]})^2 + 0.0841\cdot(E_c/N_{0[\text{dB}]}) + 1.9094, -5 < E_c/N_{0[\text{dB}]} \le 1 \\ 2, \ \ E_c/N_{0[\text{dB}]} > 1 \end{cases} \quad (3.9)$$

$$R_{b[\text{Mbps}]} = \begin{cases} 0.0231\cdot(E_c/N_{0[\text{dB}]})^2 + 0.5778\cdot(E_c/N_{0[\text{dB}]}) + 3.8283, -10 \le E_c/N_{0[\text{dB}]} < -1 \\ -0.05\cdot(E_c/N_{0[\text{dB}]})^2 + 0.31\cdot(E_c/N_{0[\text{dB}]}) + 3.77, \ -1 \le E_c/N_{0[\text{dB}]} < 2 \\ 0.0417\cdot(E_c/N_{0[\text{dB}]})^3 - 0.5429\cdot(E_c/N_{0[\text{dB}]})^2 + 2.5012\cdot(E_c/N_{0[\text{dB}]}) + 1.04, 2 \le E_c/N_{0[\text{dB}]} < 6 \\ 5.7, \ 6 \le E_c/N_{0[\text{dB}]} \le 11 \end{cases} \quad (3.10)$$

In order to obtain E-DCH throughput as a function of CPICH RSCP, it is necessary to relate the latter with E-DCH E_c/N_0. Equation (B.10) gives E_c/N_0 considering the received power in the Node B and total noise power. The Node B received power can be related with RSCP, since the path loss is approximately the same in UL and DL. Nevertheless, one should take the Node B diversity gain and masthead amplifier gain into account, (3.11).

$$P_{BS\,[\mathrm{dBm}]}^{Rx} = P_{pilot\,[\mathrm{dBm}]}^{Rx} + 10 \cdot \log\left(\frac{P_{MT\,[\mathrm{W}]}^{Tx}}{P_{pilot\,[\mathrm{W}]}^{Tx}}\right) + G_{div\,[\mathrm{dB}]} + G_{MHA[\mathrm{dB}]} \tag{3.11}$$

where:

- P_{BS}^{Rx} is the Node B received power;
- P_{MT}^{Tx} is the MT transmit power;
- G_{div} is the diversity gain;
- G_{MHA} is the masthead amplifier gain.

3.3 Assessment

Given the amount of data collected in measurements, parameters such as average and standard deviation are used throughout this thesis, (3.12) and (3.13), respectively.

$$\bar{z} = \frac{\sum_{i=1}^{N_s} z_i}{N_s} \tag{3.12}$$

where:

- z_i is the sample i;
- N_s is the number of samples.

$$\sigma = \sqrt{\frac{1}{N_s}\sum_{i=1}^{N_s}(z_i - \bar{z})^2} \tag{3.13}$$

In order to compare experimental and expected results, one uses the relative mean error and Root Mean Square Error (RMSE), (3.14) and (3.15), respectively. As reference value for the relative mean error, the theoretical value is considered.

$$\bar{e} = \left|\frac{z_r - z_i}{z_r}\right| \tag{3.14}$$

where:

- z_r is the reference value.

$$e_{RMS} = \sqrt{\frac{1}{N_s}\sum_{i=1}^{N_s}(z_r - z_i)^2} \tag{3.15}$$

The correlation factor between two variables *x* and *y* is given by:

$$r^2 = \left[\frac{\sum_{i=1}^{N_s} (x_i - \bar{x}) \cdot (y_i - \bar{y})}{\sqrt{\sum_{i=1}^{N_s} (x_i - \bar{x})^2 \cdot \sum_{i=1}^{N_s} (y_i - \bar{y})^2}} \right]^2 \tag{3.16}$$

Chapter 4

Results Analysis

This chapter presents the results of the HSPA+ measurements that were performed. A description of scenario and configurations is provided followed by the comparison between the collected data and the theoretical models in both DL and UL.

4.1 Measurements Scenario

In this work, there was the possibility of carrying out HSPA+ measurements in a single user scenario, in an Optimus site, using TEMS data collection software [Asco09]. Despite the fact that the MT was inside a car, the environment may be considered indoor, given that the car was always parked during the measurements and, therefore, mobility should not be taken into account. Since there are no retransmissions in User Datagram Protocol (UDP), this transport layer protocol was chosen for the measurements. A PERL script was used to force the continuous transfer of several files for 10 minutes.

The user was in ten locations within the cell radius to obtain results with average CPICH RSCP varying between -110 and -65 dBm, corresponding to distance from Node B to MT between 0.22 and 0.65 km, Figure 4.1. In each location, six measurements were performed in DL and two in UL, resulting in a total of eighty. In DL, one used a category 14 MT and an emulated category 8 MT by imposing the usage of a maximum number of 10 HS-PDSCH codes and modulations QPSK and 16QAM. Both MTs had linear equaliser type-2 receivers. Concerning UL, an MT category 6 was used to measure the performance with both 10 and 2 ms TTIs. Note that at the time of measurements HOM had already been introduced, unlike MIMO.

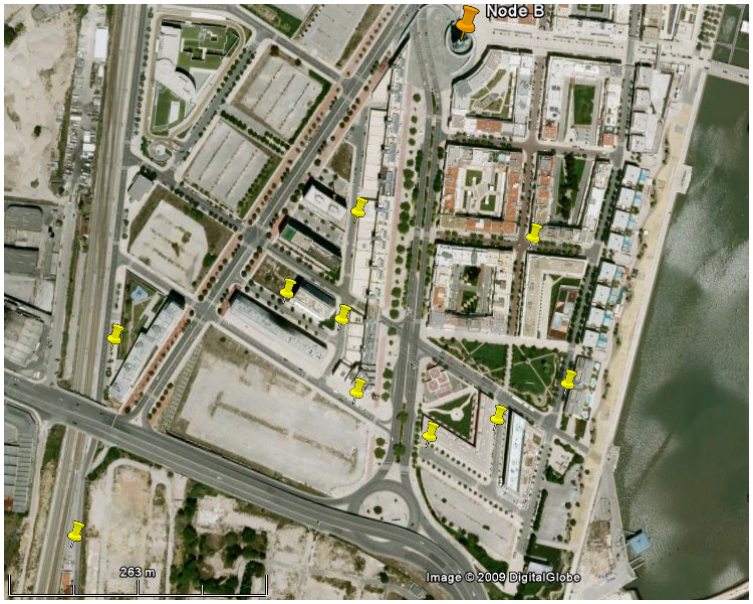

Figure 4.1. Node B and measurements' locations view (extracted from [GoEa09]).

In Table 4.1, one presents the total Node B transmit power, signalling and control power and data power values of the HSPA+ DL measurements configurations, the latter calculated by (3.2). In Table 4.2, one shows the power values and activity factors of common channels for signalling and control, which were CPICH, Broadcast Channel (BCH), Primary-Synchronisation Channel (P-SCH),

Secondary-Synchronisation Channel (S-SCH), HS-SCCH and an A-DCH for the signalling radio bearer [Opti09].

Table 4.1. Power configurations of the HSPA+ DL measurements.

	Power [dBm]		
P_{BS}^{Tx}	45	43	41
$P_{S\&C}$	32.6		
$P_{HS-DSCH}^{Tx}$	44.7	42.6	40.3

Table 4.2. Power values and activity factors of common channels for signalling and control.

Channel	Power [dBm]	Activity Factor [%]
CPICH	29	100
BCH	25.9	90
P-SCH	27.2	10
S-SCH	25.5	10
HS-SCCH	27	100
A-DCH	19	100

The activity factors in Table 4.2 refer to typical values, the one relative to HS-SCCH being traffic dependent [Opti09].

The receiver's noise figure was 6 and 2.5 dB, considering MT and Node B, respectively. In UL, there was no masthead amplifier gain, while the diversity gain was 2 dB.

4.2 HSPA+ DL

In this section, the comparison between the HSPA+ DL measurements results and the theoretical models described in Chapter 3 is presented. The addressed parameters are HS-DSCH throughput, CPICH E_c/N_0, CQI, modulation ratio, number of used HS-PDSCH codes and HS-DSCH BLER. Additional results are shown in Annex C.

4.2.1 HS-DSCH Throughput

The theoretical and experimental HS-DSCH throughputs as a function of CPICH RSCP considering total Node B transmit power of 45 dBm are shown in Figure 4.2. In Figure 4.3 and Figure 4.4, one

presents additional results considering P_{BS}^{Tx} of 43 and 41 dBm, respectively.

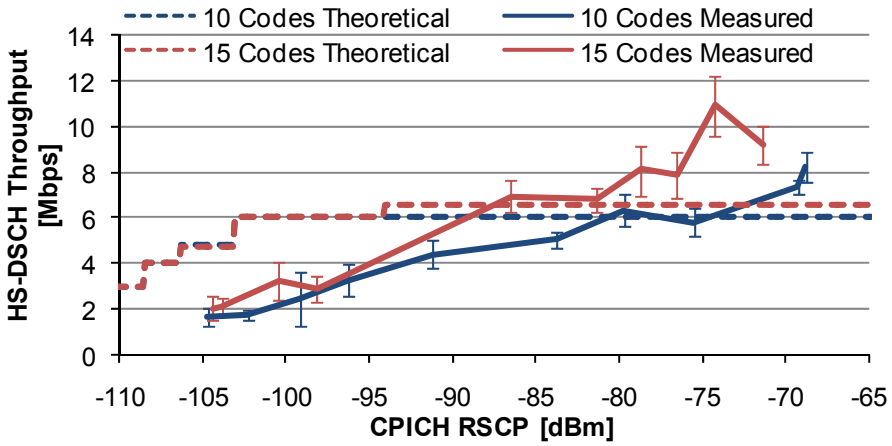

Figure 4.2. Theoretical and measured HS-DSCH throughputs as a function of CPICH RSCP using both MTs, with $P_{BS}^{Tx} = 45\,\text{dBm}$.

Series “10 Codes” and “15 Codes” refer to the category 8 and 14 MT, respectively, corresponding to the maximum number of HS-PDSCH codes used by each terminal. Since the experimental data correspond to average values measured in each of the ten locations, standard deviations are also shown. In Table 4.3, one shows the relative mean error and standard deviation between theoretical and measured curves for the category 14 MT in Figure 4.2. It was necessary to choose the α in (2.5), in order to minimise the relative mean error. Note that the orthogonality factor is not constant during the measurements, depending on the distance from Node B to MT, therefore the relative mean errors are high, the lowest being 36.9% for α equal to 0.9, with a standard deviation of 22.3%. It is also important to mention that for high α values, the error decreases when CPICH RSCP increases, while for low values of α the opposite happens. Regarding the category 8 MT, the value of α that minimises the error is also 0.9, with relative mean error and standard deviation of 35.3% and 24.3%, respectively. In this case, since the MT category was emulated, the performance was better than expected for an actual category 8 MT. It should be reminded that the receiver was an equaliser type-2, which allows greater DL orthogonality factor and, as a result, less intra-cell interference.

Table 4.3. Relative mean error and standard deviation of HS-DSCH throughput as a function of CPICH RSCP for the category 14 MT, with $P_{BS}^{Tx} = 45\,\text{dBm}$, depending on the α.

α	0.1	0.2	0.3	0.4	0.5	0.6	0.7	0.8	**0.9**
$\bar{e}$ [%]	304	244	244	209	175	149	128	72.8	**36.9**
σ [%]	215	183	183	164	142	125	107	50.7	**22.3**

In Figure 4.2, one shows that for CPICH RSCP between -105 and -95 dBm, i.e., under unfavourable radio channel conditions, the measured HS-DSCH throughput was similar for both MT categories, being in the [2, 4] Mbps range, while as RSCP increased the difference between the data rates

increased as well, given the fact that 64QAM is used with high RSCP. The highest achieved data rate was 8.26 and 10.9 Mbps, with mean CPICH RSCP of -74.1 and -74.3 dBm, using 10 and 15 HS-PDSCH codes, respectively. It should be mentioned that the theoretical HS-DSCH throughput reaches its maximum value for CPICH RSCP greater than -60 dBm for both MT categories, being constant for RSCP between -94 and -60 dBm, which denotes that the used models are pessimistic.

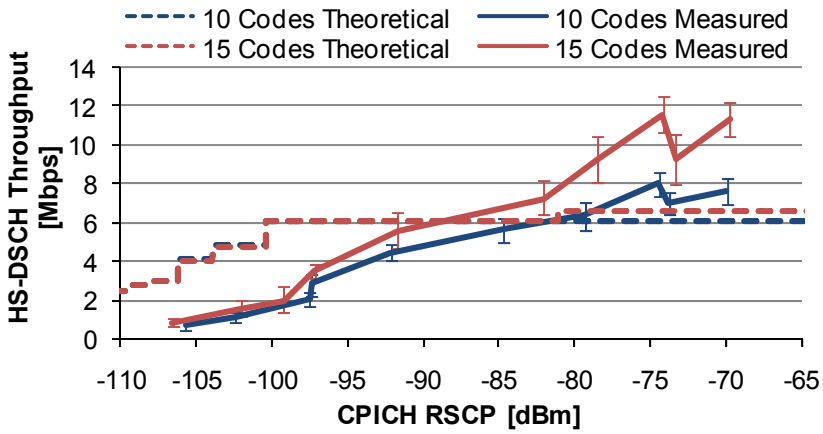

Figure 4.3. Theoretical and measured HS-DSCH throughputs as a function of CPICH RSCP for both MTs, with $P_{BS}^{Tx} = 43\,\text{dBm}$.

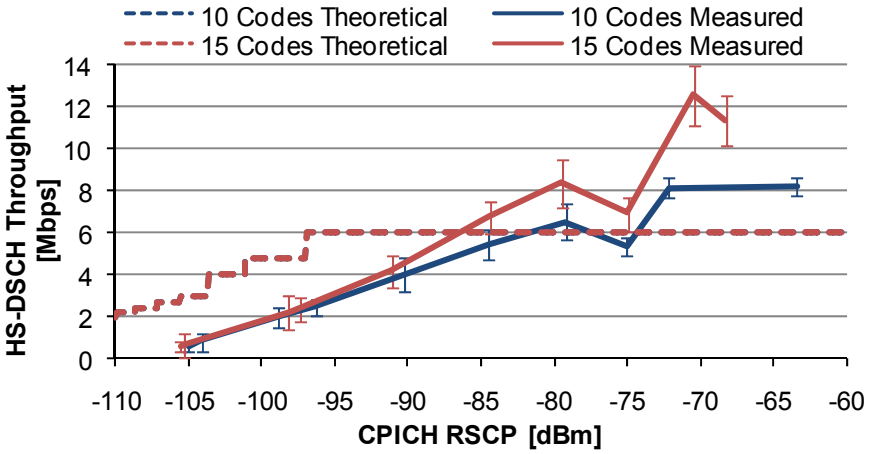

Figure 4.4. Theoretical and measured HS-DSCH throughputs as a function of CPICH RSCP for both MTs, with $P_{BS}^{Tx} = 41\text{dBm}$.

Figure 4.3 and Figure 4.4 exhibit the same trend of Figure 4.2; when there was an increase of RSCP, the average measured throughput increased as well. Once more, the difference between data rates was greater for RSCP higher than -85 dBm, i.e., only under good radio channel conditions the category 14 MT can reach its maximum performance. With P_{BS}^{Tx} of 43 dBm the highest average throughput was 7.9 and 11.6 Mbps, with mean RSCP of -74.4 and -74.2 dBm, using 10 and 15 HS-PDSCH codes, respectively, while considering P_{BS}^{Tx} equal to 41 dBm the average data rate reached 8.23 and 12.6 Mbps, with mean RSCP equal to -63.4 and -70.5 dBm, for category 8 and 14,

correspondingly. The α value chosen was 0.9 for all cases. The relative mean error is 39.4% and 50.7%, with standard deviation of 28.6% and 23.9% for P_{BS}^{Tx} of 43 dBm, using a maximum of 10 and 15 codes, in that order. With P_{BS}^{Tx} equal to 41 dBm, for the category 8 MT the error is 40.5%, with deviation of 26.5%, while for the category 14 MT the error and deviation are 55.6% and 32.6%, respectively.

HS-DSCH throughput as a function of CPICH RSCP for all power configurations in Table 4.1, is presented in Figure 4.5 and Figure 4.6, considering the usage of the category 14 and 8 MT, in that order.

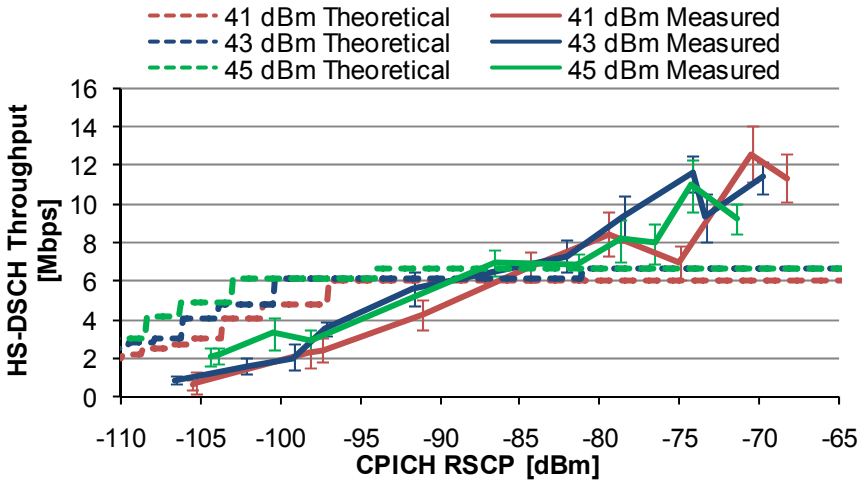

Figure 4.5. Theoretical and measured HS-DSCH throughputs as a function of CPICH RSCP for the category 14 MT, considering different power configurations.

Figure 4.5 shows that the average HS-DSCH throughput, for CPICH RSCP higher than -85 dBm, was in most cases greater with P_{BS}^{Tx} equal to 43 dBm than with 45 dBm, which can be a result of the increase of interference when the power increases. In addition, the maximum average throughput (12.6 Mbps) was achieved with 41 dBm of Node B transmit power.

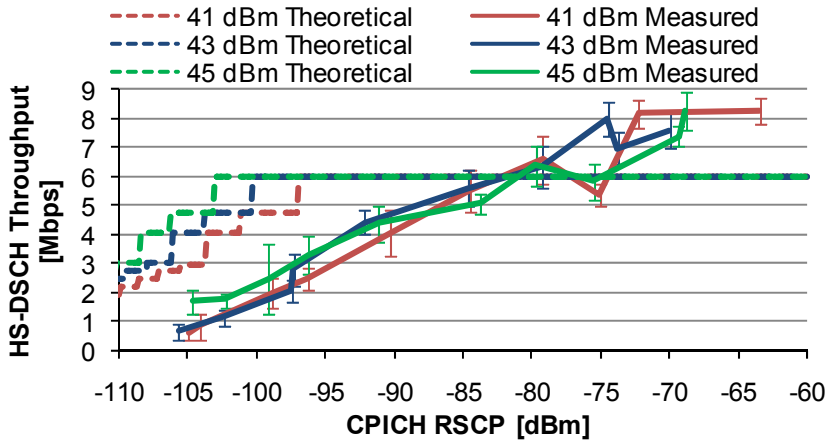

Figure 4.6. Theoretical and measured HS-DSCH throughputs as a function of CPICH RSCP for the category 8 MT, considering different power configurations.

In Figure 4.6, one shows again that the data rates were greater with less available power, in situations with high RSCP. One can conclude that it is only beneficial to have 45 dBm of P_{BS}^{Tx} when the RSCP is low, typically between -110 and -95 dBm.

Since all experimental results are expressed in mean values, it is also useful to present all measured data samples. In Figure 4.7, one shows the HSPA+ DL throughputs (theoretical and experimental) as a function of RSCP on the pilot channel for the category 14 MT, with P_{BS}^{Tx} equal to 45 dBm.

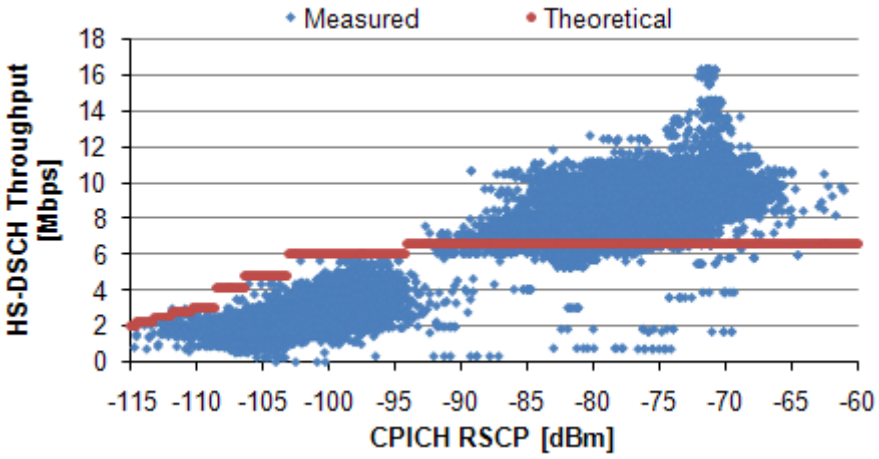

Figure 4.7. HS-DSCH throughput as a function of CPICH RSCP for the category 14 MT with $P_{BS}^{Tx} = 45\,\text{dBm}$, considering all performed measurements.

In Figure 4.7, once more one observes a trend to an increase of the measured data rate with CPICH RSCP, whereas the theoretical throughput is constant for RSCP between -94 and -60 dBm. The latter happens since there is a slight increase of HS-DSCH SINR for these RSCP values, from 21.6 to 21.8 dB with α of 0.9 in (2.5), resulting in a CQI value of 26 considering (3.6), and therefore, in data rate equal to 6.57 Mbps. In addition, it is shown that the measured throughput was, in the majority of samples, greater than the expected one for RSCP higher than -94 dBm, while for RSCP lower than this value the opposite occurs. As a consequence of these discrepancies, one obtained a correlation factor of 0.539 and RMSE of 2.61 Mbps. Table 3.2 is not strictly followed and the orthogonality factor is set to be constant, thus, contributing to the differences obtained between the models and the measurements' results.

It is also interesting to analyse HS-DSCH throughput as a function of CPICH E_c/N_0. The theoretical and measured data using both terminals and considering P_{BS}^{Tx} equal to 45, 43 and 41 dBm are presented, Figure 4.8, Figure 4.9 and Figure 4.10, respectively. Again, it should be noted that the orthogonality factor that provides the lowest relative mean errors is 0.9. In Table 4.4, one exhibits the relative mean errors and standard deviations of these comparisons. With this value of α, the highest CPICH E_c/N_0 value considered in (2.6) is -15.6, -13.6 and -11.6 dB, for available power of 45, 43 and 41 dBm, respectively.

Table 4.4. Relative mean error and standard deviation of HS-DSCH throughput as a function of CPICH E_c/N_0 with α = 0.9, considering different configurations.

P_{BS}^{Tx} [dBm]	45		43		41	
MT Category	8	14	8	14	8	14
$\bar{e}$ [%]	17.6	26.9	27.1	51.9	40.5	38.8
σ [%]	14.4	23.3	46.2	53.8	26.5	39.9

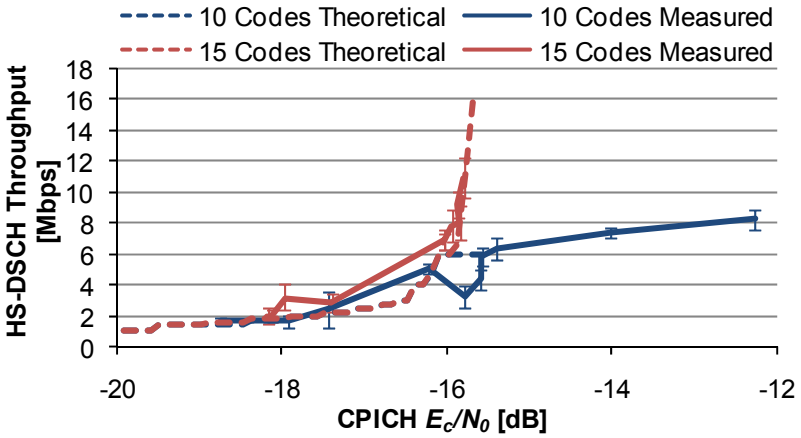

Figure 4.8. Theoretical and measured HS-DSCH throughputs as a function of CPICH E_c/N_0 using both MTs, with $P_{BS}^{Tx} = 45\,\text{dBm}$.

In Figure 4.8, a trend to an increase of data rate with CPICH E_c/N_0 is visible. According to the model, with an E_c/N_0 lower than -16 dB, the throughput should be approximately the same for both MTs, whereas the experimental data show greater average throughput using the category 14 MT, for all E_c/N_0 values. The highest mean throughput was achieved with average E_c/N_0 equal to -12.3 and -15.8 dB, in the measurements with 10 and 15 HS-PDSCH codes, respectively.

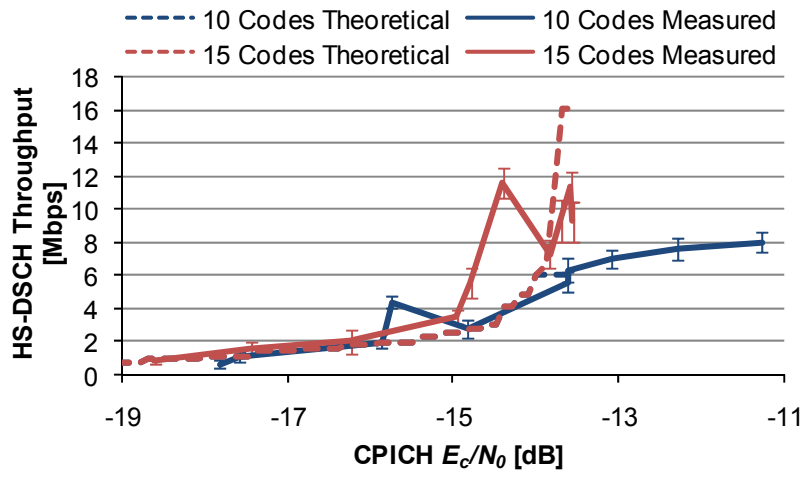

Figure 4.9. Theoretical and measured HS-DSCH throughputs as a function of CPICH E_c/N_0 for both MTs, with $P_{BS}^{Tx} = 43\,\text{dBm}$.

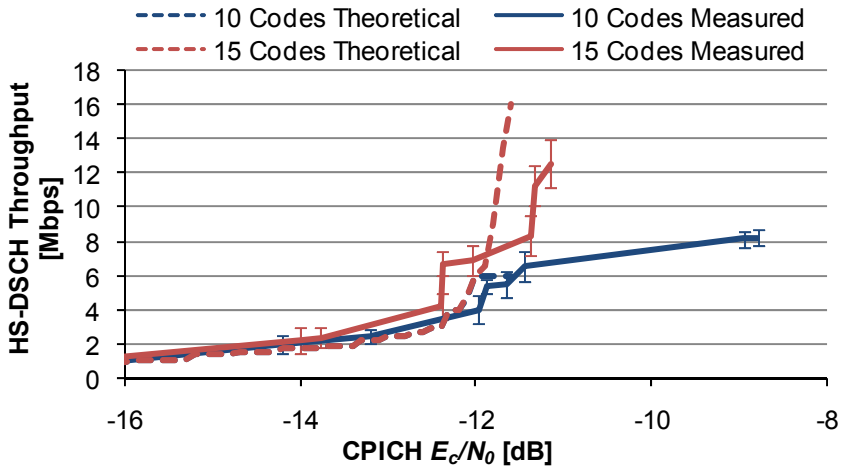

Figure 4.10. Theoretical and measured HS-DSCH throughputs as a function of CPICH E_c/N_0 for both MTs, with $P_{BS}^{Tx} = 41\text{dBm}$.

In Figure 4.9 and Figure 4.10, one can observe the same trend shown in Figure 4.8. The average data rate was approximately equal with both MTs for E_c/N_0 lower than -16 and -13 dB, considering 43 and 41 dBm, respectively. With 43 dBm of P_{BS}^{Tx}, the measured curves present better performance than expected for CPICH E_c/N_0 values lower than -14 dB, whereas the same happens with 41 dBm for E_c/N_0 values lower than -12 dB. Still, it is noticeable that every measured data rate was on average significantly lower than the theoretical peak. The highest mean throughputs with P_{BS}^{Tx} equal to 43 dBm were obtained for average E_c/N_0 equal to -11.3 and -14.4 dB, while for the 41 dBm setting, the greatest data rates presented earlier were achieved with -8.80 and -11.2 dB of E_c/N_0, considering the category 8 and 14 MT, respectively.

Figure 4.11 and Figure 4.12 present the HSPA+ DL throughputs (expected and experimental) as a function of the pilot E_c/N_0 for all power configurations chosen for the measurements, considering the usage of the category 14 and 8 MT, in that order.

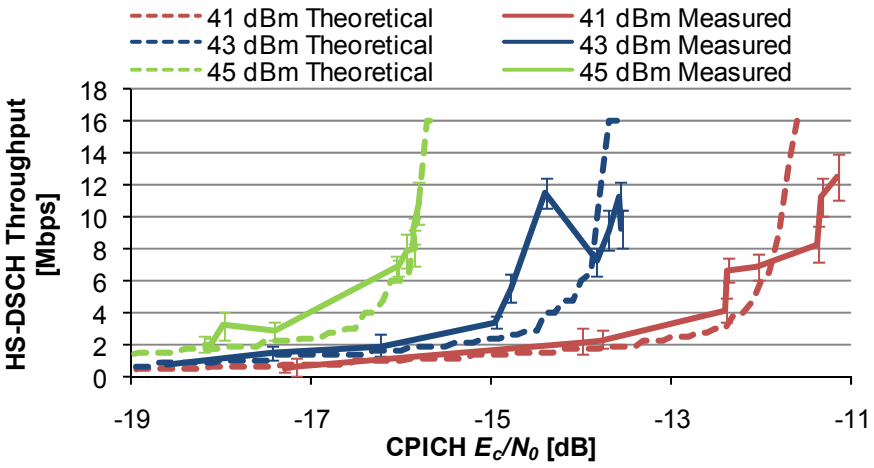

Figure 4.11. Theoretical and measured HS-DSCH throughputs as a function of CPICH E_c/N_0 for the category 14 MT, considering different power configurations.

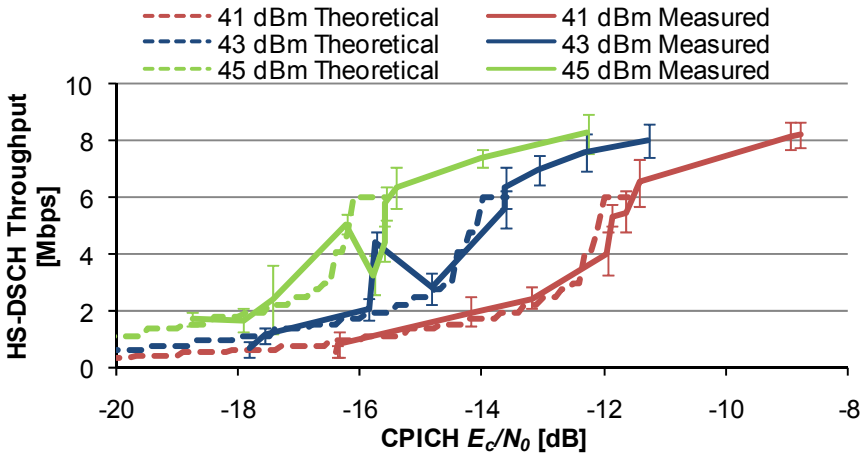

Figure 4.12. Theoretical and measured HS-DSCH throughputs as a function of CPICH E_c/N_0 for the category 8 MT, considering different power configurations.

Figure 4.11 and Figure 4.12 show that the model fits better for the setting with 45 dBm of P_{BS}^{Tx}, which is reflected in the results of Table 4.4. In Figure 4.11, the relative mean error is 26.9% for the configuration with 45 dBm, being 51.9% and 38.8% with 43 and 41 dBm, respectively. Using the category 8 MT, the errors are 17.6%, 27.1% and 40.5%, in the same order. It is visible that the higher the available power, the lower the measured and theoretical CPICH E_c/N_0. Subsection 4.2.2 addresses this parameter as a function of CPICH RSCP.

Taking all measured results into account, HS-DSCH throughputs (theoretical and experimental) as a function of CPICH E_c/N_0 for the category 14 MT with P_{BS}^{Tx} equal to 45 dBm are presented, Figure 4.13.

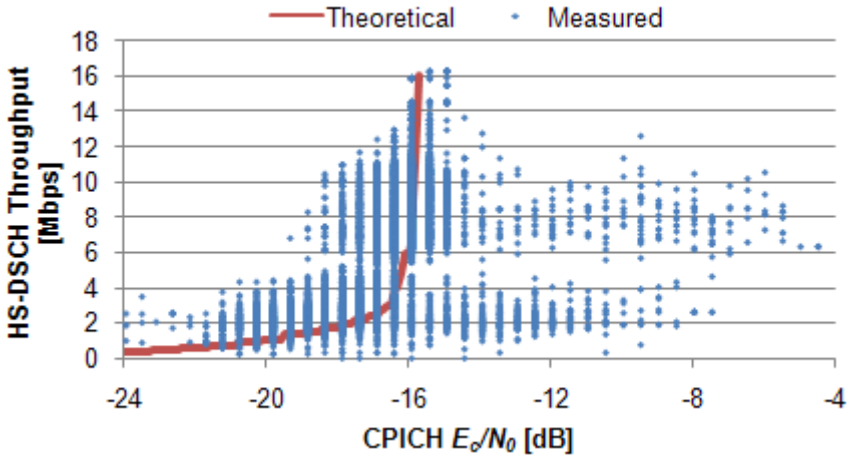

Figure 4.13. HS-DSCH throughput as a function of CPICH E_c/N_0 for the category 14 MT with $P_{BS}^{Tx} = 45\,\text{dBm}$, considering all performed measurements.

As shown in Figure 4.13, measured E_c/N_0 varied between -24 and -4.5 dB. The maximum theoretical value of this parameter, for the chosen α of 0.9, is -15.6 dB, as stated earlier. This is a clear indication that the orthogonality factor was not constant during the measurements. Note that the theoretical model defines a trend to an increase of the throughput with CPICH E_c/N_0 while the greatest measured

throughput was achieved for E_c/N_0 approximately -16 dB. For E_c/N_0 values higher than -15 dB (with lower orthogonality factor) the measured throughput shows a tendency to decrease. It is also observable that, in most cases, the experimental data rate was greater than expected, denoting the differences between Table 3.2 and the implemented models. Consequently, a correlation factor of 0.528 and RMSE of 2.91 Mbps are obtained.

Figure 4.14 illustrates the measured and theoretical HS-DSCH throughputs as a function of CQI for both MTs with total transmit power of 45 dBm. The relative mean error is 50.9% and 95.3%, with standard deviation of 27.4% and 29.2%, whether the maximum number of HS-PDSCH codes used is 10 or 15, respectively. Additional results concerning the remaining power configurations are presented, Figure 4.15 and Figure 4.16.

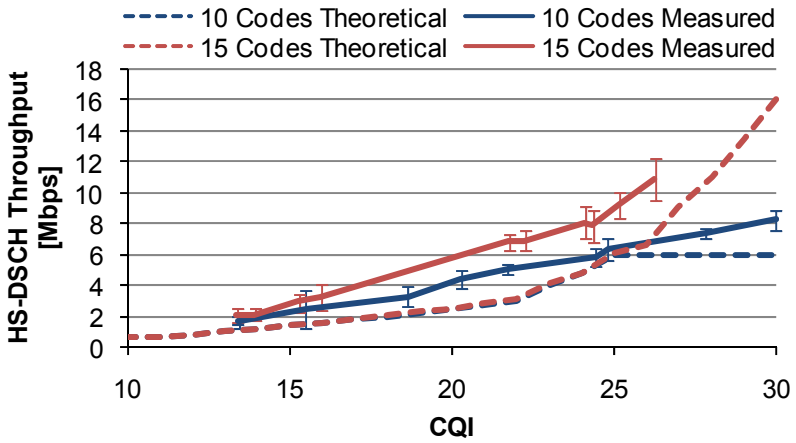

Figure 4.14. Theoretical and measured HS-DSCH throughputs as a function of CQI for both MTs, with $P_{BS}^{Tx} = 45\,\text{dBm}$.

CQI mapping tables are indicative and, as a result, the algorithms implemented by the manufacturer can be quite different from the standard. For instance, Table 3.2 shows that for a CQI value of 17 (TBS is 4200 bits) the number of codes used should be 5, while the actual number can even be 15, depending on the algorithm. According to the mapping tables, the maximum number of HS-PDSCH codes should only be used for CQI greater than 24 for category 8 MT, and equal to 30 when a category 14 terminal is being used. The number of codes used during the measurements is addressed in subsection 4.2.5. Moreover, the used category 8 MT was not authentic, so the experimental performance surpassed the theoretical one. As mentioned before, all experimental results are expressed in mean values and one should also take the standard deviations into account. These issues may explain the discrepancies between experimental and theoretical results.

Figure 4.15 and Figure 4.16 also show that the average throughputs were greater than expected in the configurations with 43 and 41 dBm of P_{BS}^{Tx}, for the same reasons pointed out earlier. The relative mean error is 60.8% and 89.6%, with standard deviations of 38.1% and 40.9%, considering the category 8 and 14 MT, respectively, for the 43 dBm configuration. Results with 41 dBm of available power have a relative mean error of 62.4% and 86.4%, with deviation equal to 21.4% and 31.6%, with

maximum usage of 10 and 15 codes, respectively. These values represent the high divergence between the models in Table 3.1 and Table 3.2 and the experimental data.

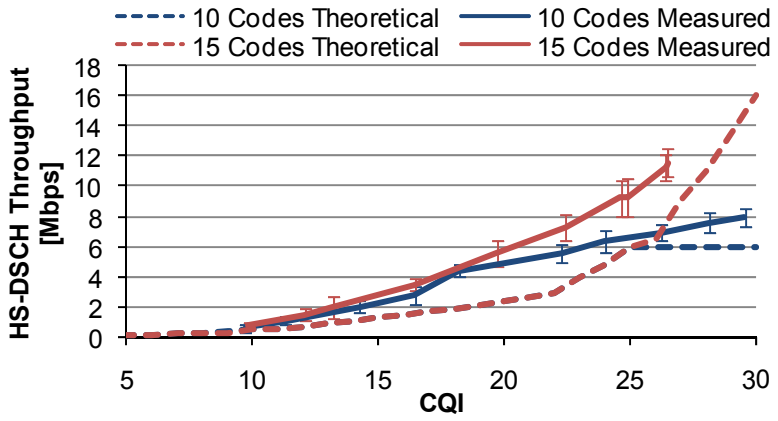

Figure 4.15. Theoretical and measured HS-DSCH throughputs as a function of CQI for both MTs, with $P_{BS}^{Tx} = 43\,\text{dBm}$.

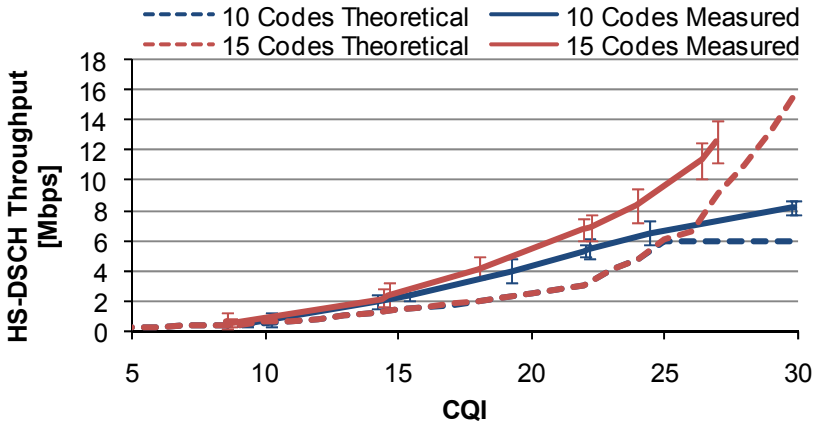

Figure 4.16. Theoretical and measured HS-DSCH throughputs as a function of CQI for both MTs, with $P_{BS}^{Tx} = 41\text{dBm}$.

The HSPA+ DL throughput as a function of CQI considering all power configurations, for the category 14 device, is shown in Figure 4.17. Figure 4.18 presents the results using the category 8 MT. One can see that the achieved throughput was similar for all power settings (being higher than the theoretical), given the same CQI. This is expected since the model is independent of the available power.

In Figure 4.19, one shows the HS-DSCH throughputs (theoretical and experimental) as a function of CQI for the category 14 MT, with P_{BS}^{Tx} equal to 45 dBm, taking all measured results into consideration. One can observe a trend to an increase of the measured HS-DSCH throughput with CQI, as predicted in the model, resulting in a correlation factor of 0.772. However, as expected from the analysis with mean values, the measured throughput was, most of time, higher than the experimental one, the RMSE being 2.91 Mbps. It is shown that the manufacturer did not take the CQI mapping tables into account, which leads to the errors obtained in the comparisons that use Table 3.1 and Table 3.2 as

theoretical models.

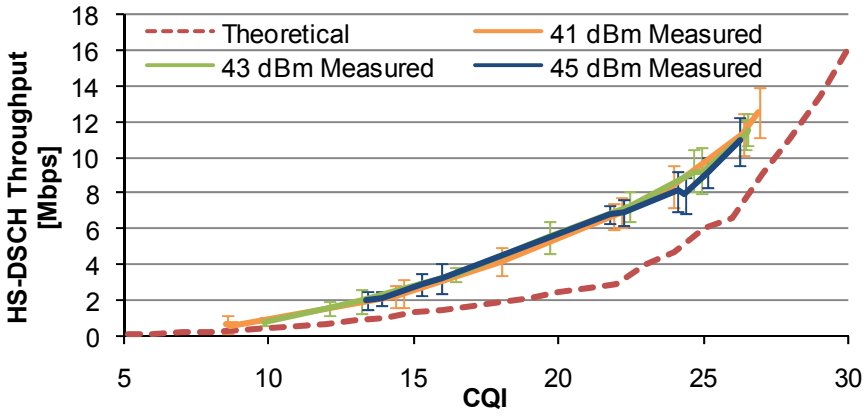

Figure 4.17. Theoretical and measured HS-DSCH throughputs as a function of CQI for the category 14 MT, considering different power configurations.

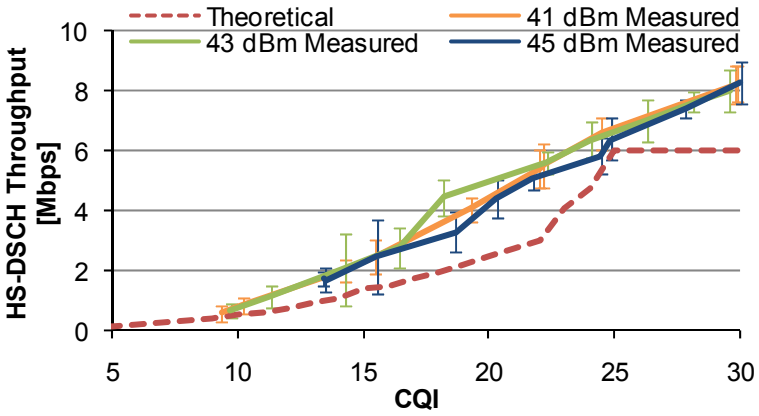

Figure 4.18. Theoretical and measured HS-DSCH throughputs as a function of CQI for the category 8 MT, considering different power configurations.

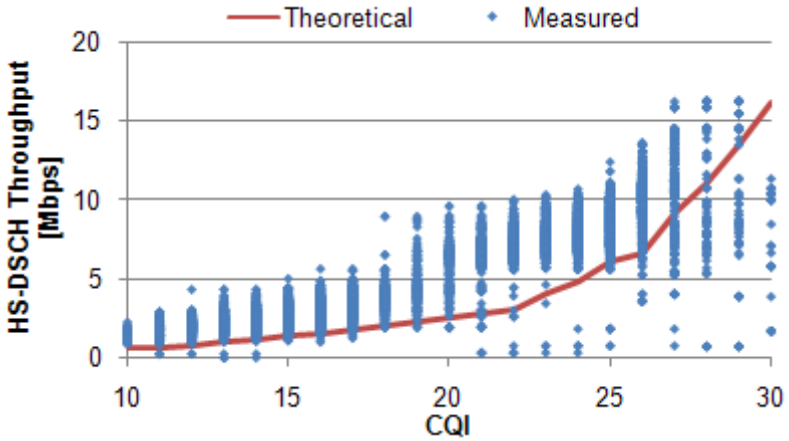

Figure 4.19. HS-DSCH throughput as a function of CQI for the category 14 MT with $P_{BS}^{Tx} = 45\,\text{dBm}$, considering all measured data.

Concluding, the differences between theory and practice are due to the implementation of algorithms

that do not follow the CQI mapping tables, together with the use of an emulated 8th category MT and the choice of fixed orthogonality factors. In addition, note that the maximum throughput measured was 16.3 and 12.6 Mbps with the category 14 MT, considering instantaneous and mean value, respectively.

4.2.2 CPICH E_c/N_0

Equation (3.3) gives CPICH E_c/N_0 as a function of CPICH RSCP. The theoretical and experimental data for this relation considering a maximum usage of 15 HS-PDSCH codes and all power configurations are presented, Figure 4.20. In Figure 4.21, one shows the results for the category 8 MT.

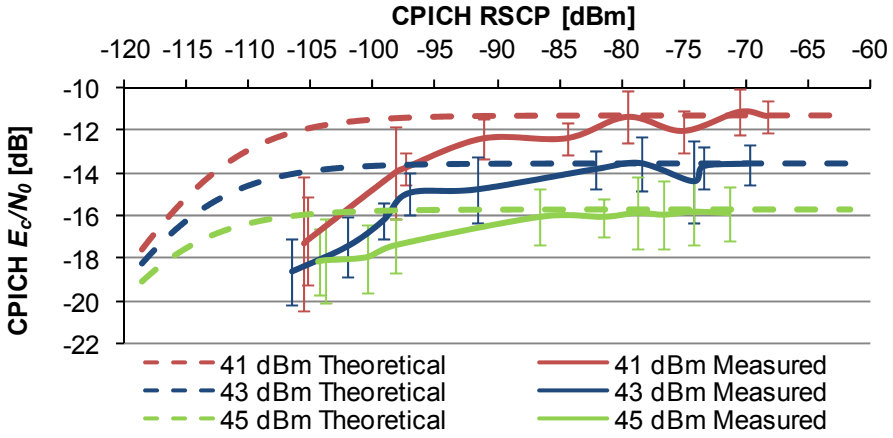

Figure 4.20. Theoretical and measured CPICH E_c/N_0 as a function of CPICH RSCP for the category 14 MT, considering different power configurations.

In Figure 4.20, one shows that the greater the available power, the lower the achieved CPICH E_c/N_0. Still, with poor channel quality, e.g., for an RSCP of -105 dBm, the differences between the obtained E_c/N_0 values were smaller than for higher RSCP. The highest average E_c/N_0 measured was -15.7, -13.6 and -11.2 dB, considering P_{BS}^{Tx} equal to 45, 43 and 41 dBm, respectively. These results can be explained with the trend to an increase of interference with power, which leads to a decrease of E_c/N_0, as the model forecasts. In theory, one should obtain the maximum CPICH E_c/N_0 for an RSCP near -100 dBm, whereas the experimental E_c/N_0 saturated for RSCP between -90 and -80 dBm, resulting in greater relative errors for low RSCP values.

In Figure 4.21, it is noticeable that the average CPICH E_c/N_0 exceeded the theoretical maximum for high RSCP. In fact, the greatest measured E_c/N_0 was -12.3, -11.3 and -8.80 dB, considering P_{BS}^{Tx} equal to 45, 43 and 41 dBm, respectively. Again, the differences between the measured E_c/N_0 present a trend to increase with RSCP.

Table 4.5 contains the relative mean error and standard deviation between the theoretical and the measured data. Note that the configuration with the highest available power and 15 HS-PDSCH codes usage has the lowest error, which is 6.13%. Moreover, all errors are lower than 20%, indicating a good

approximation between results.

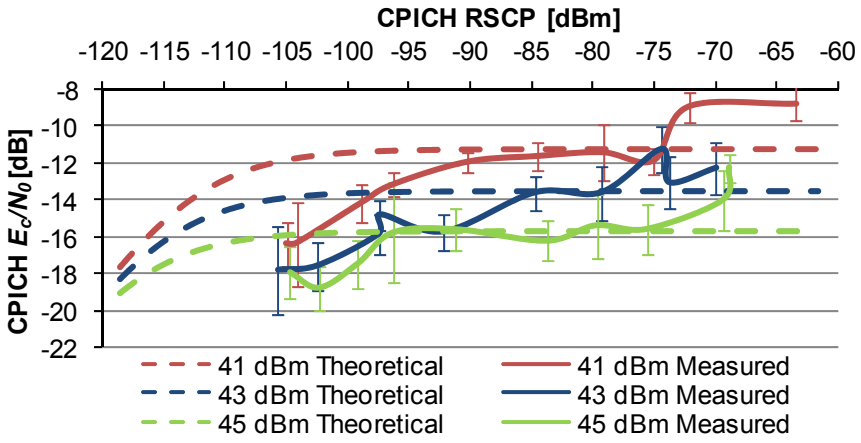

Figure 4.21. Theoretical and measured CPICH E_c/N_0 as a function of CPICH RSCP for the category 8 MT, considering different power configurations.

Table 4.5. Relative mean error and standard deviation of CPICH E_c/N_0 as a function of CPICH RSCP considering different configurations.

P_{BS}^{Tx} [dBm]	45		43		41	
MT Category	8	14	8	14	8	14
$\bar{e}$ [%]	8.14	6.13	12.7	18.5	17.5	16.1
σ [%]	7.89	6.22	10.1	9.89	13.8	16.8

E_c/N_0 as a function of RSCP on the pilot channel for the category 14 MT with P_{BS}^{Tx} equal to 45 dBm is presented, considering all measured samples and the theoretical model, Figure 4.22.

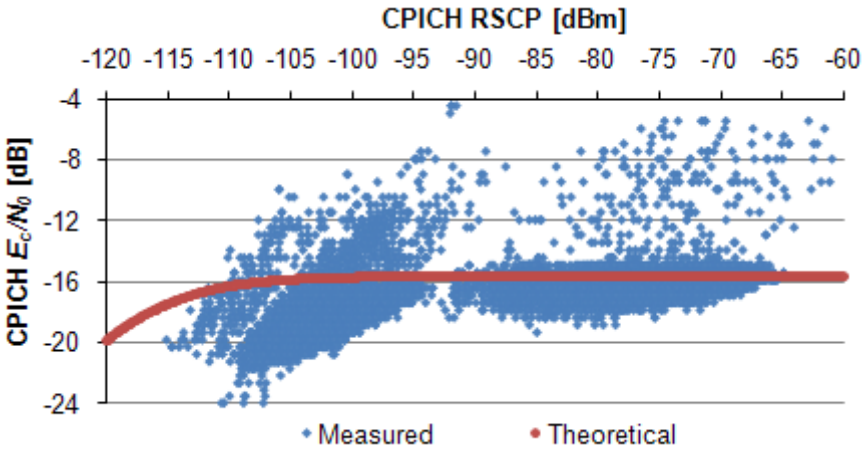

Figure 4.22. CPICH E_c/N_0 as a function of CPICH RSCP for the category 14 MT with $P_{BS}^{Tx} = 45$ dBm, considering all measured data.

As expected, given the analysis with average values, it is noticeable that the experimental E_c/N_0 was lower than the theoretical one for CPICH RSCP lower than -90 dBm, considering the majority of the

collected samples. In addition, E_c/N_0 exceeded the theoretical maximum of -15.7 dB in several occasions. As a result, one obtains an RMSE of 1.98 dB. The correlation factor is 0.544, since the measured CPICH E_c/N_0 did not always follow the theoretical trend.

It is also interesting to analyse how HSPA+ DL activity affected CPICH E_c/N_0, i.e., what was, considering the same RSCP, the degradation of E_c/N_0 between situations without and with load. In Figure 4.23, one presents this analysis using the category 14 MT with 45 dBm of available power.

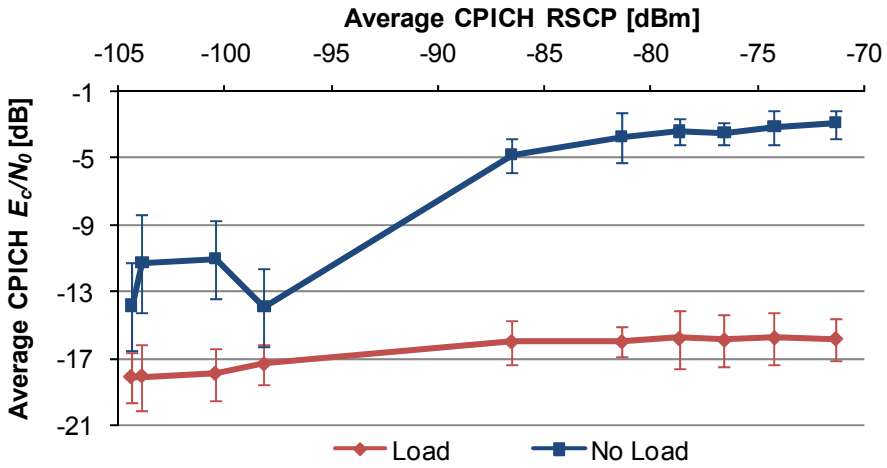

Figure 4.23. Measured CPICH E_c/N_0 as a function of CPICH RSCP using the category 14 MT with $P_{BS}^{Tx} = 45$ dBm, considering situations with and without HSPA+ DL activity.

Results denote that the difference between E_c/N_0 values increased as the path loss decreased, i.e., when there was an increase of the RSCP. In fact, while data were being transmitted the average CPICH E_c/N_0 saturated for RSCP around -88 dBm and did not exceed -15.8 dB. On the contrary, the mean E_c/N_0 without HSPA+ DL activity reached a maximum of -2.96 dB with an average RSCP equal to -71.4 dBm. In summary, E_c/N_0 degradation varied between 3.47 and 12.9 dB, with average value of 9.52 dB and standard deviation of 3.75 dB.

To sum up, one can conclude that the average measured E_c/N_0 was close to expected, considering the model in (3.3). Still, a correlation factor of 0.544 and RMSE of 1.98 dB are achieved, taking all experimental values into account.

4.2.3 CQI

As mentioned earlier, CQI can be expressed as a function of CPICH E_c/N_0 using (2.6) and (3.6). The theoretical and measured data considering 45 dBm of total transmit power are shown for both terminals, Figure 4.24. When the 15 HS-PDSCH codes were used, the highest CQI measured was 26, with -15.8 dB of E_c/N_0, while for 10 codes the maximum CQI was 30 when E_c/N_0 reached -12.3 dB. One can see a tendency to an increase of theoretical and measured CQIs with CPICH E_c/N_0, given the increase of HS-DSCH SINR.

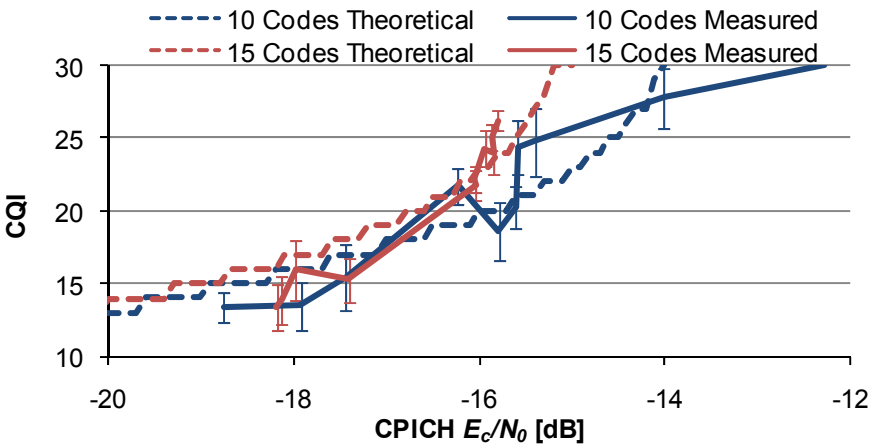

Figure 4.24. Theoretical and measured CQIs as a function of CPICH E_c/N_0 for both MTs, with $P_{BS}^{Tx} = 45\,\text{dBm}$.

In Table 4.6, one shows the relative mean error and standard deviation between the theoretical and measured curves for the category 14 MT in Figure 4.24, considering different values of orthogonality factor. The lowest relative mean error is 8.92% with 5.84% of standard deviation, for α equal to 0.8. Concerning the MT that uses a maximum of 10 HS-PDSCH codes, the α chosen was 0.6, resulting in 11.3% and 5.05% of relative mean error and standard deviation, respectively. As stated before, the orthogonality factor depends on the distance, so when it is assumed a fixed α the errors are inevitable. Nevertheless, the results show that the use of these theoretical models is appropriate.

Table 4.6. Relative mean error and standard deviation of CQI as a function of CPICH E_c/N_0 for the category 14 MT, with $P_{BS}^{Tx} = 45\,\text{dBm}$, depending on the α.

α	0.1	0.2	0.3	0.4	0.5	0.6	0.7	**0.8**	0.9
$\bar{e}$ [%]	31.9	26.7	26.4	22.8	18.6	16.5	11.9	**8.92**	11.2
σ [%]	24.6	20.2	18.2	15.2	11.9	8.81	6.72	**5.84**	6.45

In Figure 4.25 and Figure 4.26, one shows the results for both MTs, considering P_{BS}^{Tx} equal to 43 and 41 dBm, respectively.

In the measurements with the maximum usage of 10 HS-PDSCH codes the highest CQI was 30 for E_c/N_0 of -11.3 and -8.80 dB, with 43 and 41 dBm of P_{BS}^{Tx}, respectively, while using 15 codes the greatest CQI was 27 for -14.4 and -11.2 dB of E_c/N_0, in the same order. The orthogonality factors considered in Figure 4.25 and Figure 4.26 were 0.7 and 0.8, for the category 8 and 14 MT, respectively. One can see that the experimental CQI followed the theoretical trend. With 43 dBm of P_{BS}^{Tx} the relative mean error is 9.74% and 11.4%, with 8.37% and 9.08% of standard deviation, for the category 8 and 14, correspondingly, while for 41 dBm the error is 9.06% and 10.1%, with deviation of 6.86% and 6.46%, in the same order. These results are representative of the minor discrepancies between theoretical and measured data.

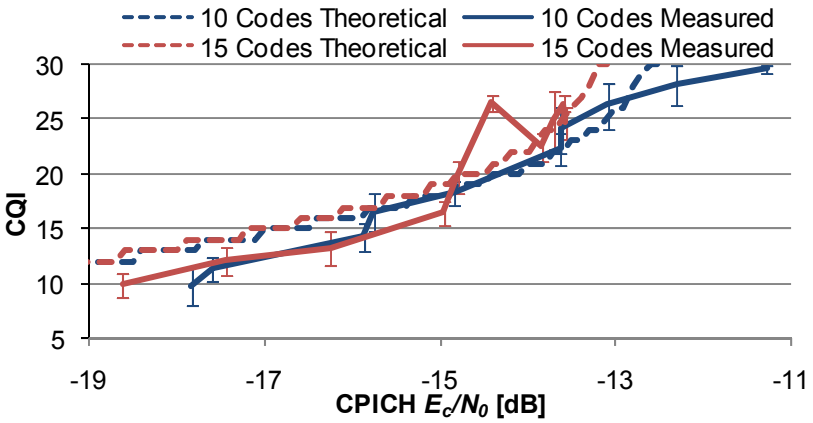

Figure 4.25. Theoretical and measured CQIs as a function of CPICH E_c/N_0 for both MTs, with $P_{BS}^{Tx} = 43\,\text{dBm}$.

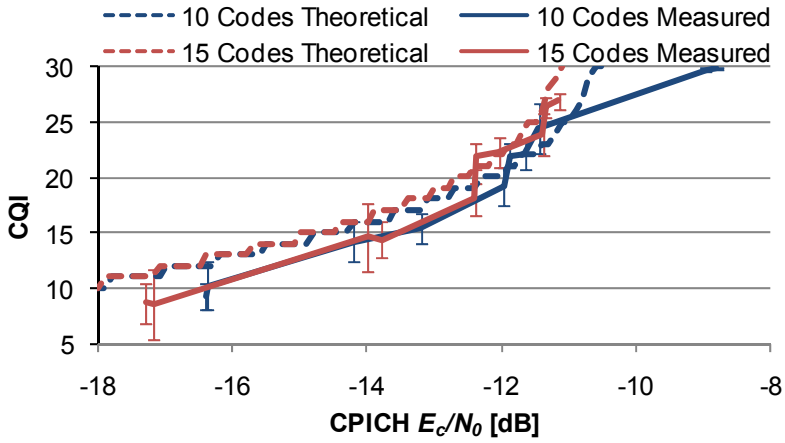

Figure 4.26. Theoretical and measured CQIs as a function of CPICH E_c/N_0 for both MTs, with $P_{BS}^{Tx} = 41\,\text{dBm}$.

CQI versus CPICH E_c/N_0 for the category 14 MT considering different power configurations, is shown in Figure 4.27. In Figure 4.28, one presents the results for the category 8 MT.

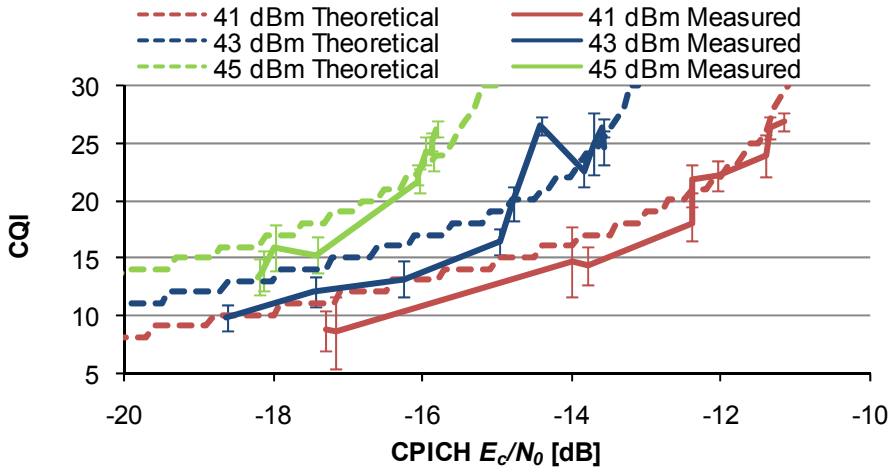

Figure 4.27. Theoretical and measured CQIs as a function of CPICH E_c/N_0 for the category 14 MT, considering different power configurations.

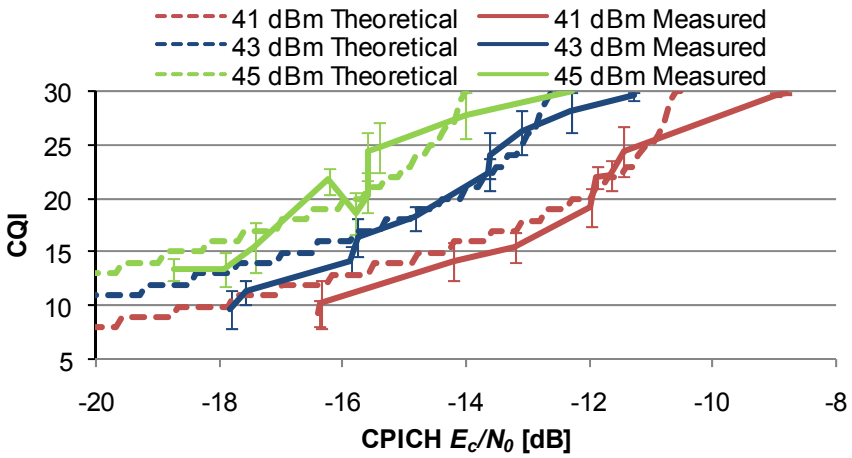

Figure 4.28. Theoretical and measured CQIs as a function of CPICH E_c/N_0 for the category 8 MT, considering different power configurations.

Figure 4.27 and Figure 4.28 show that for a given CPICH E_c/N_0, the higher the available power, the greater the achieved CQI. As shown in the previous subsection, E_c/N_0 increases with P_{BS}^{Tx}, which means that the CQIs were reached with higher E_c/N_0 when lesser power was available.

In Figure 4.29, one presents CQI as a function of CPICH E_c/N_0, considering all experimental samples and theoretical data, for the terminal of 14th category and 45 dBm of P_{BS}^{Tx}.

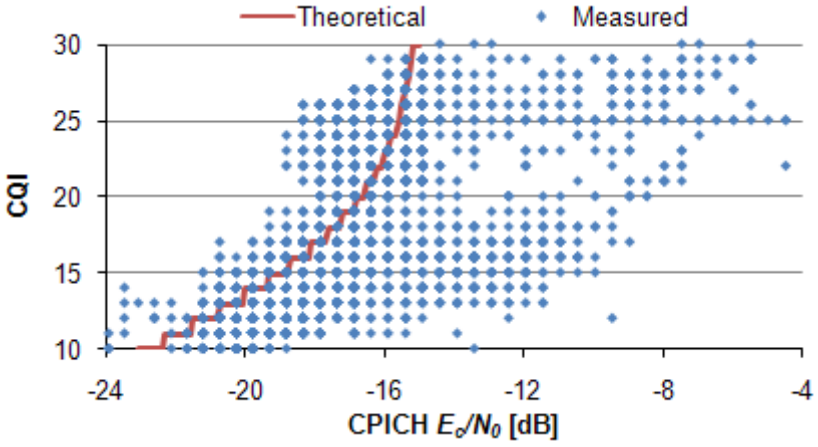

Figure 4.29. CQI as a function of CPICH E_c/N_0 for the category 14 MT with $P_{BS}^{Tx} = 45$ dBm, considering all measured data.

Again, one observes a trend to an increase of CQI with CPICH E_c/N_0, both in theory and in practice. This is reflected in the correlation factor, which is 0.639. It is noticeable that, in the great majority of cases, E_c/N_0 did not exceed the maximum theoretical value (-15 dB), being the orthogonality factor 0.8. Still, results indicate that α was varying during the measurements. First, measured CQI presents a significant variation for any given E_c/N_0, resulting in an RMSE of 3. Additionally, CPICH E_c/N_0 reached values that are only specified with lower orthogonality factor values in (2.6).

In conclusion, it was noticeable that the measured CQI increased with CPICH E_c/N_0, which is an expected behaviour, given the theoretical models. Furthermore, the obtained errors represent the minor deviations between theory and practice, even considering constant orthogonality factors.

4.2.4 Modulation Ratio

The theoretical models used in this subsection are extracted from Table 3.1 and Table 3.2. Since the models define which modulation should be used for each reported CQI, in theory the ratio is 100% or 0%, whether the modulation is used or not. Conversely, the measured data consist of average usage ratios for each modulation, i.e., the percentage of time in which QPSK, 16QAM or 64QAM were used. Both the theoretical and experimental modulation ratios as a function of CQI with P_{BS}^{Tx} equal to 45 dBm considering MT categories 8 and 14 are shown, Figure 4.30 and Figure 4.31, respectively.

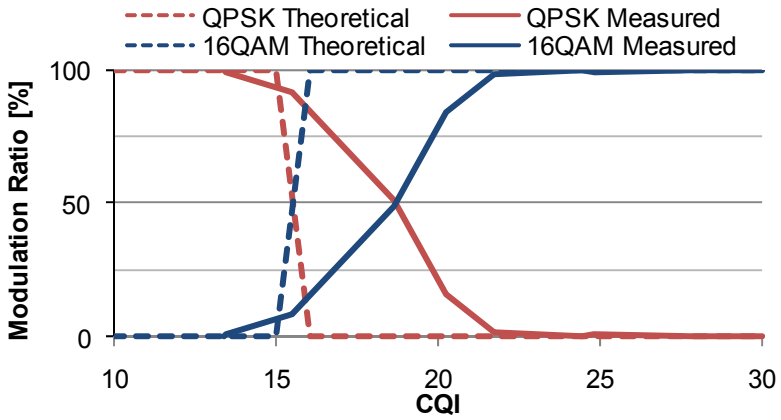

Figure 4.30. Theoretical and measured modulation ratios as a function of CQI with $P_{BS}^{Tx} = 45$ dBm, using the category 8 MT.

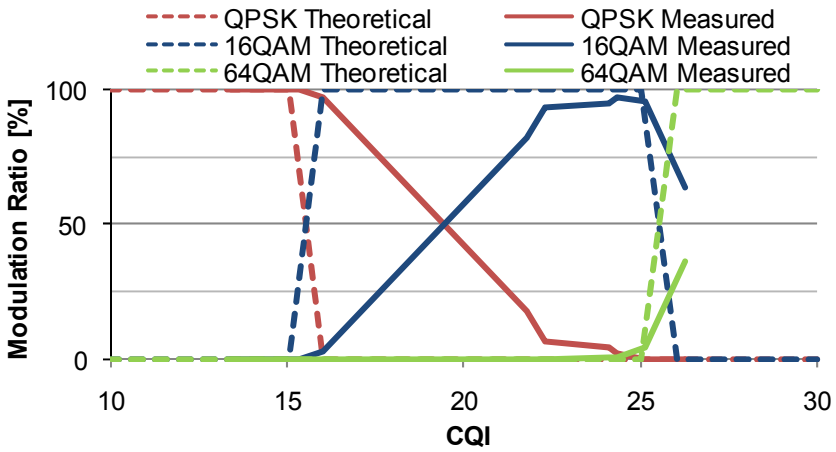

Figure 4.31. Theoretical and measured modulation ratios as a function of CQI with $P_{BS}^{Tx} = 45$ dBm, using the category 14 MT.

Figure 4.30 denotes that the 16QAM ratio reached 100% for average CQI greater than 21 while the

model predicts its usage for CQI higher than 15. Nevertheless, since the comparison is done between fixed and mean values, the model can be considered appropriate for this relation. One obtains 16.1% of relative mean error with a standard deviation of 30.9%.

Regarding the 14th category MT, the relative error and standard deviation are 20% and 33.2%, in that order. In Figure 4.31, one shows that the QPSK usage was greater than expected given the measured CQI, leading to a lower 16QAM usage. Since the measured CQI did not achieve values greater than 26, there is not enough data to analyse the 64QAM ratio. Still, it should be noted that for an average CQI of 26, the measured 64QAM ratio was 36.5%, distant from the theoretical 100%.

In Figure 4.32, one presents the comparison between the theoretical and measured modulation ratios as a function of CPICH RSCP for the terminal of 8th category, with total transmit power equal to 45 dBm. Equivalent comparison concerning the MT that can use 64QAM is also shown, Figure 4.33.

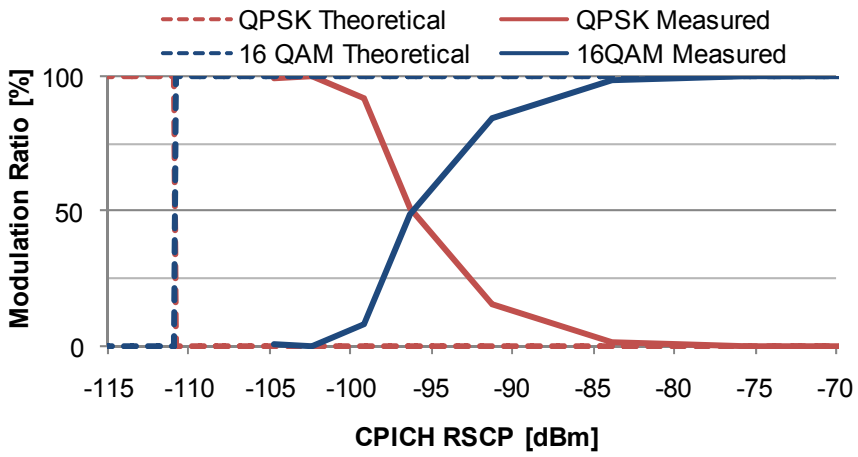

Figure 4.32. Theoretical and measured modulation ratios as a function of CPICH RSCP with $P_{BS}^{Tx} = 45\,\text{dBm}$, using the category 8 MT.

The α value in (2.5) that gives the lowest relative mean error for both MTs is 0.1. Even taking the lowest orthogonality factor into account, the model surpasses what was measured, which means that the used model is very optimistic for this relation. For all measured CPICH RSCP average values using the category 8 MT, the model indicates the usage of 16QAM for α between 0.1 and 0.9, resulting in a relative mean error of 36% with standard deviation of 44.9%. As mentioned earlier, the orthogonality factor depends on the distance and it varied during the measurements. Therefore, it is supposed to be greater in situations with high received signal, normally when the MT is near the Node B.

The relative mean error is minimised with 0.1 of orthogonality factor, being 47.2% with 45.8% of standard deviation. Nevertheless, the 64QAM theoretical curve shown in Figure 4.33 was obtained for α equal to 0.9, since that is the only value defining the usage of this modulation for RSCP lower than -60 dBm, according to the models presented in the previous chapter. Once again, the achieved errors for this relation are significant, which can be justified by the fact that the implemented algorithms differ

from the several models used, together with the use of mean experimental values in these analyses.

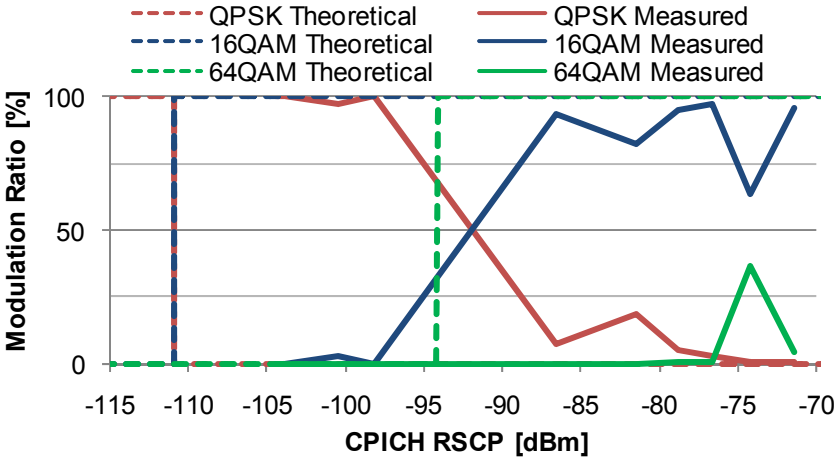

Figure 4.33. Theoretical and measured modulation ratios as a function of CPICH RSCP with $P_{BS}^{Tx} = 45$ dBm, using the category 14 MT.

The relation between the modulation ratio and the CPICH E_c/N_0 considering the MT that uses QPSK and 16QAM, for a total transmit power of 45 dBm, is presented, Figure 4.34.

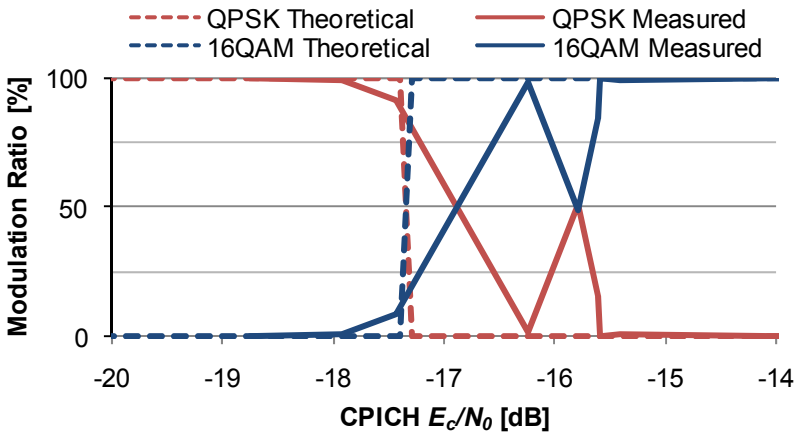

Figure 4.34. Theoretical and measured modulation ratios as a function of CPICH E_c/N_0 with $P_{BS}^{Tx} = 45$ dBm, using the category 8 MT.

The smallest relative mean error between model and measured data is 7.8%, with standard deviation equal to 16.1%, considering an α of 0.3 in (2.6). Again, there is a clear indication that this model is optimistic for this relation, i.e., if one considers higher orthogonality factor values, 16QAM is defined for lower E_c/N_0 values and the relative error increases. However, a good approximation of what was measured is achieved by taking this specific α into account, as shown in Figure 4.34.

In Figure 4.35, one shows the modulation ratio versus CPICH E_c/N_0 using the category 14 MT. The orthogonality factor chosen is again 0.3, resulting in a relative mean error of 7.8% with 11.4% of standard deviation. Despite the fact that the error is not considerable, the 64QAM curves differ from each other. In theory, only when α equals 0.9 this modulation is used for E_c/N_0 approximately -16 dB.

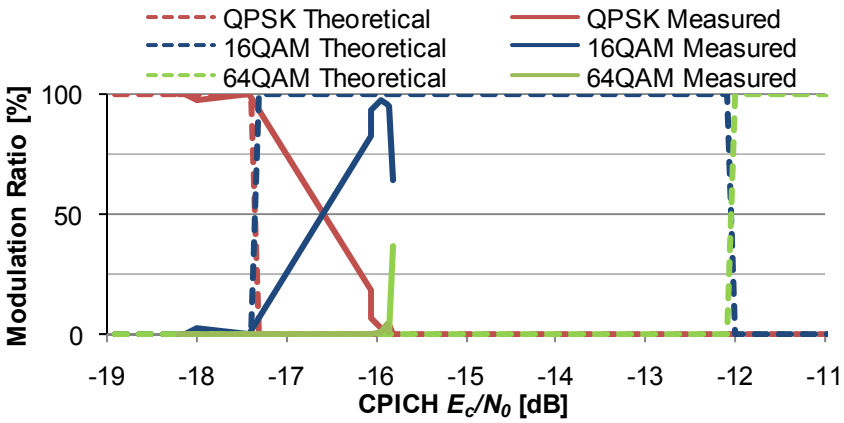

Figure 4.35. Theoretical and measured modulation ratios as a function of CPICH E_c/N_0 with $P_{BS}^{Tx} = 45$ dBm, using the category 14 MT.

To conclude, it is shown that the model based on the CQI mapping tables, being optimistic, is a good approximation of the measured modulation ratio as a function of CQI. Since this model is also used in the remaining analysis, the smallest errors are obtained with low orthogonality factor. Nevertheless, considering these α values, the 64QAM's theoretical curves are quite different from the measured ones.

4.2.5 HS-PDSCH Codes

The number of HS-PDSCH codes that an MT should use for each reported CQI is defined in Table 3.1 and Table 3.2. Both the theoretical and measured number of codes versus CQI for the 8th category MT, considering 45 dBm of transmit power, are presented, Figure 4.36. Regarding the MT that uses a maximum of 15 codes, the same relation is shown, Figure 4.37.

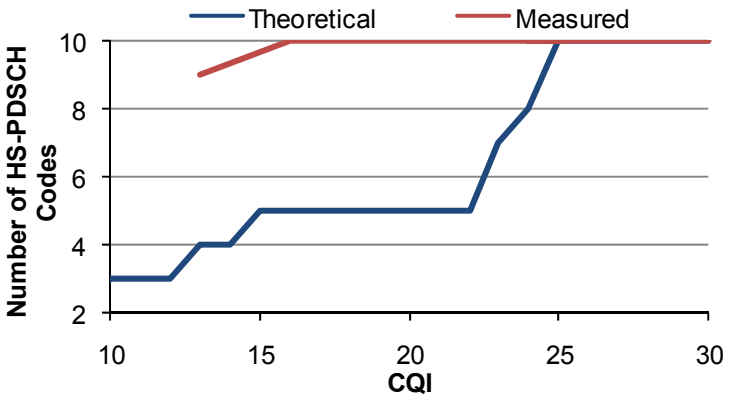

Figure 4.36. Number of HS-PDSCH codes as a function of CQI with $P_{BS}^{Tx} = 45$ dBm, using the category 8 MT, considering theoretical and measured data.

It should be noted that experimental data consist of weighted averages, taking the average code usage during the measurements into account. In Figure 4.36, one shows that for every measured CQI greater than 16, the MT used 10 HS-PDSCH codes. Since the CQI table defines the use of 10 codes

only for CQI higher than or equal to 25, the discrepancies between the CQI mapping table and the implemented algorithm are evident, leading to a relative mean error of 67.5% and standard deviation equal to 54.1%.

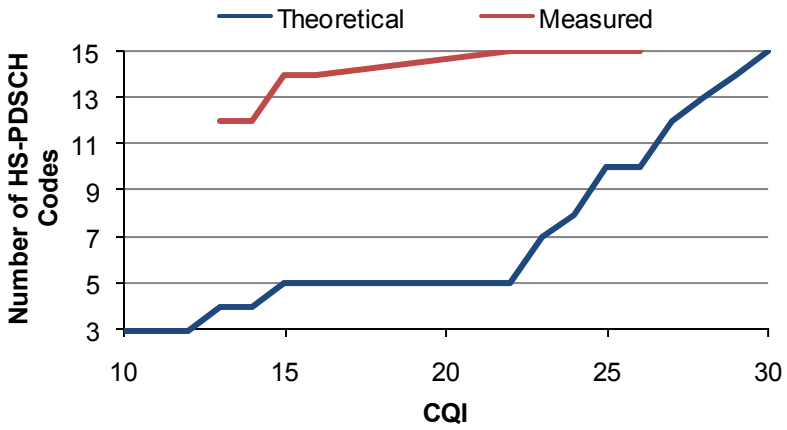

Figure 4.37. Number of HS-PDSCH codes as a function of CQI with $P_{BS}^{Tx} = 45$ dBm, using the category 14 MT, considering theoretical and measured data.

Once more, it can be seen in Figure 4.37 that the measured results are significantly different than expected. One gets a relative mean error equal to 143% and a standard deviation of 66%, representative of the great disparity between the model and experimental results. For example, for a CQI of 22 the model indicates the use of 5 codes while the actual number of codes in use was 15.

In Figure 4.38, one shows the measured HS-PDSCH average code usage considering different values of CPICH RSCP, for the category 8 terminal with 45 dBm of transmit power.

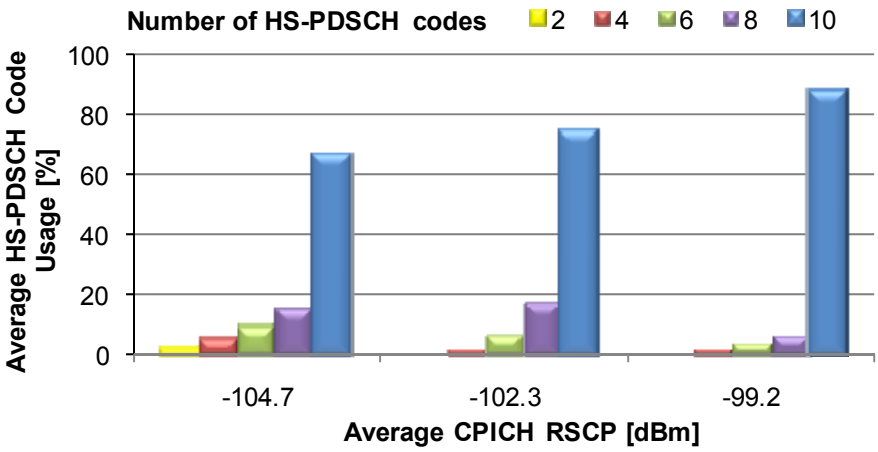

Figure 4.38. Measured HS-PDSCH code usage as a function of CPICH RSCP with $P_{BS}^{Tx} = 45$ dBm, considering the category 8 MT.

For all the remaining RSCP samples, the average usage of 10 codes surpassed 99%. Results indicate that the 10 codes usage increased as CPICH RSCP increased, varying from 66.5% to 88.3%. Adding to this, it is interesting to note that only even numbers of codes were used more than 1% of the time.

The same analysis is done for the 14th category MT, Figure 4.39.

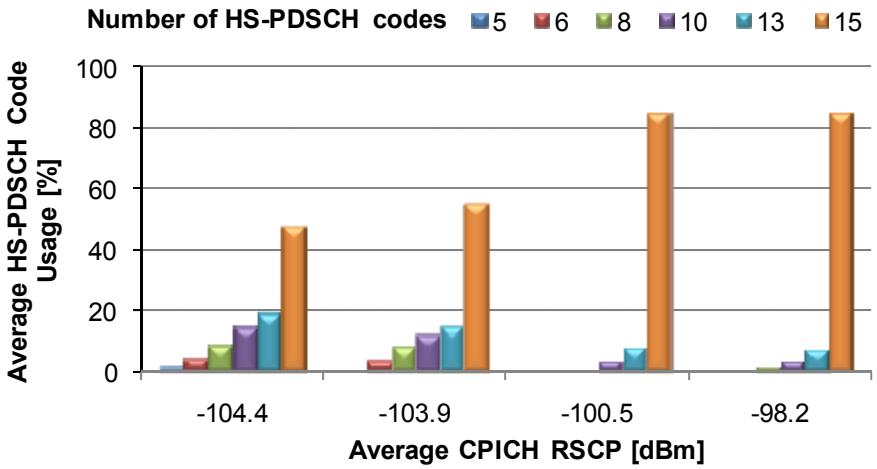

Figure 4.39. Measured HS-PDSCH code usage as a function of CPICH RSCP with $P_{BS}^{Tx} = 45$ dBm, considering the category 14 MT.

In Figure 4.39, it is shown that a larger range of codes was used in more than 1% of the 10 minutes, which is the duration of each measurement. The mean usage of 15 HS-PDSCH codes increased from 47.5% to 85%, with average RSCP equal to -104.4 and -98.2 dBm, respectively. Concerning these results, it is important to emphasise that even for low CPICH RSCP values, i.e., under unfavourable radio channel conditions, the 15 codes usage was substantial, suggesting that the implemented algorithm defines the usage of the maximum number of codes whenever possible.

Concluding, one shows that the algorithm is quite different from the theoretical model, which may explain the errors in the comparison between measured and theoretical throughput, i.e., since the actual number of codes used was higher than expected for any given CQI, the theoretical throughput tends to be lower than the measured one.

4.2.6 HS-DSCH BLER

In Figure 4.40, one presents the theoretical HS-DSCH BLER as a function of CPICH RSCP for the three power configurations, considering CQI equal to 20 and an orthogonality factor of 0.8 in (3.8) and (2.5), respectively. A CQI of 20 was chosen because this value represents a good approximation of the average measured CQI, whereas the defined α takes the fact that a linear equaliser receiver was used into account.

The model indicates that the higher the available power, the lower the CPICH RSCP needs to be in order to achieve a BLER lower than 10%. In Figure 4.41, one shows the measured HS-DSCH BLER on first transmission as a function of RSCP with different power configurations, using the terminal with 15 HS-PDSCH codes. Again, it should be noted that neither the CQI nor the orthogonality factor were constant during the measurements. In theory, BLER decreases as the radio channel conditions become more favourable; measured results show that it was not always the case. One explanation for

this fact may be the raise of TBS when RSCP increases, leading to higher BLER when the throughput increases. In addition, for most situations a tendency to an increase of BLER 1st with the available power is visible.

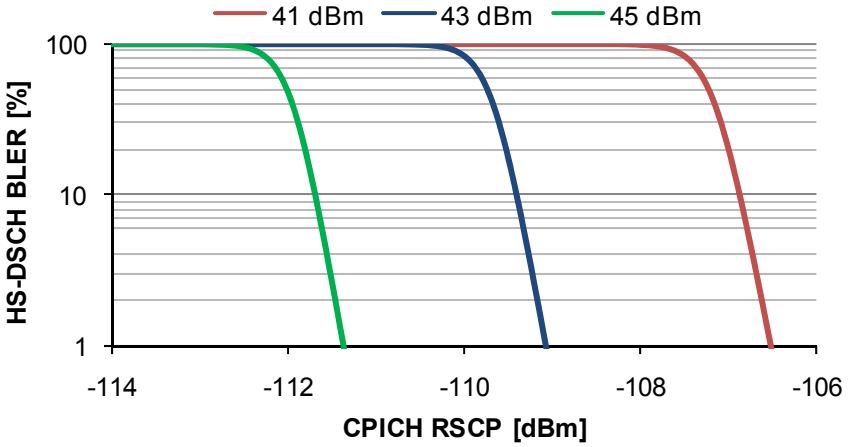

Figure 4.40. Theoretical HS-DSCH BLER as a function of CPICH RSCP with CQI = 20 and α = 0.8, for different power configurations.

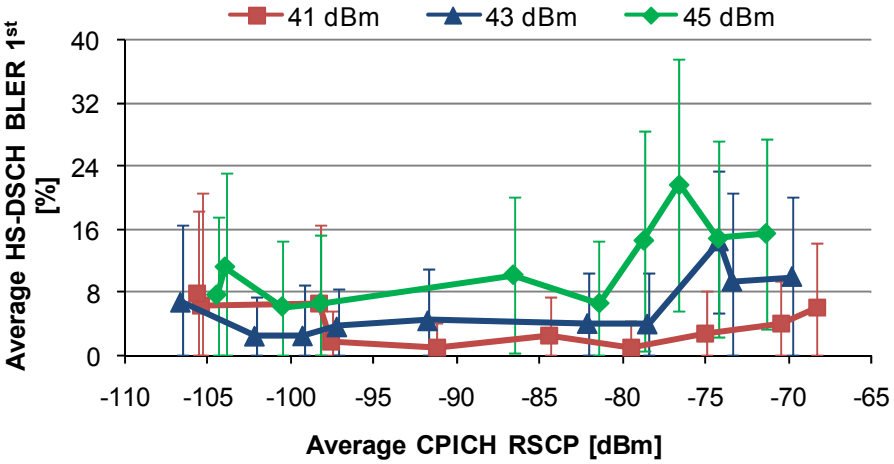

Figure 4.41. Measured HS-DSCH BLER 1st as a function of CPICH RSCP with different power configurations, using the category 14 MT.

As shown in Figure 4.41, with 45 and 43 dBm the average BLER on a first transmission was greater than 10% in few occasions. The greatest measured BLER 1st was 21.6%, 14.4% and 7.91%, with mean RSCP of -76.6, -74.2, and -105.6 dBm, while the lowest was 6.1%, 2.37% and 0.96%, with RSCP equal to -100.5, -102.1 and -79.5 dBm, considering 45, 43 and 41 dBm of P_{BS}^{Tx}, respectively. Additionally, it is noticeable that the measured BLER 1st presented high standard deviations in most cases, reaching 15.9%, 11.3% and 14.4%, in the same order.

Theoretical BLER versus CPICH E_c/N_0 is shown in Figure 4.42, taking the same assumptions of Figure 4.40 into account. In Figure 4.43, this relation is presented with the experimental data, considering all power configurations and the usage of the 14th category terminal.

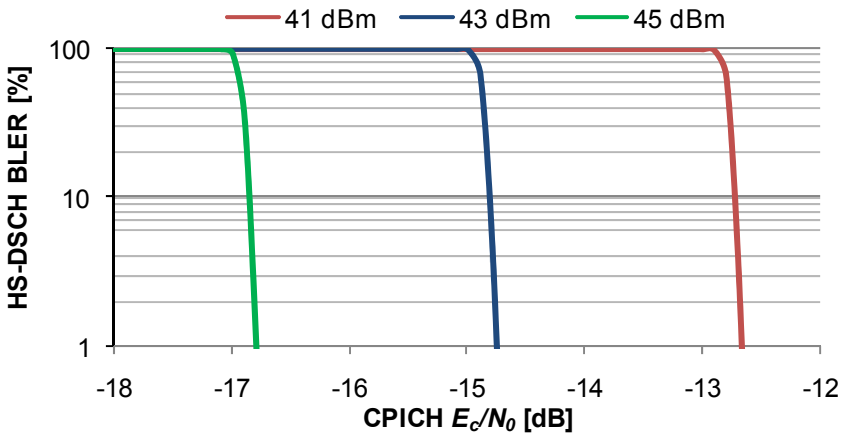

Figure 4.42. Theoretical HS-DSCH BLER as a function of CPICH E_c/N_0 with CQI = 20 and α = 0.8, for different power configurations.

The model sets that, for a given E_c/N_0 greater than -17 dB, the lower the available power, the greater the resultant BLER. Note that the theoretical HS-DSCH BLER is 10% for E_c/N_0 approximately -16.9, -14.8 and -12.8 dB, considering transmit power of 45, 43 and 41 dBm, in that order. In Figure 4.43, one shows that the highest obtained BLER was reached for an average CPICH E_c/N_0 equal to -15.8, -14.4 and -17.3 dB, while the minimum BLER was obtained for -17.9, -17.4 and -11.4 dB of E_c/N_0, with P_{BS}^{Tx} equal to 45, 43 and 41 dBm, respectively.

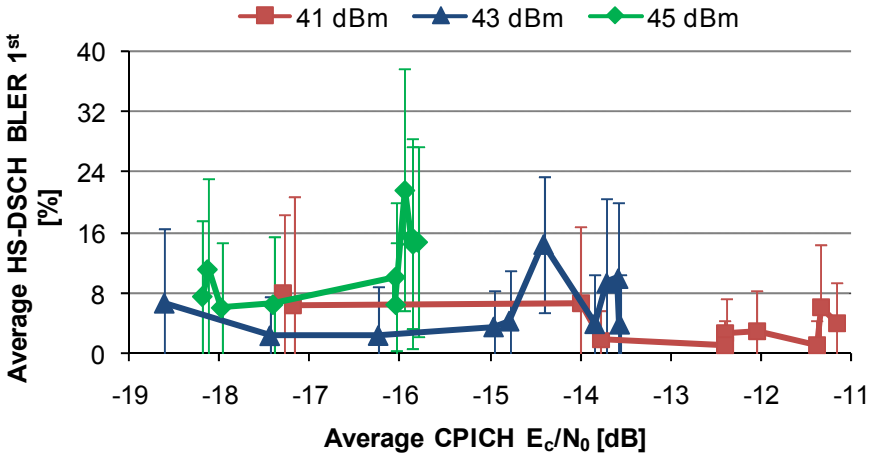

Figure 4.43. Measured HS-DSCH BLER 1st as a function of CPICH E_c/N_0 for different power configurations, using the category 14 MT.

HS-DSCH BLER on a first transmission as a function of CQI using the 15 codes MT for all power configurations is presented, Figure 4.44. Again, it should be noted that the greatest BLER values were achieved for CQI higher than 24, in the 45 and 43 dBm configurations.

One can conclude that the results are not in accordance with the model. The latter expects the decrease of the BLER with the increase of RSCP, E_c/N_0 and CQI, while the former present the opposite trend, with 45 and 43 dBm of P_{BS}^{Tx}. It was also shown that average BLER on first

transmission reached the highest values for the maximum Node B available power.

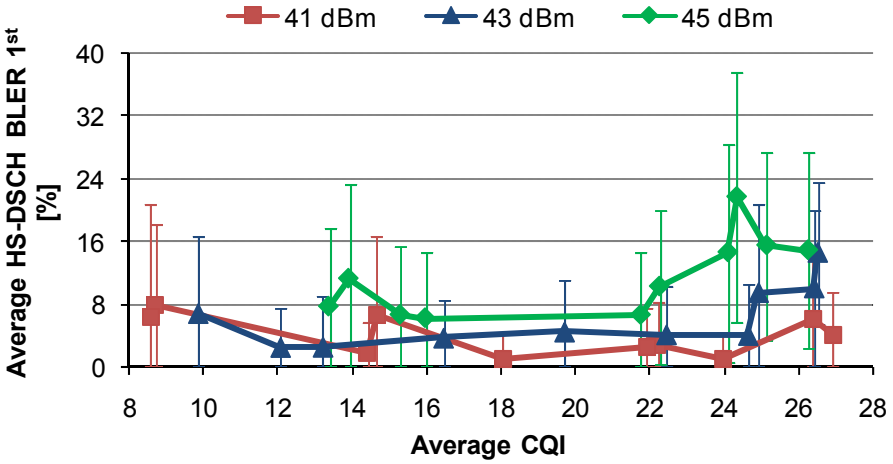

Figure 4.44. Measured HS-DSCH BLER 1st as a function of CQI for different power configurations, using the category 14 MT.

4.3 HSPA+ UL

In this section, one presents the comparison between the HSPA+ UL measurements results and the theoretical models described in Chapter 3. The parameters addressed are E-DCH throughput, MT transmit power and E-DCH BLER.

4.3.1 E-DCH Throughput

E-DCH throughput as a function of CPICH RSCP is presented, considering theoretical and experimental data, for both 10 and 2 ms TTIs, Figure 4.45. As mentioned in the previous chapter, the theoretical throughput is obtained taking the measured MT transmit power into account.

In Figure 4.45, one shows that the average throughput with 10 ms TTI was almost constant for RSCP greater than -100 dBm, not exceeding 0.9 Mbps. On the contrary, with a TTI of 2 ms there was an increase of the mean throughput as the radio channel conditions became more favourable, being 1.76 Mbps with average RSCP equal to -103.6 dBm to reach 4.27 Mbps with an RSCP of -64.9 dBm. Moreover, the variation of data rate is perceptible on standard deviations, the largest being 0.23 and 0.75 Mbps for 10 and 2 ms TTIs, correspondingly. It is noticeable that the average data do not differ significantly from the models, obtaining 31.2% and 21.4% of relative mean error, with standard deviation of 22.9% and 29.6% considering 10 and 2 ms TTIs, respectively.

E-DCH throughput as a function of CPICH RSCP with a TTI of 10 ms, considering all data collected in the measurements, is shown, Figure 4.46. In Figure 4.47, one presents the theoretical throughput

based on measured MT transmit power. Equivalent analysis with 2 ms TTI is also shown, Figure 4.48 and Figure 4.49.

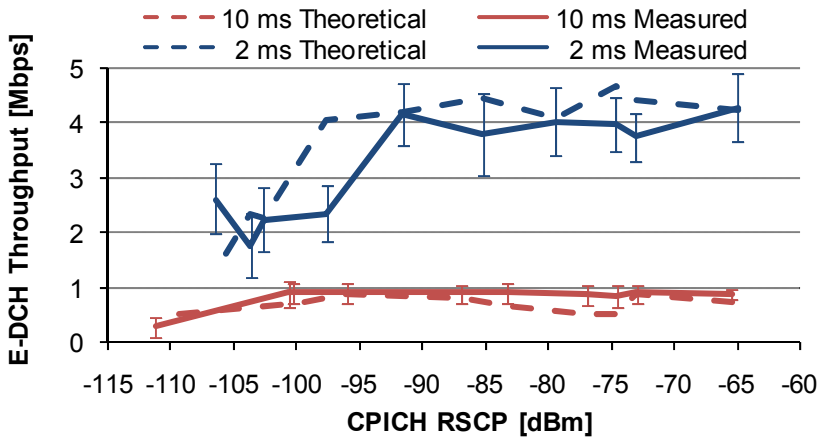

Figure 4.45. Theoretical and measured E-DCH throughputs as a function of CPICH RSCP, considering both TTIs.

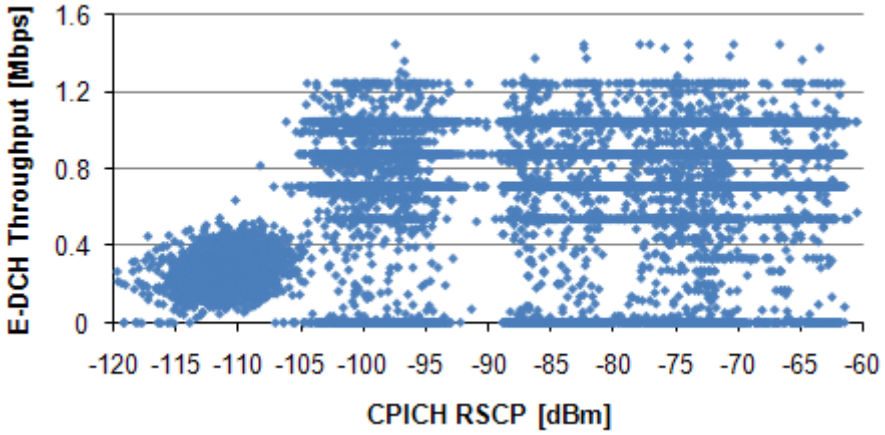

Figure 4.46. Measured E-DCH throughput as a function of CPICH RSCP with 10 ms TTI.

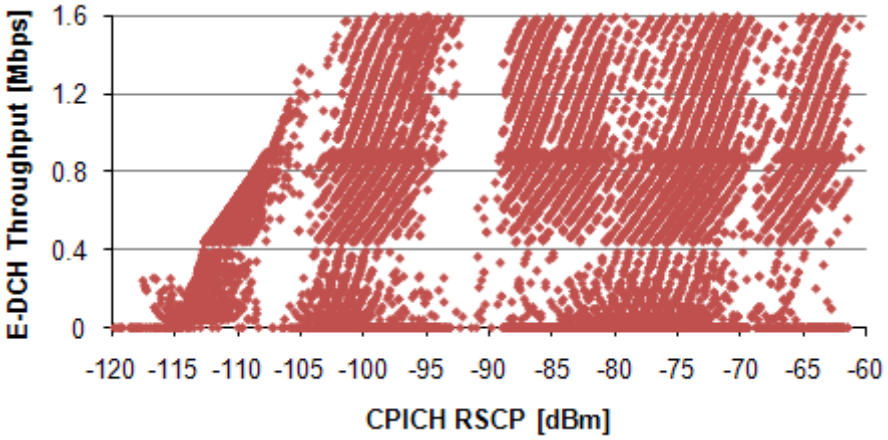

Figure 4.47. Theoretical E-DCH throughput as a function of CPICH RSCP with 10 ms TTI.

With TTI equal to 10 ms, it is noticeable the great variation of throughput, both experimental and

theoretical. In both cases, the peak throughput (1.45 and 1.6 Mbps, considering measured and expected value, respectively) is achieved for CPICH RSCP higher than -105 dBm. One obtained a correlation factor of 0.333 and the RMSE is 0.435 Mbps, consistent with the results of the analysis with average values. Additionally, one can observe several samples of E-DCH data rate equal to zero, which also happened with 2 ms TTI, due to the fact that some packets were discarded when the buffer reached its pole capacity.

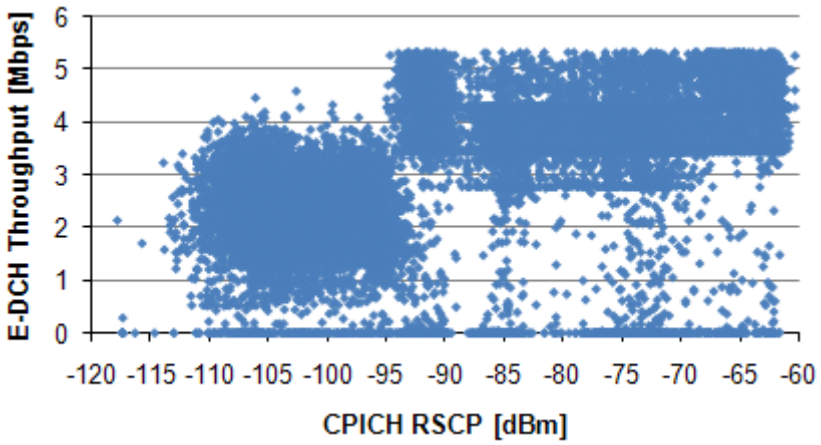

Figure 4.48. Measured E-DCH throughput as a function of CPICH RSCP with 2 ms TTI.

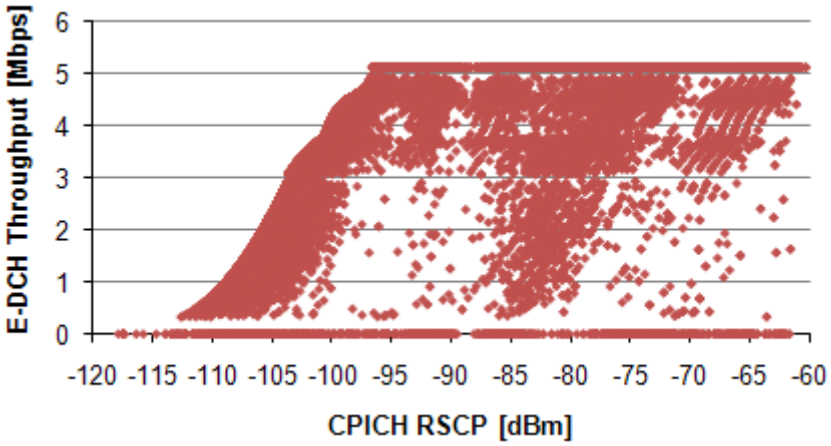

Figure 4.49. Theoretical E-DCH throughput as a function of CPICH RSCP with 2 ms TTI.

In Figure 4.48 and Figure 4.49, one can observe a trend to an increase of E-DCH throughput with RSCP, especially with RSCP between -120 and -95 dBm. Note that for RSCP lower than -100 dBm, the maximum throughput was approximately 4 Mbps, while the peak throughput (measured 5.32 Mbps and expected 5.15 Mbps) was reached for RSCP greater than -95 dBm. Still, the correlation factor is 0.444. In addition, the expected data rate is higher than the measured one in 66.6% of the samples, which indicates that the theoretical performance was not achieved in the majority of occasions, with the RMSE being 1.35 Mbps.

In conclusion, it was shown that the average E-DCH throughput was almost constant for TTI of 10 ms, not surpassing 0.9 Mbps, while in the 2 ms TTI case it increased with CPICH RSCP, reaching 4.27

Mbps, obtaining 31.2% and 21.4% of relative mean error. Additionally, when one considers all measured throughput and MT transmit power samples the correlation factor is low, being 0.333 and 0.444 for TTIs of 10 and 2 ms, respectively. The peak measured data rate was 1.45 and 5.32 Mbps, while RMSE is 0.435 and 1.35 Mbps.

4.3.2 MT Transmit Power

Since there was power control, it is interesting to analyse P_{MT}^{Tx} as a function of CPICH RSCP, considering both TTIs, Figure 4.50. Note that the maximum MT transmit power was 24 dBm.

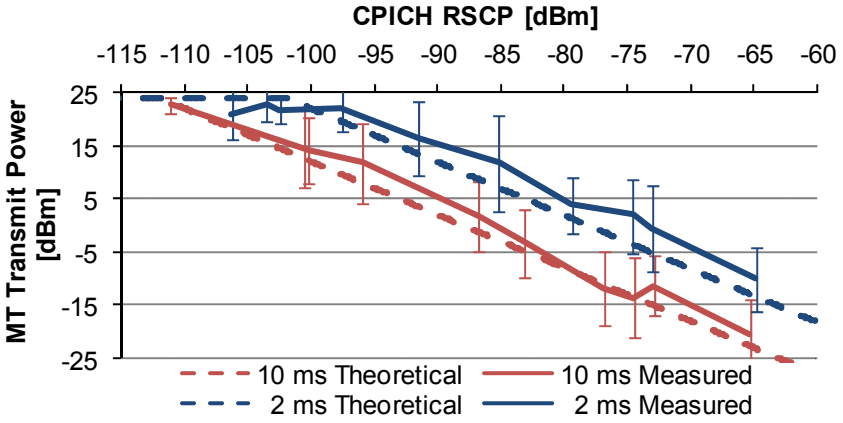

Figure 4.50. Theoretical and measured MT transmit powers as a function of CPICH RSCP, considering both TTIs.

It should be mentioned that the theoretical lines are expressed taking a constant Node B received power into account in (3.11); with 10 ms TTI, one considers P_{BS}^{Rx} equal to -115 dBm, while for 2 ms it is chosen as -105 dBm. It is noticeable that, for a given RSCP, P_{MT}^{Tx} was higher with a TTI of 2 ms, since the achieved throughputs are greater in this case. Given that, the maximum transmit power was reached for greater RSCP than with 10 ms TTI. As expected, one can observe a trend to a decrease of MT transmit power with the increase of CPICH RSCP, i.e., since the path loss decreases, the transmit power can be reduced. The average P_{MT}^{Tx} went from -22.2 to 22.7 dBm and from -10 to 22.8 dBm, considering 10 and 2 ms TTIs, in that order.

In Figure 4.51 and Figure 4.52, one shows the MT transmit power as a function of RSCP, considering all measured samples, for TTIs of 10 and 2 ms, respectively. The theoretical lines are the ones presented in Figure 4.50.

Figure 4.51 shows that the MT transmit power took several values for each RSCP, which indicates that the Node B received power was not constant. Therefore, the errors between measured and theoretical data are predictable. Despite that, the correlation factor is 0.786, since it is followed the same trend. One can also see that P_{MT}^{Tx} varied between -40 and 24 dBm. Additionally, one should

mention that the experimental transmit power is higher than expected (considering -115 dBm of P_{BS}^{Rx}) in 67.7% of the samples, so, in these cases, the received power was greater than -115 dBm.

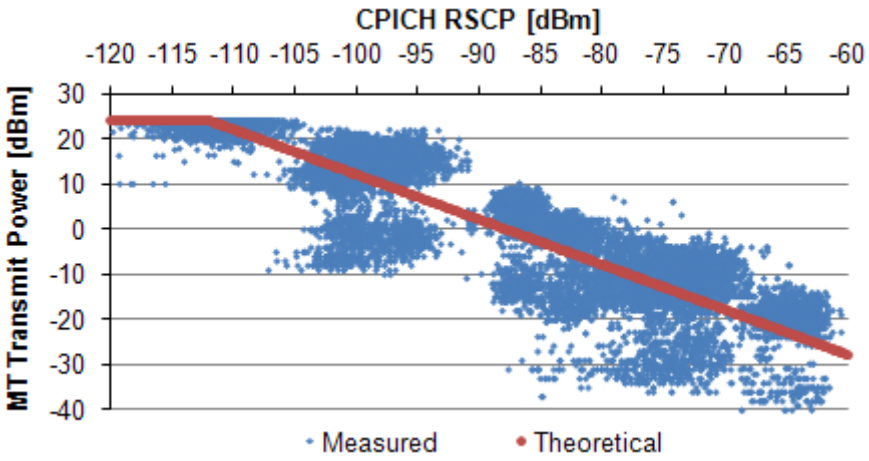

Figure 4.51. MT transmit power as a function of CPICH RSCP with 10 ms TTI.

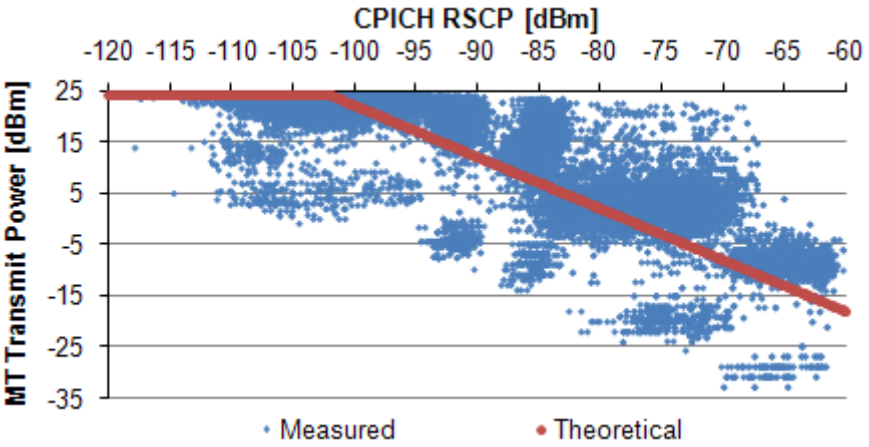

Figure 4.52. MT transmit power as a function of CPICH RSCP with 2 ms TTI.

Figure 4.52 also denotes that the Node B received power was not constant (as considered). In fact, P_{BS}^{Rx} was higher than -105 dBm in 68.9% of the time, considering measured P_{MT}^{Tx} and CPICH RSCP. Again, one can observe a trend to a decrease of MT transmit power, from 24 to -33 dBm, with increase of RSCP, i.e., as the radio channel conditions become more favourable. In this situation the correlation factor is 0.732.

To summarise, it was shown that the average measured P_{MT}^{Tx} was higher for the lowest TTI case. It was also noticeable the high correlation between measured and expected data, even considering fixed P_{BS}^{Rx}.

4.3.3 E-DCH BLER

In Figure 4.53, one presents the measured E-DCH BLER on a first transmission as a function of CPICH RSCP, for both TTIs.

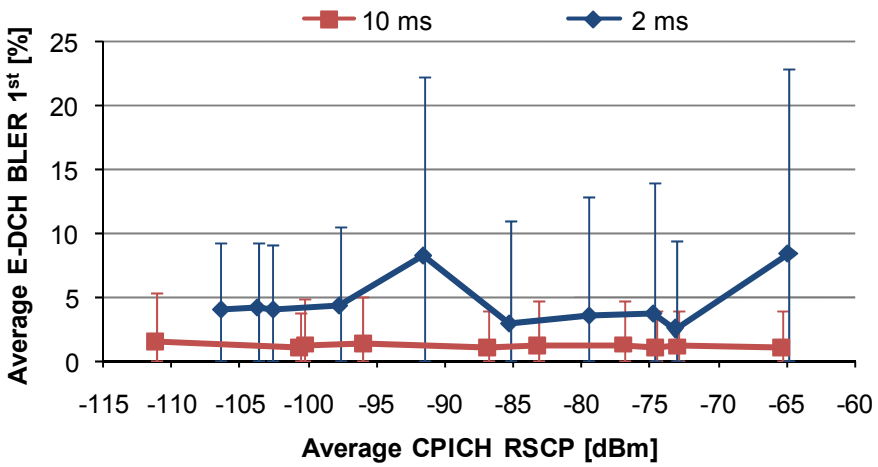

Figure 4.53. Measured E-DCH BLER 1st as a function of CPICH RSCP, considering both TTIs.

Figure 4.53 shows that the average E-DCH BLER 1st did not exceed 1.58% with 10 ms TTI, while it reached 8.52% for TTI of 2 ms. In addition, standard deviations were also greater with the smallest TTI, being the maximum deviation 3.89% and 14.42%, for 10 and 2 ms, respectively. It is noticeable that average BLER was almost constant in the 10 ms TTI case, whereas with 2 ms it was greater with average RSCP of -91.5 and -64.9 dBm. These results can be justified by the fact that the throughput is higher with TTI of 2 ms, leading to lower data coding and, consequently, greater error probability.

Chapter 5

Conclusions

In this chapter, the main conclusions of this thesis are pointed out, as well as some future work suggestions.

The main objective of this thesis was to analyse HSPA+ performance at the cellular level. This goal was accomplished through the execution of measurements in an Optimus site. In addition, the comparison between measured data and theoretical models was done.

Measurements were performed in a single user scenario. The MT was inside a parked car, so the environment may be considered indoor. The objective was to study the behaviour of HSPA+ DL and UL parameters, as HS-DSCH and E-DCH throughputs, CQI, modulation, HS-PDSCH codes, BLER and MT transmit power, using several configurations and under different radio channel conditions.

Considering P_{BS}^{Tx} equal to 45 dBm, the highest average HS-DSCH throughput was 10.9 and 8.26 Mbps, for the category 14 and 8 MTs, respectively. For the 14th category MT, the maximum average throughput increased 6.4% with available power of 43 dBm and 15.6% with 41 dBm, being 11.6 and 12.6 Mbps, correspondingly. These results demonstrate that the increase of power does not necessarily imply the achievement of higher throughputs, given the increase of interference. It was shown that, as expected, HS-DSCH throughput increased with the raise of CPICH RSCP, CPICH E_c/N_0 and CQI. Nevertheless, the measurements results exceeded what the theoretical models predict. This is due to the fact that the implemented algorithm highly deviates from the CQI mapping table, which is used to calculate the theoretical throughput. In fact, for 45 dBm of P_{BS}^{Tx} with the category 14 MT, the relative mean error between average measured data and expected results is 36.9%, 26.9% and 95.3%, for throughput as a function of RSCP, E_c/N_0 and CQI, respectively. Note that the errors are significantly lower in the analysis of data rate versus RSCP and E_c/N_0, since it was chosen a high value for the orthogonality factor (0.9) in both cases, i.e., given that the CQI table is pessimistic, higher α values lead to lower errors. Considering all experimental results, one obtains correlation factors of 0.539, 0.528 and 0.772, and the RMSE is 2.61, 2.91 and 2.91 Mbps, which confirms what was mentioned earlier. The maximum instantaneous throughput was 16.3 Mbps.

In the measurements with the category 14 terminal, the maximum average CPICH E_c/N_0 was -15.7, -13.6 and -11.3 dB, considering P_{BS}^{Tx} equal to 45, 43 and 41 dBm, respectively. These results are in accordance with the model, i.e., the increase of the power causes an increase of interference and, as a consequence, lower E_c/N_0. Additionally, it was observed that the differences between the obtained E_c/N_0 values were smaller for low CPICH RSCP. Actually, for RSCP lower than -90 dBm, the average E_c/N_0 was lower than expected, the relative mean error being 6.13%, 18.5% and 16.1%. Using all measured results, with 45 dBm of available power, the correlation factor and RMSE are 0.544 and 1.98 dB, respectively. It was also shown that the degradation of CPICH E_c/N_0 between situations without and with load was, on average, 9.52 dB.

Considering the maximum P_{BS}^{Tx}, the greatest average CQI was 26 and 30, when MT used 15 and 10 HS-PDSCH codes, respectively. As expected, there was a trend to an increase of CQI with CPICH E_c/N_0. For other power configurations, with the 14th category MT, equivalent CQI values were reached for higher E_c/N_0, i.e., taking the same E_c/N_0 into account, the higher the available power, the greater

the CQI. Again, a constant orthogonality factor (0.8) was considered in the theoretical model, the relative mean error being 8.92%, 11.4% and 10.1%, for P_{BS}^{Tx} equal to 45, 43 and 41 dBm, in that order. In the analysis with all collected data and 45 dBm of available power, one obtains a correlation factor of 0.639 and an RMSE of 3. Summarising, the adopted model proved to be a good approximation to the measured results.

Regarding the modulation ratio, for the 8th category MT with 45 dBm of P_{BS}^{Tx}, the average usage of 16QAM reached 100% for mean CQI greater than 21, with CPICH RSCP and CPICH E_c/N_0 higher than 83.8 dBm and -16.2 dB, respectively. For the 14th category device, the maximum 64QAM usage was 36.5%, with an average CQI of 26, RSCP of -74.3 dBm and E_c/N_0 equal to -15.8 dB. Note that the theoretical modulation ratio is 100% or 0%, whether the modulation is used or not, while the experimental results correspond to mean values during the measurements. The relative mean error for modulation ratio as a function of CQI, RSCP and E_c/N_0 is 16.1%, 36% and 7.8%, in that order, considering the category 8 MT, and 20%, 47.2% and 7.8%, using the category 14 MT. It was shown that the model based on the CQI mapping tables, being optimistic, is a good approximation of the measured modulation ratio as a function of CQI. Since this model is also used in the remaining analysis, the smallest errors are obtained with low orthogonality factor values (0.1 and 0.3 for RSCP and E_c/N_0, respectively). Nevertheless, considering these α values, the 64QAM's theoretical curves are quite different from the measured ones, given that the orthogonality factor was not constant during the measurements.

The number of used HS-PDSCH codes was another parameter analysed. Using the category 8 MT, 10 HS-PDSCH codes were used for CQI greater than 16, while the CQI mapping table only defines the usage of 10 codes for CQI higher than or equal to 25. In the measurements with the category 14 MT, 15 codes were used with CQI greater than 22, whereas, in theory, the usage of the maximum number of codes is defined only for CQI equal to 30. The relative mean error is 67.5% and 143%, using the category 8 and 14 MTs, respectively. It should be mentioned that even for low CPICH RSCP values, i.e., under unfavourable radio conditions, the average usage of the greatest number of codes varied from 66.5% to 88.3% and from 47.5% to 85%, using 10 and 15 codes, respectively, suggesting that the implemented algorithm defines the usage of the maximum number of HS-PDSCH codes whenever possible. These results are representative of the discrepancies between model and experimental data, revealing why the theoretical throughput is generally lower than the measured.

During the measurements with the 14th category terminal, one observed a trend to an increase of the average HS-DSCH BLER on a first transmission with the available power. In addition, with 45 and 43 dBm of P_{BS}^{Tx}, the average BLER 1st increased with the raise of CPICH RSCP, CPICH E_c/N_0 and CQI. This is due to the increase of TBS, achieving higher throughput as well as greater BLER. The greatest experimental BLER 1st was 21.6%, 14.4% and 7.91%, while the lowest was 6.1%, 2.37% and 0.96%, considering 45, 43 and 41 dBm of P_{BS}^{Tx}, respectively.

The average E-DCH throughput was almost constant with 10 ms TTI for CPICH RSCP greater than -100 dBm, while with a 2 ms TTI there was an increase of throughput with RSCP. The average data rate ranged between 0.27 and 0.90 Mbps, and 1.76 and 4.27 Mbps, considering 10 and 2 ms TTI, in that order. Experimental results do not differ significantly from the models; one obtains 31.2% and 21.4% of relative mean error. Considering all available data, it was noticeable the wide variation of throughput, with some samples equal to zero, due to the fact that there were packets discarded when the buffer reached its pole capacity. The peak instantaneous E-DCH throughput was 1.45 and 5.32 Mbps, for 10 and 2 ms TTIs, respectively. With a TTI of 10 ms, one obtains a correlation factor of 0.333 and the RMSE is 0.435 Mbps, while with the smallest TTI the correlation factor and RMSE are 0.444 and 1.35 Mbps, correspondingly.

It was observed a trend to a decrease of MT transmit power with the increase of CPICH RSCP, i.e., when the path loss decreased. The average P_{MT}^{Tx} varied between -22.2 and 22.7 dBm, and between -10 and -22.8 dBm, considering 10 and 2 ms TTI, in that order. Given the same RSCP, the average P_{MT}^{Tx} was greater with the lowest TTI, since the achieved throughputs were higher. Moreover, considering -115 and -105 dBm of Node B received power for 10 and 2 ms TTIs, the correlation factor is 0.786 and 0.732, considering fixed P_{BS}^{Rx}. The instantaneous MT transmit power ranged from -40 to 24 dBm with a 10 ms TTI, and from -33 to 24 dBm with a 2 ms TTI.

The average E-DCH BLER 1st did not exceed 1.58% with 10 ms TTI, while it reached 8.52% for TTI of 2 ms. UL BLER on first transmission was almost constant in the 10 ms TTI case, whereas with 2 ms TTI presented higher values with mean CPICH RSCP of -91.5 and -64.9 dBm. These results can be explained by the fact that the throughput is higher with TTI of 2 ms, leading to lower data coding and, consequently, greater error probability.

For future work, it is suggested the study of HSPA+ performance with the introduction of MIMO and 16QAM in UL, by performing measurements with these capabilities, and comparing the measured data with theoretical models. Other suggestion is to carry out measurements in different environments. Also the impact of introducing more users in the same cell, it is interesting to analyse. One could also suggest the study of LTE performance at the cellular level, both in single and multiple user scenarios, by developing a simulator.

Annex A – MIMO

A brief overview over the general and capacity aspects of MIMO is presented in this annex.

MIMO takes advantage of the multipath propagation, where the Receiver (Rx) antenna is reached by many copies of the transmitted signal. The difference in each component propagation path results in diversity of Time of Arrival (ToA), Angle of Arrival (AoA), signal amplitude and phase. With the purpose of achieving a better performance, MIMO systems take advantage of all arriving arrays [Maćk07]. It exploits independently the transmission between the Transmitter (Tx) and Rx antennas.

The MIMO scheme, which is the result of parallel deployment of several space-separated antennas at input and output, improves not only BER performance but also causes an increase of channel capacity [Maćk07]. Even so, the capacity in such system strongly depends on the propagation conditions in the radio channel and can vary considerably [Dziu04].

A MIMO system is composed of N_T Tx antennas and N_R Rx antennas, Figure A.1.

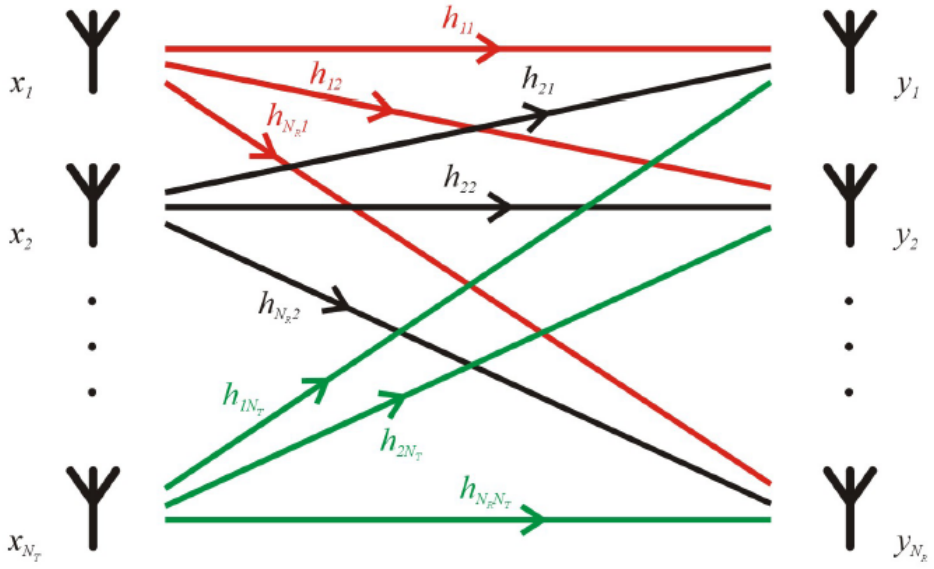

Figure A.1. MIMO scheme (extracted from [Maćk07]).

$\bar{\xi}$ is the mean correlation between links in a MIMO system, and is defined by:

$$\bar{\xi} = \frac{1}{(N_T N_R)^2} \sum_{k=1}^{N_T} \sum_{l=1}^{N_R} \sum_{m=1}^{N_T} \sum_{n=1}^{N_R} \xi(h_{kl}, h_{mn}) \quad \text{(A.1)}$$

where:

- h_{kl} is a Channel Impulse Response (CIR) between signal from the l^{th} Tx antenna to the k^{th} Rx antenna.

According to the general principles of information theory, the capacity of the radio channel is bounded by Shannon's rule, [Proa01], which represents the capacity of a Single Input Single Output (SISO) system, usually taken as a reference:

$$C_{SISO[\text{bps/hz}]} = \log_2(1+\rho_N) \tag{A.2}$$

where:

- C_{SISO} is the capacity of a radio channel;
- ρ_N is the SNR.

In an ideal case, it can be shown that the channel capacity grows linearly with the number of Tx and Rx antennas [ECGF05]. In MIMO systems is possible to establish multiple parallel subchannels, which operate simultaneously at the same time and on the same frequency band. The theoretical capacity of such a system has been presented in [FoGa98]:

$$C_{MIMO[\text{bps/Hz}]} = \log_2\left\{\det\left[\mathbf{I_{NR}} + \frac{\rho_N}{N_T}\mathbf{H_n}\mathbf{H_n^H}\right]\right\} \tag{A.3}$$

where:

- $\mathbf{I_{NR}}$ is the N_R dimensional identity matrix;
- ρ_N is defined at each Rx antenna as:

$$\rho_N = \frac{P_{total}}{P_{noise}}b \tag{A.4}$$

  where:

  - P_{noise} is the noise power at the Rx antenna.

- $\mathbf{H_n}$ is the normalised channel transfer matrix related to **T** as:

$$\mathbf{H_n} = \frac{\mathbf{T}}{b} \tag{A.5}$$

- **T** is the non-normalised channel transfer matrix, containing the channel transfer gains for each pair of antennas;
- b is defined as:

$$b^2 = R\left[\left|\mathbf{T}\right|\right]^2 = \frac{1}{N_T N_R}\sum_{m=1}^{N_R}\sum_{n=1}^{N_T}\left|T_{mn}\right|^2 \tag{A.6}$$

It is possible to obtain the upper and lower bounds for capacity from (A.3) since the correlation varies between zero and one. The maximum capacity is achieved if there is no correlation between parallel paths (ξ=0):

$$C_{MIMO(\xi=0)} = \min(N_T; N_R)\log_2\left(1+\frac{\rho_N}{N_T}\right) \tag{A.7}$$

On the other hand, when all subchannels are totally correlated (ξ=1), the minimum capacity of a MIMO channel occurs:

$$C_{MIMO(\xi=1)} = \log_2(1 + \min(N_T; N_R)\frac{\rho_N}{N_T}) \quad \text{(A.8)}$$

When the channel is known at the Tx, meaning the correlation between subchannels is known at the Tx, the waterfilling power distribution can be performed. In specified conditions this allows to operate with the maximum achievable capacity.

The Relative MIMO Gain (RMG) can be defined as the relation between the capacities of a MIMO system related to the SISO one, [KuCo08]:

$$G_{M/S} = \frac{C_{MIMO}}{C_{SISO}} \quad \text{(A.9)}$$

Annex B – Link Budget

The presented link budget is based on the Release 99 one, described in detail in [CoLa06] and [Sant04], adapted to HSPA+.

The path loss can be calculated by [Corr06]:

$$L_{P\,[\mathrm{dB}]} = P_{t\,[\mathrm{dBm}]} + G_{t\,[\mathrm{dBi}]} - P_{r\,[\mathrm{dBm}]} + G_{r\,[\mathrm{dBi}]} = EIRP_{[\mathrm{dBm}]} - P_{r\,[\mathrm{dBm}]} + G_{r\,[\mathrm{dBi}]} \quad \text{(B.1)}$$

where:

- L_p is the path loss;
- P_t is the transmitting power at antenna port;
- G_t is the transmitting antenna gain;
- P_r is the available receiving power at antenna port;
- G_r is the receiving antenna gain.

If diversity is used, G_r in (B.1) is replaced by:

$$G_{rdiv\,[\mathrm{dB}]} = G_{r\,[\mathrm{dBi}]} + G_{div\,[\mathrm{dB}]} \quad \text{(B.2)}$$

where:

- G_{div} represents the diversity gain.

The Equivalent Isotropic Radiated Power (EIRP) can be calculated for DL by (B.3), and for UL by (B.4).

$$EIRP_{[\mathrm{dBm}]} = \left(P_t - P_{S\&C}\right)_{[\mathrm{dBm}]} - L_{c\,[\mathrm{dB}]} + G_{t\,[\mathrm{dBi}]} \quad \text{(B.3)}$$

$$EIRP_{[\mathrm{dBm}]} = \left(P_t - P_{S\&C}\right)_{[\mathrm{dBm}]} - L_{u\,[\mathrm{dB}]} + G_{t\,[\mathrm{dBi}]} - G_{MHA\,[\mathrm{dB}]} \quad \text{(B.4)}$$

where:

- L_c are the cable losses between transmitter and antenna;
- L_u are user losses;
- G_{MHA} is the masthead amplifier gain;
- $P_{S\&C}$ is the signalling and control power.

The received power can be calculated by (B.5) for DL and (B.6) for UL:

$$P_{Rx\,[\mathrm{dBm}]} = P_{r\,[\mathrm{dBm}]} - L_{u\,[\mathrm{dB}]} \quad \text{(B.5)}$$

$$P_{Rx[\text{dBm}]} = P_{r[\text{dBm}]} - L_{c[\text{dB}]} \quad \text{(B.6)}$$

where:

- P_{Rx} is the received power at receiver input.

The HSPA+ receiver sensitivity can be approximated by:

$$P_{Rx\min[\text{dBm}]} = N_{[\text{dBm}]} - G_{p[\text{dB}]} + \rho_{IN[\text{dB}]} \quad \text{(B.7)}$$

where:

- $P_{Rx\min}$ is the receiver sensitivity;
- N is the total noise power given by (B.8);
- G_p is the processing gain, Table B.1;
- ρ_{IN} is the signal to noise ratio, Table B.1;
- R_b is the data rate;
- R_c is the WCDMA chip rate;
- E_c/N_0 is the energy per chip to noise power spectral density ratio.

Table B.1. HSPA+ processing gain and SNR definition.

System	Processing Gain	SNR/SINR
HSPA+ DL	Fixed and equal to 16 (SF_{16})	ρ_{IN}
HSPA+ UL	R_c/R_b	E_c/N_0

The total noise power is:

$$N_{[\text{dBm}]} = -174 + 10 \cdot \log(\Delta f_{[\text{Hz}]}) + F_{[\text{dB}]} + M_{I[\text{dB}]} \quad \text{(B.8)}$$

where:

- Δf is the signal bandwidth;
- F is the receiver's noise figure;
- M_I is the interference margin.

For HSPA+ UL, the metric used for SNR is the E_c/N_0. The E-DPDCH throughput is a continuous function of the E_b/N_0 at the Node B.

The E_b/N_0 is necessary being obtained from interpolation of E_c/N_0:

$$E_b/N_{0\,[\text{dB}]} = E_c/N_{0\,[\text{dB}]} + G_{p[\text{dB}]} \quad \text{(B.9)}$$

In HSPA+ UL, manipulating (B.7) and (B.9), the E_c/N_0 for a certain user's distance is given by:

$$E_c / N_{0\,[\mathrm{dB}]} = P_{Rx\,[\mathrm{dBm}]} - N_{[\mathrm{dBm}]} \quad \text{(B.10)}$$

For HSPA+ DL, rearranging (B.7), the SINR associated to a certain user distance is calculated by:

$$\rho_{IN\,[\mathrm{dB}]} = P_{Rx\,[\mathrm{dBm}]} - N_{[\mathrm{dBm}]} + G_{p\,[\mathrm{dB}]} \quad \text{(B.11)}$$

Some margin values must be considered, to adjust additional losses due to radio propagation and others:

$$M_{[\mathrm{dB}]} = M_{SF\,[\mathrm{dB}]} + M_{FF\,[\mathrm{dB}]} + L_{int\,[\mathrm{dB}]} \quad \text{(B.12)}$$

where:

- M_{SF} is the slow fading margin;
- M_{FF} is the fast fading margin;
- L_{int} are the indoor penetration losses.

Annex C – HSPA+ DL Additional Results

Modulation ratio as a function of CPICH RSCP is presented for the 8th category MT, considering P_{BS}^{Tx} equal to 43 and 41 dBm, Figure C.1 and Figure C.2. The analysis regarding the category 14 terminal is also shown, Figure C.3 and Figure C.4, for 43 and 41 dBm, respectively.

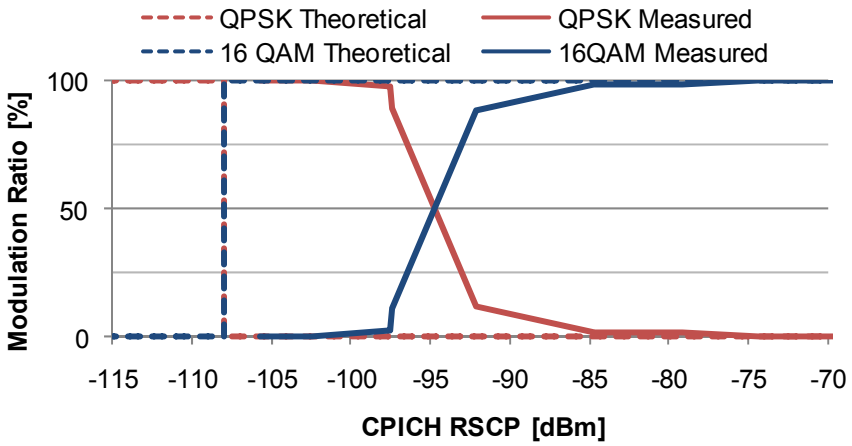

Figure C.1. Theoretical and measured modulation ratios as a function of CPICH RSCP for the category 8 MT, with $P_{BS}^{Tx} = 43\,\text{dBm}$.

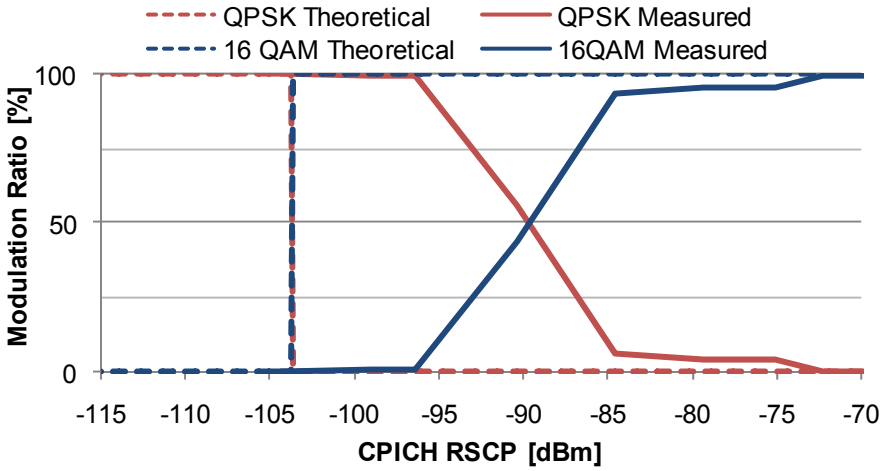

Figure C.2. Theoretical and measured modulation ratios as a function of CPICH RSCP for the category 8 MT, with $P_{BS}^{Tx} = 41\text{dBm}$.

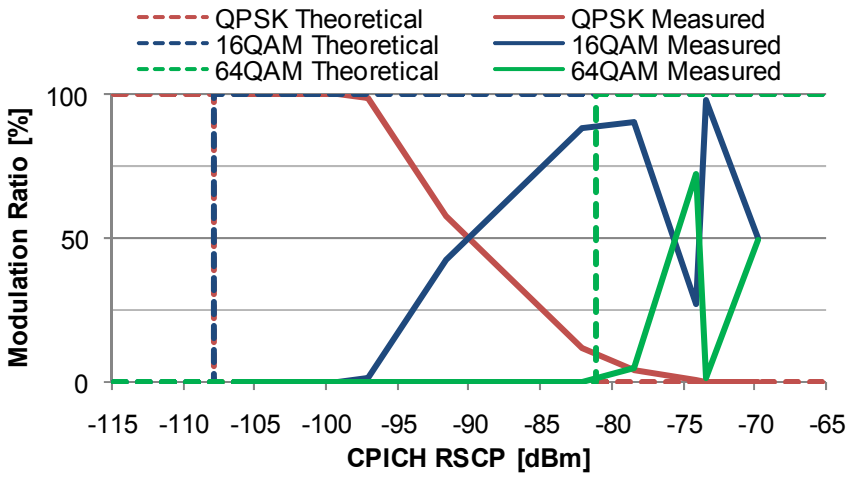

Figure C.3. Theoretical and measured modulation ratios as a function of CPICH RSCP for the category 14 MT, with $P_{BS}^{Tx} = 43\,\text{dBm}$.

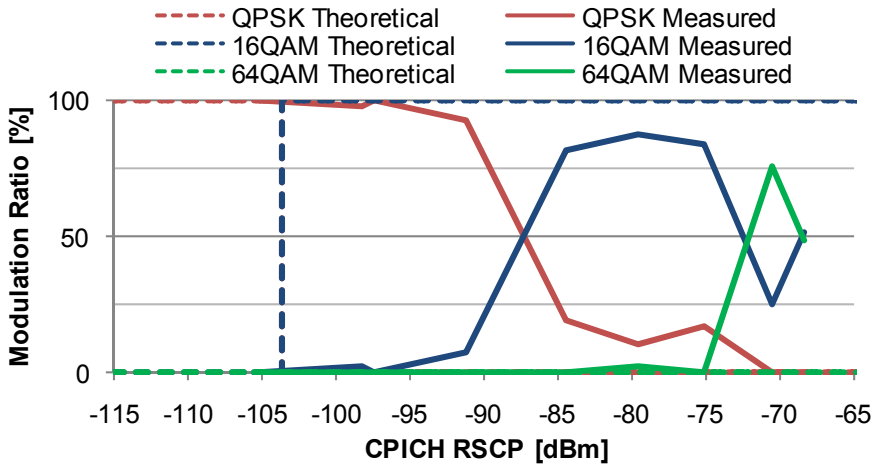

Figure C.4. Theoretical and measured modulation ratios as a function of CPICH RSCP for the category 14 MT, with $P_{BS}^{Tx} = 41\text{dBm}$.

In Figure C.5, one shows the modulation ratio versus E_c/N_0 for the category 8 MT, with P_{BS}^{Tx} equal to 43 dBm. Results concerning the minimum available power are also presented, Figure C.6. In addition, the same analysis for the 14th category MT is done, Figure C.7 and Figure C.8.

In Figure C.9 and Figure C.10, one presents the modulation ratio as a function of CQI, for the terminal that only uses QPSK and 16QAM, considering the power configurations with 43 and 41 dBm, respectively. Again, results regarding the usage of 64QAM are also shown, Figure C.11 and Figure C.12.

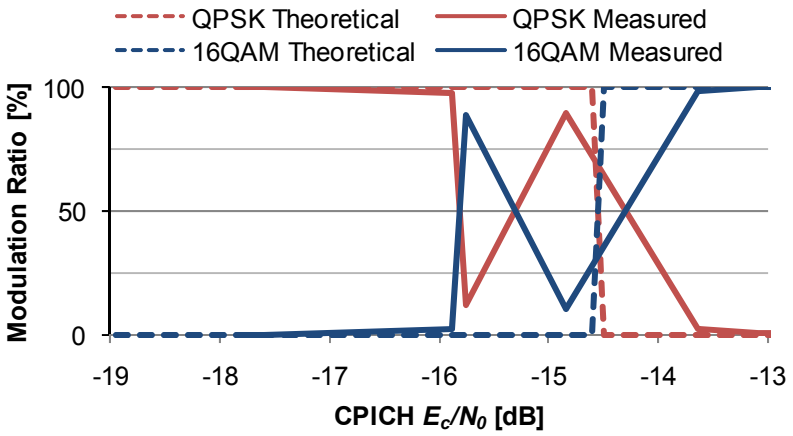

Figure C.5. Theoretical and measured modulation ratios as a function of CPICH E_c/N_0 for the category 8 MT, with $P_{BS}^{Tx} = 43\,\text{dBm}$.

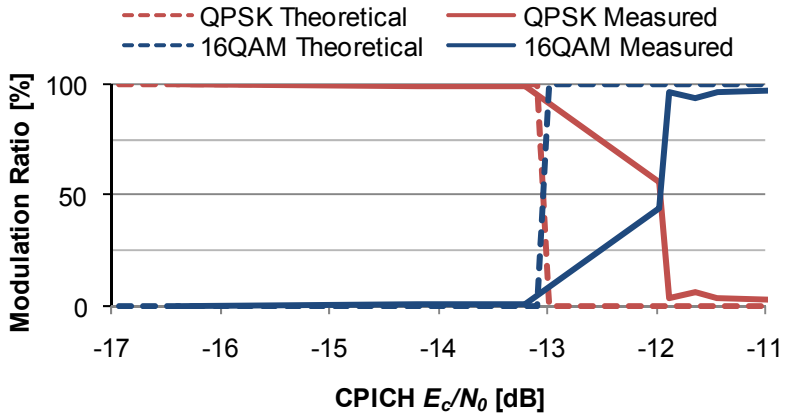

Figure C.6. Theoretical and measured modulation ratios as a function of CPICH E_c/N_0 for the category 8 MT, with $P_{BS}^{Tx} = 41\text{dBm}$.

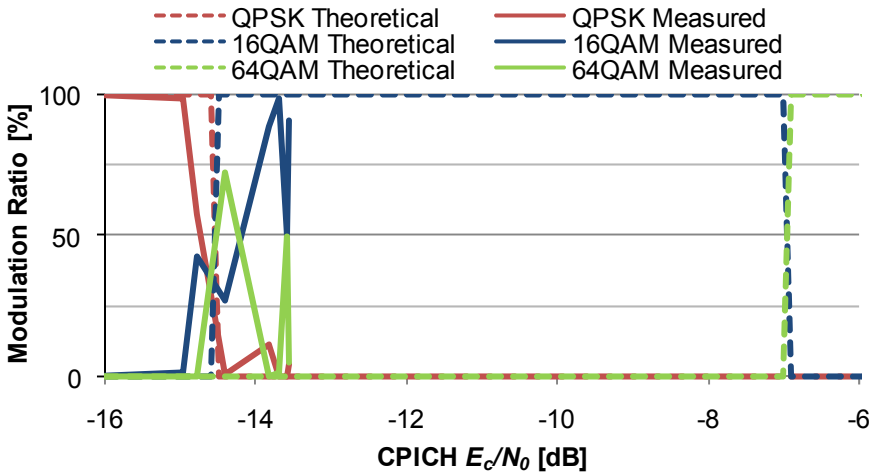

Figure C.7. Theoretical and measured modulation ratios as a function of CPICH E_c/N_0 for the category 14 MT, with $P_{BS}^{Tx} = 43\,\text{dBm}$.

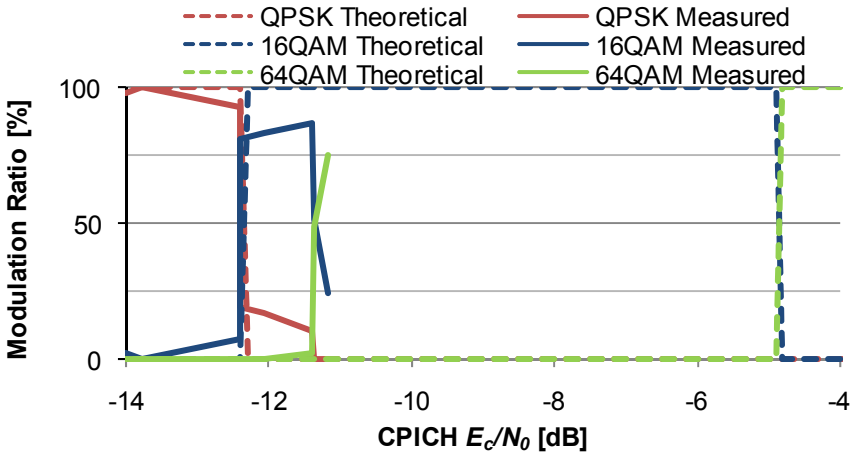

Figure C.8. Theoretical and measured modulation ratios as a function of CPICH E_c/N_0 for the category 14 MT, with $P_{BS}^{Tx} = 41\text{dBm}$.

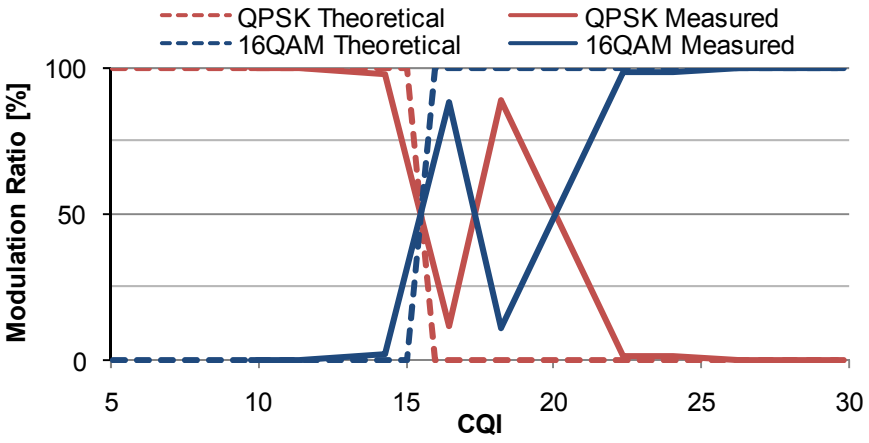

Figure C.9. Theoretical and measured modulation ratios as a function of CQI for the category 8 MT, with $P_{BS}^{Tx} = 43\,\text{dBm}$.

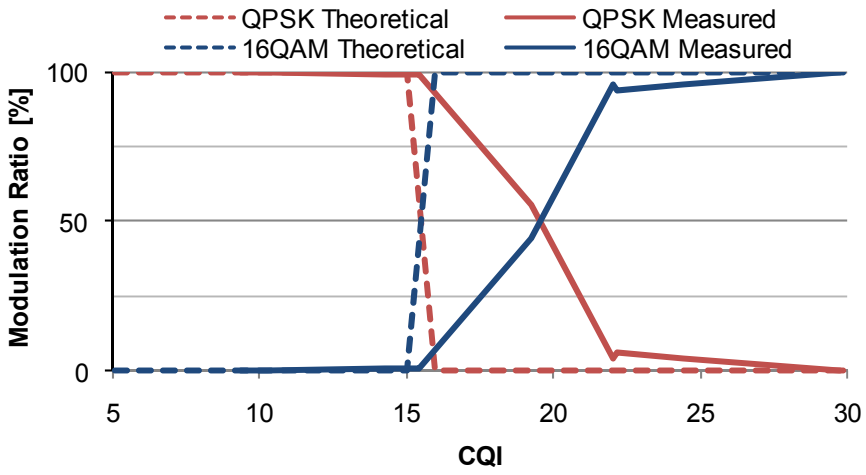

Figure C.10. Theoretical and measured modulation ratios as a function of CQI for the category 8 MT, with $P_{BS}^{Tx} = 41\text{dBm}$.

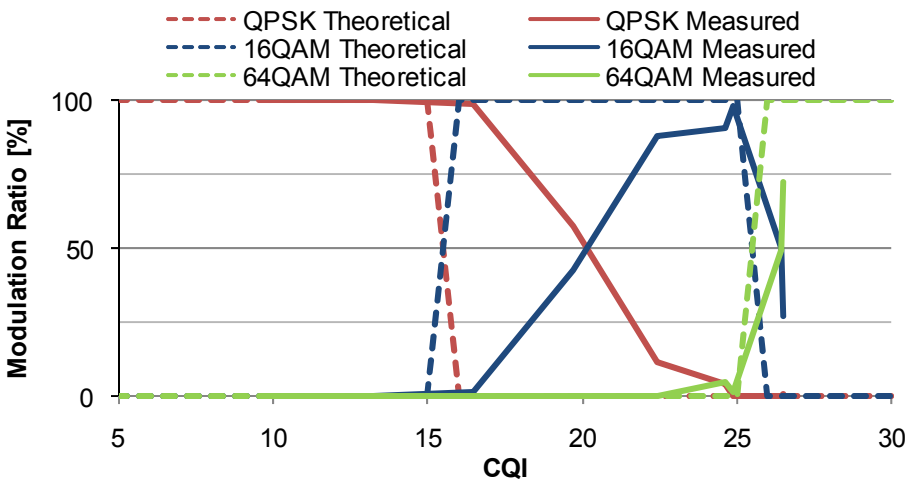

Figure C.11. Theoretical and measured modulation ratios as a function of CQI for the category 14 MT, with $P_{BS}^{Tx} = 43\,\text{dBm}$.

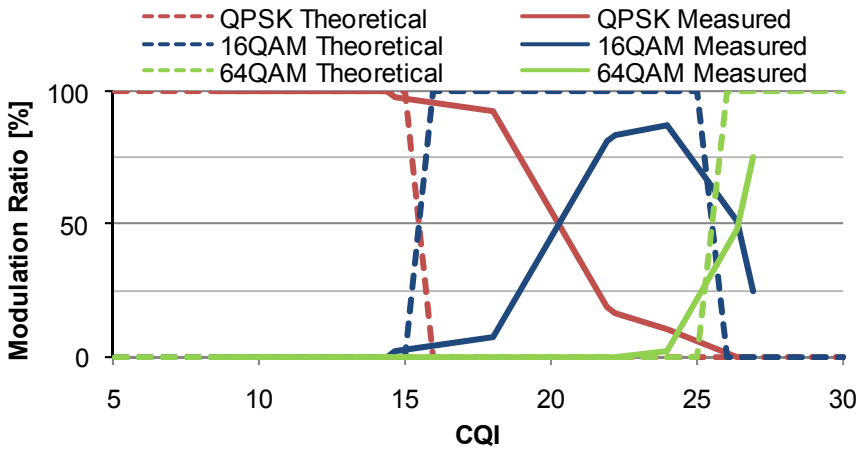

Figure C.12. Theoretical and measured modulation ratios as a function of CQI for the category 14 MT, with $P_{BS}^{Tx} = 41\text{dBm}$.

A comparison between the theoretical and measured number of HS-PDSCH codes as a function of CQI for the 8th category MT, with 43 and 41 dBm of P_{BS}^{Tx}, is presented in Figure C.13 and Figure C.14, respectively. In Figure C.15 and Figure C.16, one shows the same comparison regarding the usage of the 15 codes terminal.

In Figure C.17 and Figure C.18, one shows the measured HS-PDSCH average code usage considering different values of CPICH RSCP, for the category 8 terminal with 43 and 41 dBm of total Node B transmit power, respectively. Again, results when the 14th category MT was used are also shown, Figure C.19 and Figure C.20.

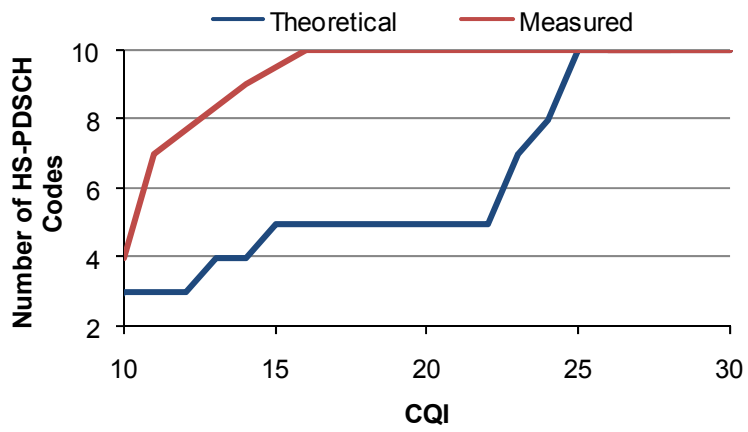

Figure C.13. Number of HS-PDSCH codes as a function of CQI with $P_{BS}^{Tx} = 43$ dBm, using the category 8 MT, considering theoretical and measured data.

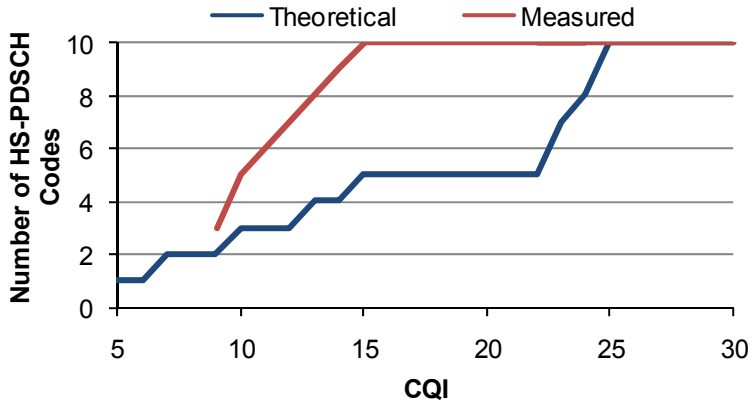

Figure C.14. Number of HS-PDSCH codes as a function of CQI with $P_{BS}^{Tx} = 41$dBm, using the category 8 MT, considering theoretical and measured data.

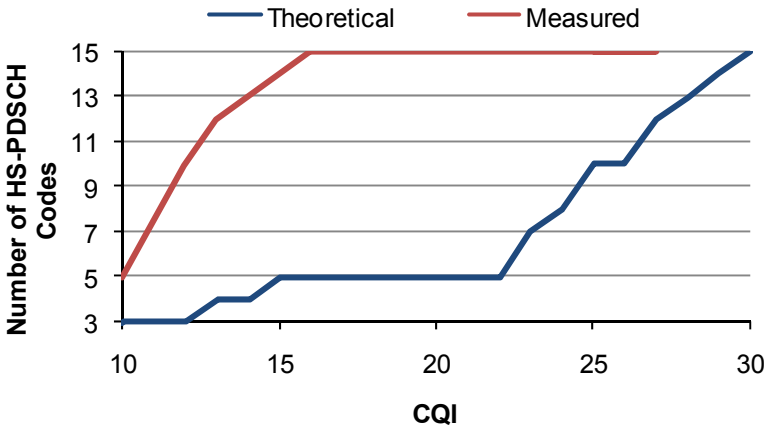

Figure C.15. Number of HS-PDSCH codes as a function of CQI with $P_{BS}^{Tx} = 43$ dBm, using the category 14 MT, considering theoretical and measured data.

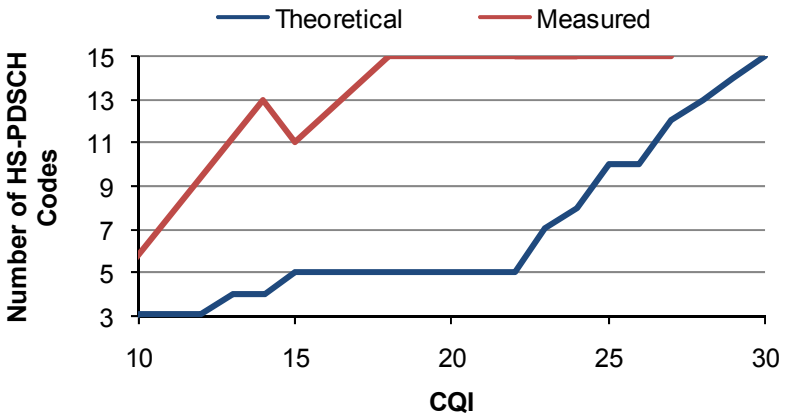

Figure C.16. Number of HS-PDSCH codes as a function of CQI with P_{BS}^{Tx} = 41dBm, using the category 14 MT, considering theoretical and measured data.

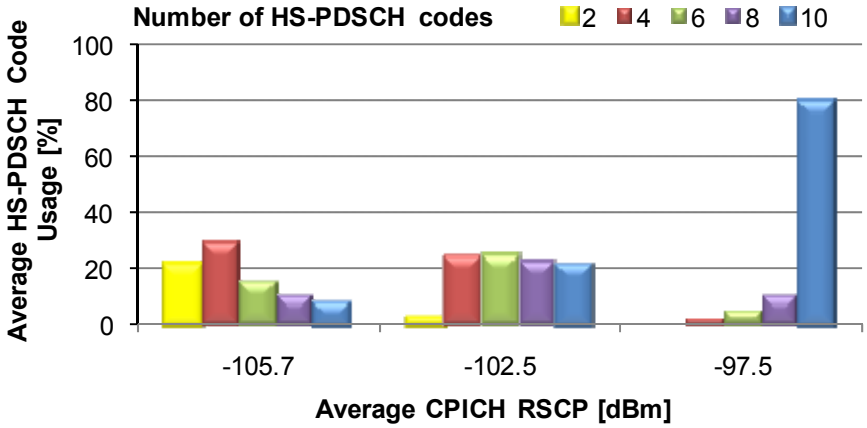

Figure C.17. Measured HS-PDSCH code usage as a function of CPICH RSCP with P_{BS}^{Tx} = 43 dBm, considering the category 8 MT.

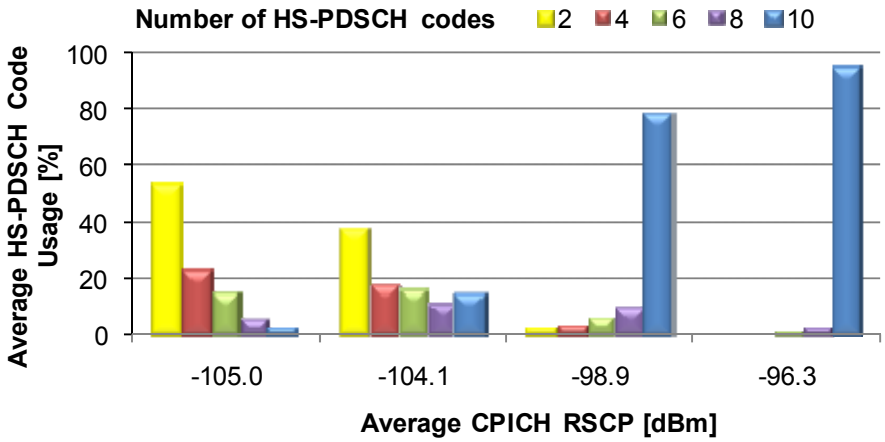

Figure C.18. Measured HS-PDSCH code usage as a function of CPICH RSCP with P_{BS}^{Tx} = 41dBm, considering the category 8 MT.

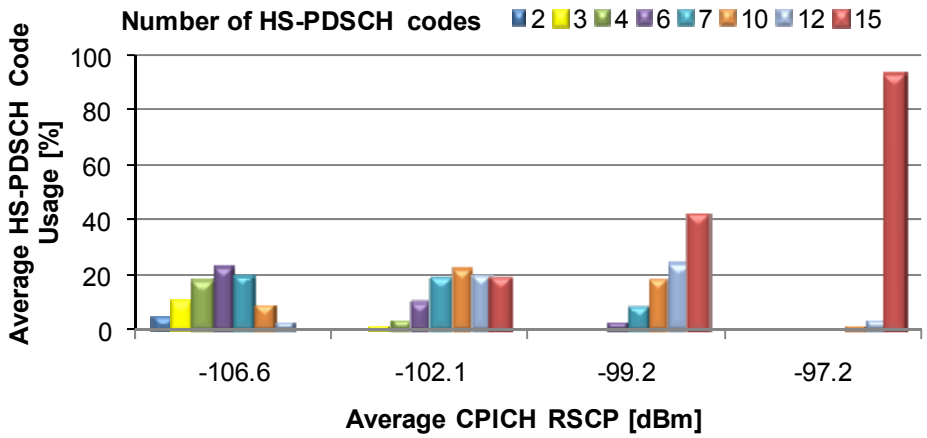

Figure C.19. Measured HS-PDSCH code usage as a function of CPICH RSCP with $P_{BS}^{Tx} = 43$ dBm, considering the category 14 MT.

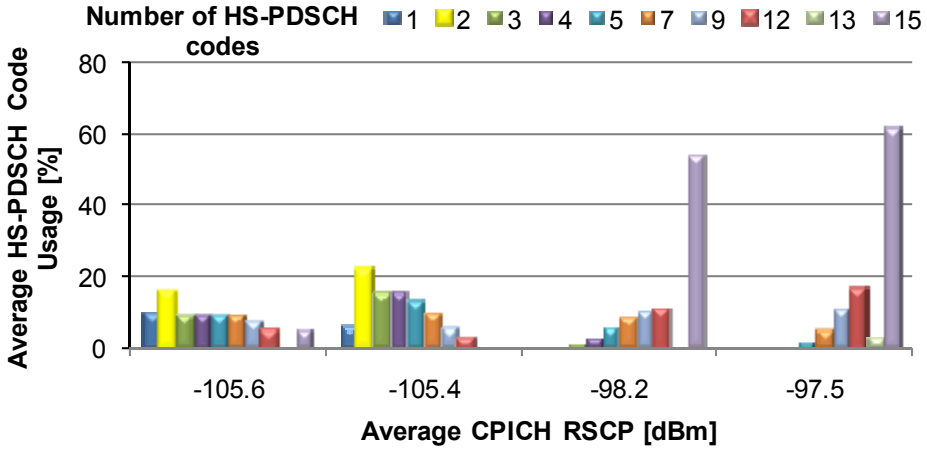

Figure C.20. Measured HS-PDSCH code usage as a function of CPICH RSCP with $P_{BS}^{Tx} = 41$dBm, considering the category 14 MT.

HS-DSCH BLER on first transmission as a function of CPICH RSCP, CPICH E_c/N_0 and CQI, for the category 8 MT, is presented, Figure C.21, Figure C.22 and Figure C.23, respectively.

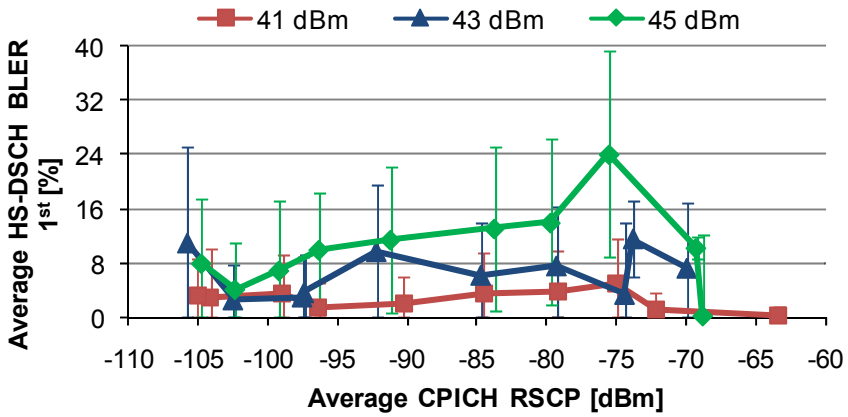

Figure C.21. Measured HS-DSCH BLER 1st as a function of CPICH RSCP for different power configurations, using the category 8 MT.

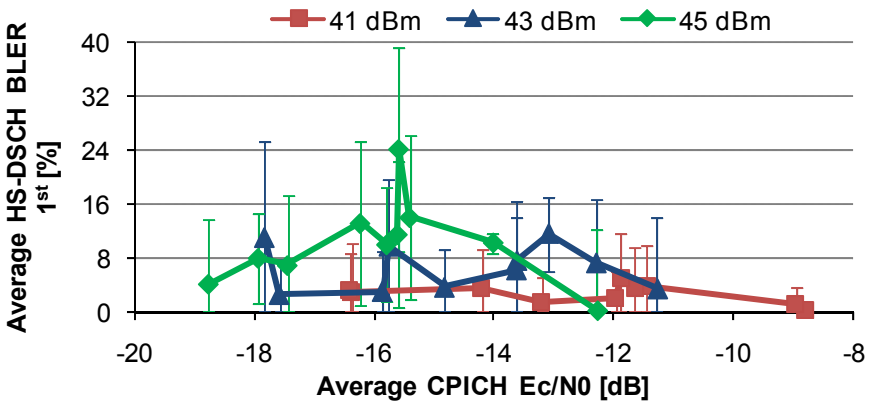

Figure C.22. Measured HS-DSCH BLER 1st as a function of CPICH E_c/N_0 for different power configurations, using the category 8 MT.

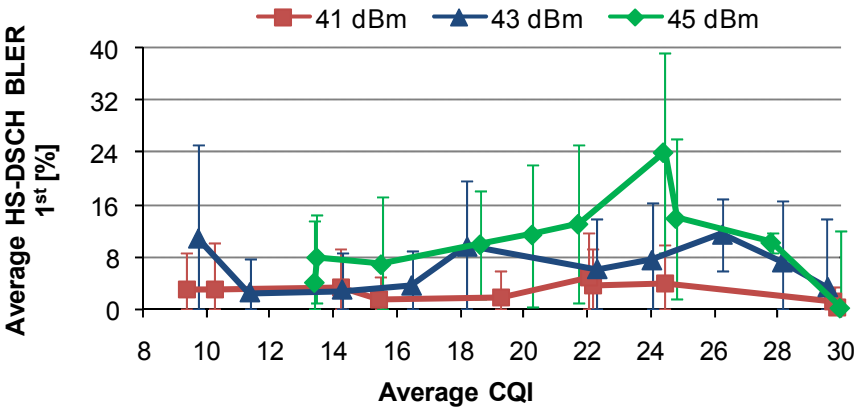

Figure C.23. Measured HS-DSCH BLER 1st as a function of CQI for different power configurations, using the category 8 MT.

References

[3GAM09] http://www.3gamericas.org/index.cfm?fuseaction=page&pageid=565, Set. 2009.

[3GPP02] 3GPP, Technical Specification Group - Radio Access Network Working, *Revised CQI Proposal*, Motorola, Ericsson, Report R1-020675, Paris, France, Apr. 2002.

[3GPP08] 3GPP, Technical Specification Group Services and System Aspects, *Service aspects; Services and Service Capabilities (Release 9)*, Report TS 22.105, V9.0.0, Dec. 2008 (http://www.3gpp.org/ftp/Specs/html-info/22105.htm).

[3GPP09a] 3GPP, Technical Specification Group Radio Access Network, *UE Radio Access capabilities (Release 8)*, Report TS 25.306, V8.7.0, Jun. 2009 (http://www.3gpp.org/ftp/Specs/html-info/25306.htm).

[3GPP09b] 3GPP, Technical Specification Group Radio Access Network, *Physical layer - Measurements (FDD) (Release 8)*, Report TS 25.215, V8.3.0, Mar. 2009 (http://www.3gpp.org/ftp/Specs/html-info/25215.htm).

[3GPP09c] 3GPP, Technical Specification Group Radio Access Network, *Physical Layer Procedures (FDD) (Release 8)*, Report TS 25.214, V8.6.0, May 2009 (http://www.3gpp.org/ftp/Specs/html-info/25214.htm).

[3GPP09d] 3GPP, Technical Specification Group Radio Access Network, *User Equipment (UE) conformance specification; Radio transmission and reception (FDD); Part 1: Conformance specification (Release 8)*, Report TS 34.121-1, V8.7.0, Jun. 2009 (http://www.3gpp.org/ftp/Specs/html-info/34121-1.htm).

[Asco09] http://www.ascom.com/en/index/products-solutions/technology-platforms/platform/tems/solutionloader.htm, Oct. 2009.

[BBSS04] Brouwer,F., Bruin,I., Silva,J., Souto,N., Cercas,F. and Correia,A., “Usage of Link-Level Performance Indicators for HSDPA Network-Level Simulations in E-UMTS”, in *Proc. of ISSSTA-2004 - IEEE International Symposium on Spread Spectrum Techniques and Applications*, Sydney, Australia, Sep. 2004.

[BEGG08] Bergman,J., Ericson,M., Gerstenberger,D., Göransson,B., Peisa,J. and Wager,S., *HSPA Evolution – Boosting the performance of mobile broadband access*, Ericsson Review, Nº1, 2008.

[CoLa06] Costa,P. and Ladeira,D., *Planning of UMTS Cellular Networks for Data Services Based on HSDPA* (in Portuguese), Graduation Thesis, Instituto Superior Técnico, Lisbon, Portugal, Jun. 2006.

[Corr06] Correia,L.M., *Mobile Communication Systems – Course Notes*, IST-TUL, Lisbon, Portugal, Mar. 2006.

[Dziu04] Dziunikowski,W., *Multiple-Input Multiple-Output (MIMO) Antenna Systems*, in Chandran, S. (ed.), *Adaptive Antenna Arrays*, Springer, Berlin, Germany, 2004.

[ECGF05] El Zein,G., Cosquer,R., Guillet,J., Farhat,H. and Sagnard,F., "Characterisation and Modeling of the MIMO Propagation Channel: An Overview", in *Proc. of European Conference Wireless Technology*, Paris, France, *O*ct. 2005.

[Eric09] White Paper, *Accelerating global development with mobile broadband*, Ericsson Research, Feb. 2009 (http://www.ericsson.com/technology/whitepapers/acc-global-dev-with-mbb.pdf).

[GoEa09] http://earth.google.com/, Sep. 2009.

[GSMW09] http://gsmworld.com/newsroom/press-releases/2009/2521.htm#nav-6, Sep. 2009.

[HGMT05] Hagerman,B., Gunnarsson,F., Murai,H., Tadenuma,M. and Karlsson,J., "WCDMA Uplink Parallel Interference Cancellation - System Simulations and Prototype Field Trials", *EURASIP Journal on Applied Signal Processing*, Vol. 2005, Issue 11, Nov. 2005, pp. 1725-1735.

[HoTo04] Holma,H. and Toskala,A., *WCDMA for UMTS – Radio Access For Third Generation Mobile Communications*, John Wiley & Sons, Chichester, UK, 2004.

[HoTo06] Holma,H. and Toskala,A., *HSDPA/HSUPA for UMTS – High Speed Radio Access for Mobile Communications*, John Wiley & Sons, Chichester, UK, 2006.

[HoTo07] Holma,H. and Toskala,A., *WCDMA for UMTS – HSPA Evolution and LTE* (4^{th} Edition), John Wiley & Sons, Chichester, UK, 2007.

[HoTo09] Holma,H. and Toskala,A., *LTE for UMTS – OFDMA and SC-FDMA Based Radio Access*, John Wiley & Sons, Chichester, UK, 2009.

[KuCo08] Kuipers,M. and Correia,L.M., "Modelling the Relative MIMO Gain", in *Proc. of PIMRC'08 - IEEE Personal, Indoor and Mobile Radio Communications*, Cannes, France, Sep. 2008.

[Lope08] Lopes,J., *Performance of UMTS/HSDPA/HSUPA at the Cellular Level*, M.Sc. Thesis, Instituto Superior Técnico, Lisbon, Portugal, Mar. 2008.

[Maćk07] Maćkowiak,M., *Geometrically Based Multibounce MIMO Channel Models*, M.Sc. Thesis,

Instituto Superior Técnico, Lisbon, Portugal, Sep. 2007.

[Moli05] Molisch,A.F., *Wireless Communications*, John Wiley & Sons, Chichester, UK, 2005.

[Opti09] Private Communication, Optimus, 2009.

[Pede05] Pedersen,K.I., "Quality Based HSDPA Access Algorithms", in *Proc of VTC Fall 2005* – 62nd *IEEE Vehicular Technology Conference*, Dallas, TX, USA, Sep. 2005.

[Preg08] Preguiça,R., *Comparison between UMTS/HSPA+ and WiMax/IEEE 802.16e in Mobility Scenarios*, M.Sc. Thesis, Instituto Superior Técnico, Lisbon, Portugal, Sep. 2008.

[Proa01] Proakis,J.G., *Digital Communications*, MacGraw Hill, New York, NY, USA, 2001.

[Salv08] Salvado,L., *UMTS/HSDPA comparison with WiMAX/IEEE 802.16e in mobility scenarios*, M.Sc. Thesis, Instituto Superior Técnico, Lisbon, Portugal, Fev. 2008.

[Sant04] Santo,L., *UMTS Performance in Multi-Service Non-Uniform Traffic Networks*, M.Sc. Thesis, Instituto Superior Técnico, Lisbon, Portugal, Dec. 2004.